MAX-PLANCK-INSTITUT
FÜR POLYMERFORSCHUNG

Thiol-ene miniemulsion photopolymerization towards functional and reactive sulfur polymer latex

Dissertation

zur Erlangung des Grades
„Doktor der Naturwissenschaften“
im Promotionsfach Chemie

am Fachbereich Chemie, Pharmazie,
Geographie und Geowissenschaften
der Johannes Gutenberg-Universität Mainz

vorgelegt von Lorena Infante Teixeira
geboren in: Belo Horizonte, Brasilien

Mainz, 2021

This thesis was carried out from August 2018 until October 2021 in the Department of Physical Chemistry of Polymers at the Max-Planck-Institute for Polymer Research, Mainz.

1. Berichterstatter:
2. Berichterstatter:

Tag der mündlichen Prüfung:

Declaration

I hereby declare that I wrote the dissertation submitted without any unauthorized external assistance and used only sources acknowledged in the work. All textual passages, which are appropriated verbatim or paraphrased from published and unpublished texts, as well as all information obtained from oral sources are duly indicated and listed in accordance with bibliographical rules. In carrying out this research, I complied with the rules of standard scientific practice as formulated in the statutes of Johannes Gutenberg-University Mainz to insure standard scientific practice.

Mainz, 2021 Lorena Infante Teixeira

Abstract

Polymerization in miniemulsion has drawn a great deal of attention in the last few decades. One of the main reasons for that is the concept of nanoreactors, i.e., every droplet acts as an individual reaction locus. The use of such geometrically restricted environments unravels several advantages and breakthroughs for polymer science. For example, it provides an additional way to control the design of particles and enable the reaction to be performed in a waterborne medium, also appealing to environmental concerns of the industrial sector. Besides being an elegant way to produce well-defined nanoparticles, the confinement effect of the droplets formed in miniemulsion preparations has been reported to be extremely beneficial in other aspects, such as in the encapsulation of sensitive payloads, such as pharmaceuticals and catalysts, and in accelerating and enhancing reactions that occurred within the nanoreactor boundaries.

Although many polymer nanoparticles have been prepared by miniemulsion polymerization, the rational design of new nanoparticles is still needed to optimize their composition for specific applications. For example, in the case of biomedical applications for instance, nanoobjects, e.g., particles and capsules could be employed as drug carriers, but they need to have a well-controlled composition and surface chemistry to harness their full potential. This can be difficult to achieve considering the high complexity of the immense number of biochemical interactions possible. To improve delivery, it is necessary to design nanosystems with controlled composition that could protect the encapsulated drug until it reaches its destination, that are inert to foreign interactions, being only responsive to environmental cues that are specific to the targeted tissue, to locally release the cargo and improve the therapeutic effect.

To address these challenges, the polymerization using thiol-ene chemistry adds layers of possibilities to tailor the properties of polymer nanomaterials produced by miniemulsion. To begin with, the hydrothiolation can proceed under several mild conditions compatible with biological media and enable a fine control of the structure-property relationship, due to the wide range of thiol- and ene-containing monomers available. In addition, the ubiquitous presence of thiol-moieties in biological molecules makes thiol-ene chemistry an attractive method for the post-polymerization biofunctionalization of polymer materials. In addition, the thiol-ene reaction are extremely fast, oxygen and moisture tolerant, regioselective and quantitative, and display all the advantages of a click-reaction.

From an application standpoint, thiol-ene chemistry coupled with miniemulsion technique is a powerful combination to produce several types of polymer nanoparticles. Occurring through a step-growth mechanism, this polymerization allows the formation of functional end-groups on the polymer chain of thiols or enes, especially under off-stoichiometric ratios of monomers, which could be used as anchors for further functionalization of the surfaces of the particles in post-polymerization modifications. Therefore, with the same chemistry, this platform allows not only the formation of polymer networks but also their tailored functionalization.

Different from other click-chemistry that have also been used to prepare such nanosystems, thiol-ene provides an extra feature that relies on the sulfur chemistry. Sulfur centers within the main backbone of polysulfide (polythioether) chains are prone to oxidation. These atoms can adopt different oxidation-states. In addition to the sulfide, sulfoxides (IV) and sulfones (VI) can be produced by oxidation, which dramatically changes the physiochemical properties of the material, such as their thermo-mechanical resistance, as well as their hydrophilicity and protein adhesion profile. Consequently, nanocarriers produced by thiol-ene chemistry are widely adaptable for several industrial applications and can be modified both on their surface and in their core network.

In this thesis, thiol-ene polymer nanoparticles were prepared via photopolymerization in miniemulsion. The coupling of click-chemistry in dispersed media with photoinitiation confers spatiotemporal selectivity and facilitate tailoring the materials properties. The main goal of this project was to synthesize novel polymer nanoparticles, whose properties could be tailored, either by functionalization with biomolecules through thiol-ene chemistry, or core-modified by oxidation of the sulfur centers and be used as drug-delivery systems. To do so, it was important to control certain aspects of the reaction, in particular, the kinetics under confinement, defining the rate and degree of polymerization. For that, different thiol-ene monomer pairs were prepared and their rates of polymerization were followed by Raman spectroscopy (Section 4.1). The comparison between formulations in bulk, and in miniemulsion provided a full description of the effect of confinement on this step-growth polymerization and how it could be harnessed to favor high-performance properties to the material. The results described could even help understanding the phenomenon in other types of step-growth mechanisms. More interestingly, the polymerizations performed in miniemulsion in the presence of either diene or dithiol monomers show significant improvement in terms of conversion and degree of polymerization compared to the same reaction performed in bulk, and this allow the further thiol-ene functionalization of the excess enes (or thiols) after the polymerization.

Post-polymerization functionalization of these particles prepared with an excess of dienes was then employed to functionalize the remaining functional groups on the surface with either thiolated or ene-functionalized biomolecules, such as carbohydrates and peptides, or polymer, such as polyethylene glycol (PEG), well-known in biomedical applications for its role in controlling the interaction between the nanocarriers and the environment (Section 4.3). Furthermore, since hydrophilicity of a nanoparticle is crucial in determining the fate of a nanoparticle *in vivo*, namely its interactions with proteins, this property was tuned by subsequential oxidation, transforming the parent polysulfide nanoparticles into polysulfoxide and polysulfone latexes (Section 4.2). Moreover, results showed an increase in the hydrodynamic ratio of polysulfoxides and even degradation of the particles under over-oxidation conditions that could be used as release mechanisms in inflamed tissues, which intrinsically exhibit high concentrations of reactive oxidation species that could induce the delivery of the cargo.

The outcomes of this thesis are multiple. On one hand, the use of the miniemulsion technique was used to tune the nanoparticles physicochemical properties by controlling their size, distribution, and composition of the initial droplets. On another hand, the thiol-ene step-growth photopolymerization could, within such well-defined droplets, selectively and quantitatively produce modifiable polymer particles either through oxidation or surface modification to optimize the properties of the system for a wide array of specific applications. More generally, this project also provided new insights on reaction kinetics in nanoconfinement.

Zusammenfassung

Polymerisationen in einem heterogenen Medium wie der Miniemulsion haben in den letzten Jahrzehnten viel Aufmerksamkeit erregt. Einer der Hauptgründe dafür ist das Konzept der Nanoreaktoren, d. h. jedes dispergierte Tröpfchen der Miniemulsion fungiert als individueller Reaktionsort. Die Verwendung solcher geometrisch eingeschränkten Umgebungen bringt eine Reihe von Vorteilen und Durchbrüchen für die Polymerwissenschaft mit sich. So bietet sie beispielsweise eine zusätzliche Möglichkeit, das Design der Partikel zu kontrollieren und ermöglicht die Durchführung der Reaktion in einem wasserbasierten Medium, was den Umweltbelangen des industriellen Sektors entgegenkommt. Abgesehen davon, dass es sich um eine elegante Methode zur Herstellung wohldefinierter Nanopartikel handelt, hat sich der Begrenzungseffekt der in Miniemulsionszubereitungen gebildeten Tröpfchen auch in anderer Hinsicht als äußerst vorteilhaft erwiesen, z. B. bei der Verkapselung empfindlicher Substanzen wie Arzneimittel und Katalysatoren und bei der Beschleunigung und Verstärkung von Reaktionen, die innerhalb der Grenzen des Nanoreaktors ablaufen.

Obwohl bereits viele Polymer-Nanopartikel durch Miniemulsionspolymerisation hergestellt wurden, ist die rationelle Gestaltung neuer Nanopartikel nach wie vor erforderlich, um ihre Zusammensetzung für bestimmte Anwendungen zu optimieren. Im Falle biomedizinischer Anwendungen könnten Nanoobjekte, z. B. Partikel und Kapseln, als Arzneimittelträger eingesetzt werden, aber sie müssen eine gut kontrollierte Zusammensetzung und Oberflächenchemie aufweisen, um ihr volles Potenzial auszuschöpfen. Dies kann angesichts der hohen Komplexität der immensen Anzahl möglicher biochemischer Wechselwirkungen schwierig zu erreichen sein. Um die Verabreichung zu verbessern, müssen Nanosysteme mit kontrollierter Zusammensetzung entwickelt werden, die den eingekapselten Wirkstoff schützen, bis er seinen endgültigen Bestimmungsort erreicht, und die inert gegenüber fremden Wechselwirkungen sind und nur auf Umweltreize reagieren, die für das Zielgewebe spezifisch sind, um die Ladung lokal freizusetzen und die therapeutische Wirkung zu verbessern.

Um diese Herausforderungen zu bewältigen, bietet die Polymerisation durch die Thiol-En-Chemie eine Reihe von Möglichkeiten, die Eigenschaften der durch Miniemulsion hergestellten Polymer-Nanomaterialien anzupassen. Zunächst einmal kann die Hydrothiolierung unter einer Reihe von milden, mit biologischen Medien kompatiblen Bedingungen ablaufen und ermöglicht aufgrund der breiten Palette an Thiol- und En-haltigen Substraten eine feine Kontrolle der Struktur-Eigenschafts-Beziehung. Darüber hinaus macht die ubiquitäre Präsenz von Thiol-Molekülen in

biologischen Molekülen die Thiol-En-Chemie zu einer attraktiven Methode für die Biofunktionalisierung von Polymermaterialien nach der Polymerisation. Darüber hinaus ist die Thiol-En-Reaktion extrem schnell, sauerstoff- und feuchtigkeitstolerant, regioselektiv und quantitativ, weshalb sie auch als Klick-Reaktion bezeichnet wird.

Vom Anwendungsstandpunkt aus betrachtet ist die Thiol-En-Chemie in Verbindung mit der Miniemulsionstechnik eine leistungsstarke Kombination zur Herstellung verschiedener Arten von Polymer-Nanopartikeln. Diese Polymerisation, die nach einem schrittweisen Wachstumsmechanismus abläuft, ermöglicht die Bildung funktioneller Endkappen aus Thiolen oder Enen, insbesondere bei ungleichmäßigen Monomerverhältnissen, die als Anker für die weitere Funktionalisierung der Partikeloberflächen bei Modifikationen nach der Polymerisation verwendet werden können. Daher ermöglicht diese Plattform mit derselben Chemie nicht nur die Bildung von Polymernetzwerken, sondern auch deren maßgeschneiderte Veränderungen.

Im Gegensatz zu anderen Klick-Reaktionen, die ebenfalls zur Herstellung solcher Nanosysteme verwendet wurden, bieten Thiol-En-Reaktionen eine zusätzliche Funktion, die auf der Schwefelchemie beruht. Die Schwefelzentren im Hauptgerüst der Polysulfidketten (Polythioether) sind anfällig für Oxidation. Diese Atome können verschiedene Oxidationszustände annehmen. Neben dem Sulfid können durch Oxidation auch Sulfoxide (IV) und Sulfone (VI) entstehen, was wiederum die physiochemischen Eigenschaften des Materials, wie z. B. seine thermomechanische Beständigkeit, sowie seine Hydrophilie und sein Proteinhaftungsprofil, drastisch verändern. Infolgedessen sind die mit Hilfe der Thiol-En-Reaktion hergestellten Nanoträger für eine Vielzahl industrieller Anwendungen geeignet und können sowohl an ihrer Oberfläche als auch in ihrem Kernnetz modifiziert werden.

In dieser Arbeit wurden Thiol-En-Polymer-Nanopartikel durch Photopolymerisation in Miniemulsion hergestellt. Die Kopplung der Klick-Chemie in dispergierten Medien mit der Photoinitiation verleiht räumliche und zeitliche Selektivität und erleichtert die Anpassung der Materialeigenschaften. Das Hauptziel dieses Projekts war die Synthese neuartiger Polymer-Nanopartikel, deren Eigenschaften entweder durch Funktionalisierung mit Biomolekülen durch Thiol-En-Chemie oder durch Kernmodifikation durch Oxidation der Schwefelkerne maßgeschneidert werden können, um als Arzneimittelabgabesysteme verwendet zu werden. Zu diesem Zweck war es wichtig, bestimmte Aspekte der Reaktion zu kontrollieren, insbesondere die Kinetik unter Einschluss, welches die Geschwindigkeit und den Grad der Polymerisation bestimmt. Dazu wurden verschiedene Thiol-En-Monomer-Paare hergestellt und ihre Polymerisationsgeschwindigkeiten mittels Raman-Spektroskopie verfolgt (Abschnitt 4.1). Der Vergleich zwischen den Formulierungen im Bulk und in Miniemulsion lieferte eine vollständige Beschreibung der Auswirkungen des Einschlusses auf diese

Stufenpolymerisation und wie diese genutzt werden könnten, um dem Material Hochleistungseigenschaften zu verleihen. Die beschriebenen Ergebnisse könnten sogar zum Verständnis des Phänomens bei anderen Arten von Schrittwachstumsmechanismen beitragen. Interessanterweise zeigen die in Miniemulsion durchgeführten Polymerisationen in Anwesenheit von Dien- oder Dithiolmonomeren eine signifikante Verbesserung in Bezug auf den Umsatz und den Polymerisationsgrad im Vergleich zu der gleichen Reaktion, die in Masse durchgeführt wird, und dies ermöglicht die weitere Thiol-En-Funktionalisierung der überschüssigen Ene (oder Thiole) nach der Polymerisation.

Die mit einem Überschuss an Dienen hergestellten Partikel wurden dann nach der Polymerisation funktionalisiert, um die verbleibenden funktionellen Gruppen auf der Oberfläche entweder mit thiolierten oder En-funktionalisierten Biomolekülen wie Kohlenhydraten und Peptiden oder mit Polymeren wie Polyethylenglykol (PEG) zu funktionalisieren, das in biomedizinischen Anwendungen für seine Rolle bei der Kontrolle der Interaktion zwischen den Nanoträgern und der Umgebung bekannt ist (Abschnitt 4.3). Da die Hydrophilie eines Nanopartikels entscheidend für das Schicksal eines Nanopartikels *in vivo* ist, nämlich seine Wechselwirkungen mit Proteinen, wurde diese Eigenschaft durch eine anschließende Oxidation eingestellt, wodurch die ursprünglichen Polysulfid-Nanopartikel in Polysulfoxid- und Polysulfon-Latexe umgewandelt wurden (Abschnitt 4.2). Darüber hinaus zeigten die Ergebnisse eine Zunahme des hydrodynamischen Verhältnisses der Polysulfoxide und sogar einen Abbau der Partikel unter Überoxidationsbedingungen, die als Freisetzungsmechanismen in entzündeten Geweben genutzt werden könnten, die von Natur aus hohen Konzentrationen reaktiver Oxidationsspezies aufweisen, die die Freisetzung der Ladung einleiten könnten.

Die Ergebnisse dieser Arbeit sind vielfältig. Einerseits wurde die Miniemulsionstechnik eingesetzt, um die physikochemischen Eigenschaften der Nanopartikel durch Kontrolle ihrer Größe, Verteilung und Zusammensetzung der Ausgangströpfchen einzustellen. Andererseits konnten durch die Thiol-En-Photopolymerisation mit schrittweisem Wachstum in solchen wohldefinierten Tröpfchen selektiv und quantitativ modifizierbare Polymerpartikel entweder durch Oxidation oder Oberflächenmodifikation hergestellt werden, um die Eigenschaften des Systems für eine breite Palette spezifischer Anwendungen zu optimieren. Ganz allgemein lieferte dieses Projekt auch neue Erkenntnisse über die Reaktionskinetik bei der Nanoveredelung.

Table of Contents

1 Motivation

1.1 Introduction

Polymers are widely used chemical products, present in almost all the sectors such as aerospace, packaging, automotive, construction, electrical appliances, and medical sector. From households to our industrial needs, polymers permeate every aspect of human life due to their unique capacity of offering broad and customizable properties. Today, the polymer industry is going through one of the most significant changes in priorities in its history. Driven by current and future environmental regulations in Europe and beyond, the development of processes and products combining ecological and economic efficiency has become necessary. When it comes to eco-efficient processes and zero-VOC polymer products, two technologies stand out in terms of production level, growth, and broad application range: polymerization in dispersed media and photopolymerization.

To tackle this challenge PHOTO-EMULSION, a European project in the framework of the Horizon 2020 actions, aimed to develop and promote the use of photopolymerization in dispersed media as means to produce polymer nanoparticles to a wide range of applications, while keeping up with economical and environmental regulations. One of the cornerstones of the project is the polymerization in dispersed media, mostly in waterborne emulsions and suspensions, which already accounts for 20% of the polymer production worldwide[1] and is an important step toward zero-VOC process. The second technology explored is the photopolymerization, which is an important energy-saving polymerization process, applied today for example as a film curing technique. The combination of these two manufacturing practices offers many possibilities in a wide spectrum of fields. Besides the manufacturing aspect, the type of polymerization mechanism should be fully adaptable to this system, i.e., able to perform in waterborne dispersed media and be photochemically latent, as well as intrinsically tunable to allow the production of materials with varied properties.

With that in mind, the step-growth thiol-ene polymerization in miniemulsion seemed to be well-suited all-in-one platform to the design of finely tuned nanoparticles. Firstly, the polymerization of monomers with two or more moieties of thiols and enes produces stable networks of polysulfide chains. When this polymerization is carried out in well-defined droplets prepared by miniemulsion polymer nanoparticles can be obtained.

Furthermore, the potential of thiol-ene photopolymerization in miniemulsion has not yet been fully harnessed. For this technological platform to gain in prominence, the range of materials produced, and the range of properties obtained from those materials need to be expended. Thiol-ene photopolymerization in miniemulsion has the potential to be a very versatile and tunable strategy to

generate a broad range of innovative polymer materials. In addition to the versatility in the building blocks used in the polymerization itself more factors can be controlled. For example, the fine control of the stoichiometry ratio between the reacting species allows the presence of unreacted functionalities of thiols or enes at the end of the polymerization process, which can be used to anchor different molecules at the surface of the polysulfide nanoparticles, through the same thiol-ene click chemistry. In addition, and distinguishing itself from other click-like reactions, the thiol-ene platform enables the modification of the chemical composition of the core by the oxidation of the sulfur-centers, without any detrimental effect to the colloidal stability nor to the integrity of the polymer network. Therefore, it is created a highly tunable strategy for the design of smart nanomaterials.

The hybrid process proposed by the thiol-ene miniemulsion photopolymerization paves the way to a novel range of high sulfur content dispersed products, such as latex, films, powder nanoparticles, monoliths. The outstanding properties conferred by thiol-ene, and sulfur-chemistries could be applied to produce non-leaching materials, nanocarriers for biomedical use, high barrier packaging film, and chromatography columns.

Overall, the main goal of this thesis was to explore the features of the thiol-ene photopolymerization in miniemulsion and the properties of the resulting products. More than only expanding the scope of materials synthesized, the objectives here were to explore the fundamental aspects of the chemistry to design functional and highly tunable nanoparticles, understand and control important thermodynamic and kinetic parameters to optimize the processes of synthesis and modification of the thiol-ene polymer nanoparticles, from their core to their surface.

2 State of the art

2.1 Thiol-ene chemistry

First introduced by Posner in 1905,[2] the radical addition of thiols to olefins has emerged as one of the most important methods for the construction of carbon–sulfur bonds. Since then, the thiol-ene reaction was used in applications ranging from polymers to biomedical field. The hydrothiolation of carbon-carbon double bonds is generally considered as a member of the so-called "click"-reactions.

Click-reactions are a class of chemical reactions that are characterized by nearly quantitative yields, fast reaction rates, processing under mild conditions, little to no sensitivity to moisture or oxygen, and orthogonality to other reactions.[3,4] Since the introduction of this archetypal concept by Sharpless and co-workers,[3] the number of publications on the use of click chemistry have exponentially increased through the years. The click-chemistry universe, once represented mainly by the copper(I)-catalyzed azide-alkyne cycloaddition, counts today with a wide range of reactions, from hetero-Diels–Alder reaction, nucleophilic ring-opening of strained cyclic electrophiles, carbonyl conversion into oxime ethers and hydrazones, to the addition to carbon–carbon multiple bonds such as epoxidation, and additions. Thiol-ene coupling is another example of classical chemistry that have been reinvented by this concept.

The thiol-ene reaction, and the click reactions in general, displays great potential for the synthesis of high-value materials, since it overcome hurdles often inherent to classical organic synthesis, such as the presence of side products, and the need of exhaustive clean-up steps. Beyond its click-nature, thiol-ene chemistry has several advantages that it stands out from other click-reactions. For example, there is a wide range of available molecules containing enes and thiol-moieties, with different structures and reactivities, making the reaction highly adaptable to different needs. In addition, the reaction enables the establishment of a robust ligation with substrates through high stability of the thioether linkages in different chemical environments. Different from most click-chemistries, thiol-ene also counts with the redox-sensitive sulfur chemistry as a tool for further modifications of materials. Consequently, thiol-ene coupling is an exceptional tool for applications that are sensitive to by-products, and require high performance materials, such as in the optical, biomedical, and sensing fields. [5,6]

2.1.1 Thiol-ene reaction

The mechanism of the thiol-ene reaction starts with the formation of a thiyl radical by the abstraction of a hydrogen atom from the thiol moiety, either by a thermal- or photo-initiator (free-radical thiol-ene) or use of a nucleophile (thiol-Michael) that typically creates a thiol-centered anion rather than a radical. It is then followed by the direct addition of the thiyl species on the carbon-carbon double bond, yielding a carbon-centered intermediate, which in turn do a hydrogen abstraction from a other thiol, in an anti-Markovnikov orientation (Figure 2.1.1)[4] Since the mechanism relies on the formation of radical or ionic intermediates, the chemical structure of the species involved play an importance role on their stabilization and thus in the fate of the reaction.

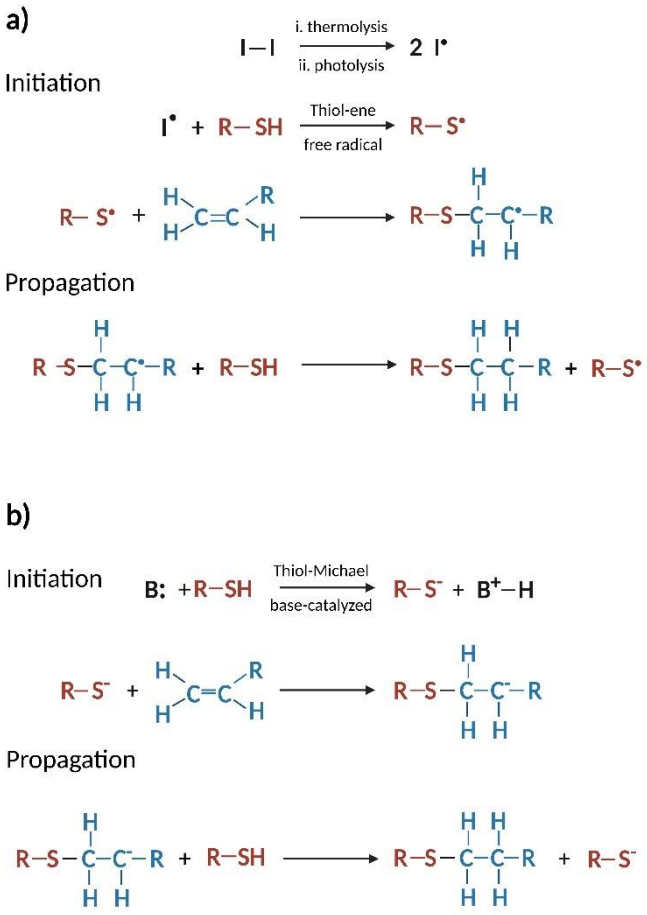

Figure 2.1.1. General mechanism of a thiol-ene reaction: In the initiation process, a thiyl radical/ion forms by a) the aid of a thermal or photoinitiator, - or b) nucleophile-mediated hydrogen abstraction. Propagation involves a two-step process, where the thiyl species adds to a C=C double bond, forming a carbon-center radical. The carbon-centered radical reacts with another thiol molecule to form the thiol-ene product and create a second thiyl radical/ion to complete the cycle.

The reactivity of the thiol-ene reaction can vary depending on the electron-density and degree of substitution of the thiol and ene-containing components. The reaction order is controlled by the balance between the propagation steps. While thiols with less abstractable hydrogen atoms would show reduced chain-transfer to a carbon-centered radical, electron-poor enes tends to limit the addition of thiyl radicals. A wide library of ene-containing monomers has been evaluated and ranked in terms of their reactivity, ranging from highly reactive norbornene and vinyl, allyl ethers, methacrylate, acrylate, styrene, to the least reactive conjugated enes. The decrease in reactivity thiol-ene generally follows the electron density of the C=C double bonds, with exception of norbornene, highly reactive in favor of an entropic gain following the release of the constrain of the strained monomer, and poorly thiol-ene reactive conjugated enes, whose radicals are stabilized by conjugation. Steric effects are also important, with terminal double bonds reacting faster than internal and substituted ones. Thiol structures can also impact the kinetic of the reaction, for example the presence of groups that weakens the sulfur-hydrogen bond increase the reaction rate. Propionates and glycolates are significantly more reactive than simple alkyls due to the effect of the polarity of the carbonyl influencing the abstraction of the hydrogen atom by the neighboring thiol.[7]

Overall, the increasing popularity of the thiol-ene chemistry as a multi-functional synthetic tool in a number of fields stems from a series of factors, ranging from its click-like nature, its fast and clean kinetics, to the ubiquitous presence of thiols in proteins and peptides.[8,9] A century after its discovery, thiol-ene chemistry has evolved from the synthesis of discreet organic molecules to a synthetic platform that allows the construction of macromolecular polymer networks and complex tailored materials by the selection of building blocks containing thiol and ene-moieties.

2.1.2 Thiol-ene functionalization

Thiol-ene reactions, like many other click reactions are increasingly used in the functionalization of surfaces,[10–12] polymer,[13,14] or biomolecules.[15,16] The high yield associated with click-reactions such as thiol-ene make those reactions particularly interesting as functionalization tools due to their simplicity and quantitative yields, offering a straightforward relationship between chemical structure and the final properties of the systems. For example, photo-initiated thiol-ene reaction has been used to pattern of 3D hydrogels with proteins for cell recognition, [16–18] affording remarkable control over site-specific immobilization of virtually any desired protein under conditions that are adequate to preserve the integrity of biomolecules.

Bioconjugation strategies make extensive use of thiol-ene coupling to modify structures. In addition to the convenient presence of thiol-moieties in peptides sequences,[19] one important asset of click chemistries such as thiol-ene is the orthogonality towards other reactions. A group successfully demonstrated the feature by promoting the patterning of cysteine-modified proteins onto microarrays hydrogel in the presence of multiple functionalities without mutual interference. In Figure 2.1.2, microscopy images evidence the copresence of both cell-adhesive proteins and fluorescent dye, conjugated by thiol-ene and NHS-active ester chemistry.

Maleimide chemistry is a staple strategy in thiol-ene bioconjugation. The presence of distinct functions in maleic anhydride units allows the functionalization from one side to amine-containing groups, without interfering with the C=C double bond on the other extremity that is left available for further thiol-ene attachment. In that way, the thiol-maleimide link serves as an universal chemical anchor between biomolecules, since it can react in an orthogonal manner with -NH_2 and -SH, two functionalities ubiquitous in biological environments.[20–22] In addition to maleimide spacers, bioconjugation via thiol-ene is often achieved through glycopolymers[15] derivatized with ene-moieties, peptides, and thiolated-polyethylene glycol (PEG-SH).[23–25] This latter is of particularly interest for biomedical applications.

The covalent binding of PEG moieties to drug, surfaces, or nanoparticles, is a standard technique in the control of the interactions between proteins and biomaterials. More specifically, the attachment of such chemical structures has the power to tune the adsorption of proteins present in the blood stream once the system is introduced *in vivo*. In addition, it reduces non-specific cellular uptake, thus leading to longer blood half-lives than unmodified drug and carriers. This phenomenon is also known as “stealth-effect”.[25,26] As a click-like reaction, the thiol-ene coupling is often selected to promote the attachment of PEG moieties to different materials, given the fast rates and quantitative yields of its conjugation reaction.

Other examples of thiol-ene functionalization techniques range from bio-patterning of hydrogels,[27] biofunctionalization of drugs and nanocarriers with molecules for cell-line targeting, such as RGD sequences,[28] lecithin[29], or carbohydrates like galactose[30] and mannose[31], to microarrays with site-specific protein-immobilization.[16]

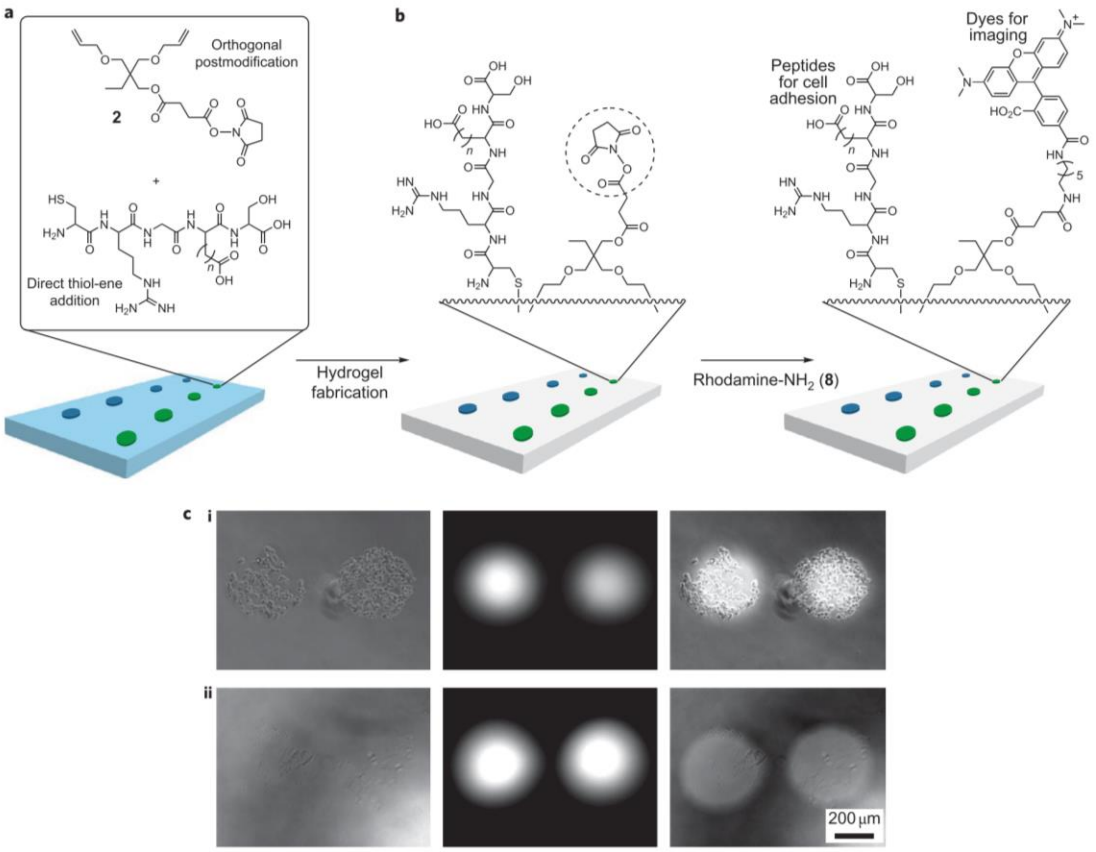

Figure 2.1.2. Combination of direct printing of peptides with orthogonal post-functionalization on individual microarray spots. a) microarray fabrication: Thiol-functional peptides (CRGDS and CRGES) and the heterobifunctional NHS cross-linker 2 were printed from a single solution and b) transferred to the hydrogel as a microarray. The activated esters were coupled with an amino-rhodamine dye (8), and these arrays were seeded with fibroblast cells. c) Microscopy images shown are of the printed cell adhesive CRGDS (i) and non-adhesive control CRGES (ii), in combination with the dye. Bright field images (left column), fluorescence images (center column) and overlay of brightfield and fluorescence images (right column). Cell grow and fluorescence are in the same area. Reprinted by permission from Springer Nature: Nature Chemistry, a versatile approach to high-throughput microarrays using thiol-ene chemistry, Gupta, N., Lin, B., Campos, L. et al. Copyright 2009. [27]

Another interesting application of the thiol-ene conjugation strategy is in the modification of surfaces. The presence of terminal thiol or ene on substrates enables to uniformly modify or selectively pattern the surface with molecules containing the counterpart moiety.[32] The possibility of a photo-mediated process makes thiol-ene coupling even more attractive for these applications, as the selectivity and grafting density in films can be tune by parameters such as power output and irradiation intervals.[10] Figure 2.1.3 shows an application of the thiol-ene photoreaction to create patterned surfaces promoting site-specific immobilization of proteins with spatio-temporal resolution. The versatility of thiol-ene functionalization is also illustrated by the functionalization of microspheres of poly(divinylbenzene) by thiol-modified poly(n-isopropylacrylamide), imparting hydrophilicity to hydrophobic particles and improving their compatibility in aqueous environment.[33]

Another case of tailored properties is the thiol-ene conjugation in polydimethylsiloxane biomedical devices, where anti-fouling polymers were readily grafted to their surface using thiol-ene chemistry, resulting in a substantial reduction of bacterial colonization.[11]

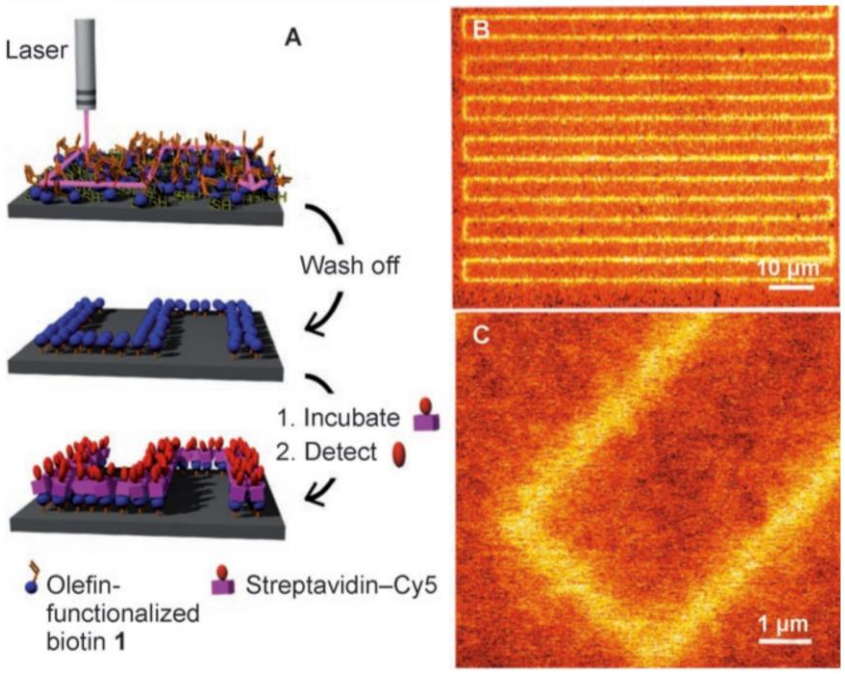

Figure 2.1.3. Photochemical nanopatterning. A) Olefin-functionalized biotin is deposited onto a thiol-modified surface. After laser-assisted (l=411 nm) nanopatterning in square-wave mode, the pattern is visualized by incubating the surface with streptavidin conjugated to a dye (SAv–Cy5). B, C) Scanning confocal fluorescence microscopy images of the nanopatterns (λ_{exc}= 630 nm). Reprinted with permission from *Angew. Chemie – Int. Ed.* 2008, 47, 23, 4421-4424. Copyright 2008 John Wiley and Sons. [18]

2.1.3 Thiol-ene polymerization

When a combination of multifunctional ene and thiol are used, the thiol-ene coupling lead to a thiol-ene polymerization. Thiol-ene polymerization is a type of step-growth polyaddition, where a polythioether network is formed by the stepwise addition of thiol groups to carbon-carbon double bonds. The evolution of the molecular weight of the oligomers and polymers formed is highly dependent of the conversion rates.

On the one hand, the delayed formation of high molecular weight species is advantageous from a manufacturing standpoint, maintaining the viscosity of the system and improving processability. Thiol-ene photopolymerization overcome crucial limitations of chain-growth mechanisms, including inhibition by oxygen and stress development, and the formation of highly heterogeneous polymer networks. But the step-growth mechanism is also the main pitfall of the thiol-ene polymerization. Since high conversions are challenging to be achieved, the reaction usually yields

low molecular weight products with limited thermo-mechanical properties, such as stiffness and low glass transition polymers.[34–36] Solutions to circumvent the issue include the use of hyperbranched and rigid monomer structures, blends with other materials, post-polymerization modifications such as oxidation of the sulfur-centers in the main chains,[37,38] or use of different reaction media that favor high conversions.[39–41]

The growth of chains and evolution of the average molecular weight in a step-growth mechanism are described by Carother's equation, where only at high degrees of conversion of the functions it is possible to achieve considerable values of molecular weights (Figure 2.1.4). In a system composed by A-A and B-B, where A and B are chemical functions of homofunctional monomers, the step-growth mechanism starts with the formation of (A-A)-(B-B) dimers. These dimers still bear free terminal moieties for further additions, and thus two dimers can add to each other forming (A-A-B-B)-(A-A-B-B). As it follows, oligomers react together through their unreacted terminal functions, slowly building up the network chains until the free functionalities are exhausted (Figure 2.1.4).

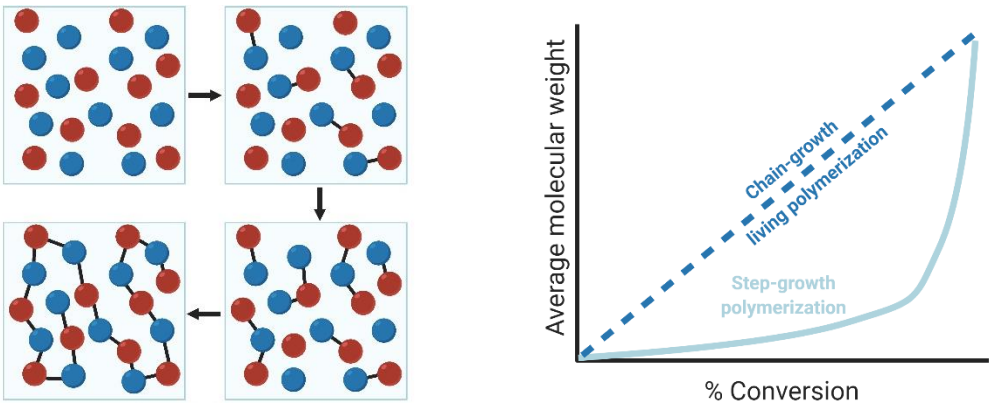

Figure 2.1.4. Scheme of a step-growth mechanism polymerization. Red and blue spheres represent the two functions present in the medium. The sequential formation of bonds illustrates the stepwise addition of functions and the build-up of the polymer network. To the right, a model graph compares the relationship between the increase of the average molecular weight of a polymer with the conversion of functionalities in both step-growth and chain-growth polymerizations.

The conversion of the end groups determines the progress of the step-growth polymerization. Each reaction step implies that the reactive end of a monomer or polymer encounters another species with which it can form a link. The functional group at the end of a monomer is usually assumed to have the same reactivity as that on a polymer chain of any size. Through the relationship shown in equation 2.1.1, the extent of conversion (p) is given by the ratio between the number of converted moieties (N_0 - N) to the number of moieties initially present in the system (N_0).

$$p = \frac{N_0 - N}{N_0} \qquad \text{(eq. 2.1.1)}$$

This equation is valid when the opposite functionality is present in equal concentration and there are no side reactions. The number-average of the degree of polymerization ($\bar{X}_n$) of the mixture is defined as the average number of monomeric units in a polymer molecule (equation 2.1.2). For an A-A-B-B polymerization, a repeating unit is made of two monomeric units. The theoretical average molecular weight $\bar{M}_n$ is then the number-average of repeating units $\bar{X}_n$ times the molecular weight of a repeating unit M_{rp} (equation 2.1.3). As the polymerization process yields polymer chains of different sizes, a more realistic depiction of the distribution of molecular weight around the average is given by the dispersity index ($Đ$). In a purely step-growth linear polymerization, $Đ$ can reach a maximum of 2 for p = 1 (100%) (equation 2.1.4). Impurities and side reactions can provoke deviations in this value. This value is also defined as the ration between the weight-average molecular weight ($\bar{M}_w$) and the number-average molecular weight ($\bar{M}_n$) of a polymer.

$$\bar{X}_n = \frac{1}{(1 - p)} \qquad \text{(eq. 2.1.2)}$$

$$\bar{M}_n = M_{rp} \times \bar{X}_n \qquad \text{(eq. 2.1.3)}$$

$$Đ = 1 + p \equiv \frac{\bar{M}_w}{\bar{M}_n} \qquad \text{(eq. 2.1.4)}$$

Here it is possible to observe how the average molecular weight evolves with the polymerization: at time t = 0, the process has not yet started and therefore p = 0 and $\bar{X}_n$ is equal to 1, illustrating the presence only of the initiating monomers. Halfway the polymerization process, where 50% of the A-A (or B-B) have been converted, $\bar{X}_n$ yields only 2 monomeric units in the main chain. When the reaction reaches 98%, 50 monomeric units can in average be found. This number is still moderate to build a high molecular weight polymer. Steep increases are only reached at nearly complete conversions, as illustrated by a model conversion of 99% that yields chains with 100 monomeric units per polymer chain (Figure 2.1.4).

In an ideal thiol-ene system, the only mechanism controlling the polymerization process is the step-growth mechanism. In the case where the only reaction occurring is the one where the thiyl radicals reacts with the C=C double bonds, forming carbon-centered radicals to produce a thioether linkage and produce a new radical, the polymerization will follow a classical step-growth kinetics. The resulting stepwise addition of reactive species with free terminal functionalities will form dimers, then small oligomers, and so on in a sequence of individual reactions until the full conversion of all free

functionalities. However, this cycle can be disrupted by the presence of monomers that also react through other processes (Figure 2.1.5).

The thiol-ene chemistry is highly dependent of the chemical structures of its components, and the polymerization process is also affected by the choice of monomers. Ene-containing monomers such as (meth)acrylates are well-known to undergo chain-growth homopolymerization (Figure 2.1.5), as their structures present electron-withdrawing ester groups that polarize their C=C double bonds and stabilizes radical intermediates, favoring free-radical mechanism in detriment step-growth additions. Therefore, thiol-ene polymerizations done with this class of monomers are difficult to control and the prediction of the properties of the final polymer is challenging, since the products will likely present a blend of chain- and step-growth characteristics.

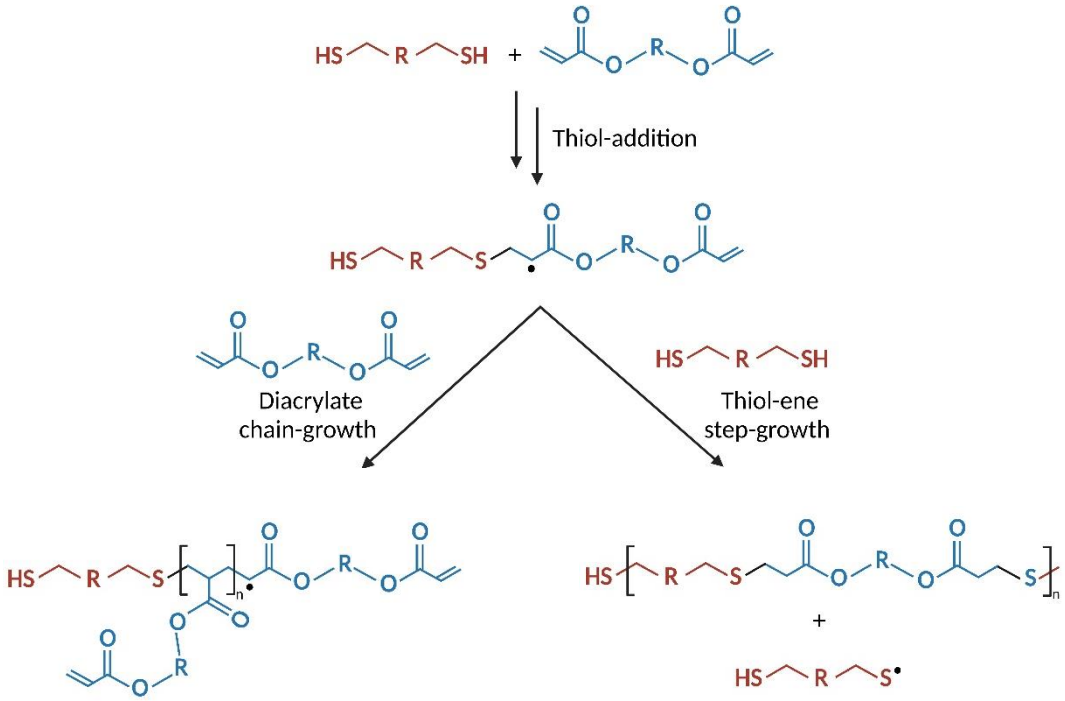

Figure 2.1.5. An ideal thiol-ene polymerization is controlled by a step-growth mechanism. Side chain-growth reactions can occur for homopolymerization-prone monomers such as (meth)acrylates.

2.1.4 Post-polymerization modifications

Polymers have been for a long time used as platform for the design of several functional materials. Post-modification is a common approach to tune the properties of polymer materials, with modification or conjugation happening after the polymerization reaction itself. Traditional post-polymerization modifications are often plagued by long reaction time to insure high functionalization yield and to complex purification procedures.[16,42] Thiol-ene polymers offers alternative strategies to tune their chemical functionality creating functional polymers, e.g. degradable, stimuli-responsive, self-healing, bio-compatible, high-performance polymers, etc., with highly tunable backbones and side chains.

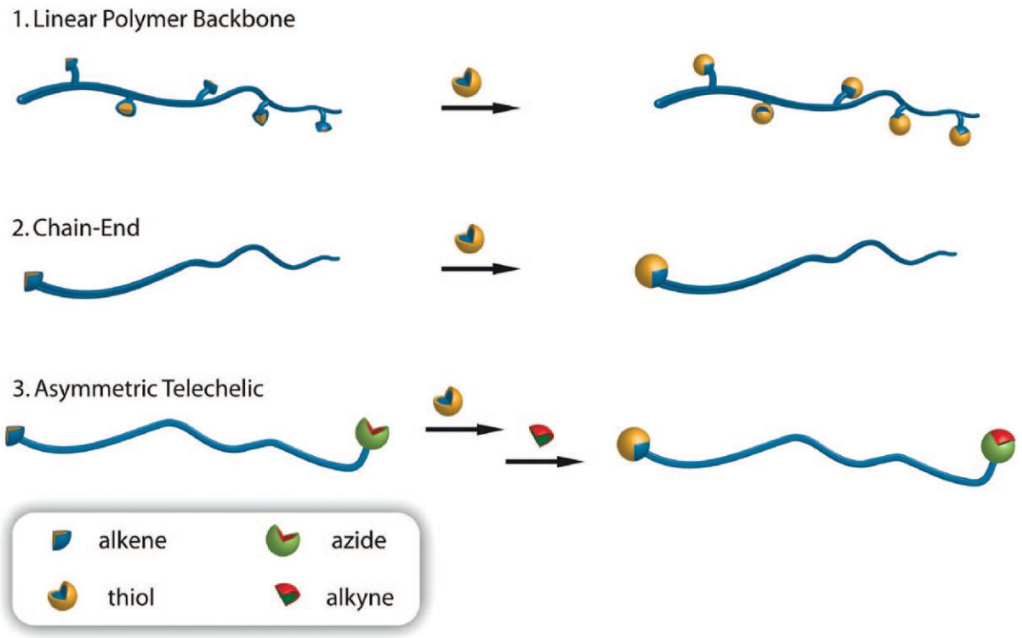

Figure 2.1.6. Schematic representation of polymer functionalization reactions examined using thiol-ene click chemistry. Reprinted with permission from Macromolecules 2008, 41, 19, 7063–7070.[14] Copyright 2008 American Chemical Society.

Modification of thiol-ene polymers by thiol-ene coupling

Polymer modifications can be made through the functionalization of end-groups in the main chain or side chains bearing thiol- or ene- moieties that can act as handles for other groups (Figure 2.1.6). A strategy that has been explored is the preparation of polymer networks with an excess of one of the reacting components, so to increase the density of the respective unreacted function, thus creating more opportunities for further post-modifications. Off-stoichiometry thiol-ene reactions provide means to prepare multi-purpose heterofunctional networks that can layer and attach target molecules via sequential thiol-ene reactions (Figure 2.1.7).[43,44] By tuning the stoichiometry during polymerization towards an excess of either thiol or ene moieties, this strategy creates a versatile and

straightforward way to control the end-groups of the polymer chains.[13,45] Then, thiol-ene functionalization reaction can be used with these remaining functionalities to react with other (macro)molecules bearing thiol- or ene-groups and build a complex conjugates with specific features.

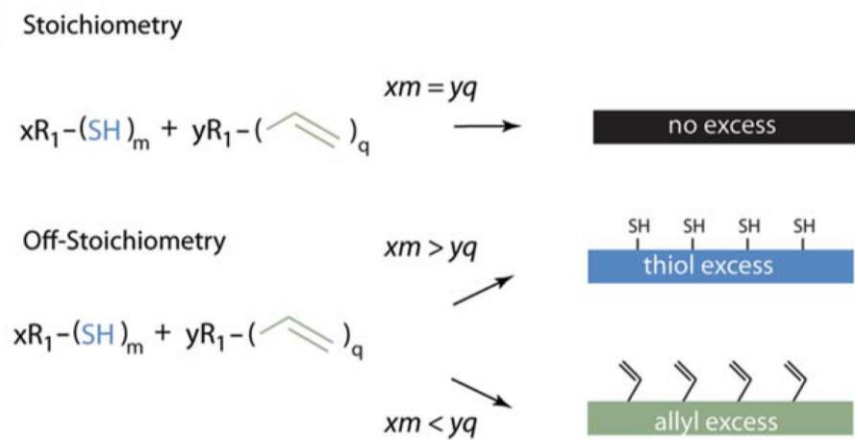

Figure 2.1.7. Standard stoichiometric formulations of thiol–ene systems lead to a complete polymerization and the absence of functional groups on the surface and in the bulk. Off-stoichiometry formulations of thiol–enes allow for a well-defined amount of unreacted thiol or allyl anchors on the surface and in the bulk. Republished with permission of Royal Society of Chemistry, from Beyond PDMS: off-stoichiometry thiol-ene(OSTE) based soft lithography for rapid prototyping of microfluidic devices, Carl Fredrik Carlborg et al., 11, 18, 2011; permission conveyed through Copyright Clearance Center, Inc. [44]

Modification of thiol-ene polymers by oxidation

The inherent versatility, facile implementation, quantitative conversions, and insensitivity to oxygen and moisture, makes the thiol-ene photopolymerization a valuable tool in polymer synthesis. On the one hand, the polythioethers prepared by thiol-ene exhibit thioether linkages with high flexibility and uniform network that are valuable for soft lithography and adhesive applications.[46] On the other hand, these properties prevents which prevents them from implementation in numerous applications that require more mechanically and thermally robust networks that are common, often offered by other polymers, such as (meth)acrylate-based materials. Furthermore, the lack of toughness of polythioethers is also limiting for otherwise suitable applications. For that reason, efforts have been devoted to improving the thermomechanical properties of thioether linkages, ranging from blending of polythioethers with epoxy or (meth)acrylate networks to the incorporation of vinyl sulfone to increase their glass transition temperatures, for example. [41,47]

Indeed, sulfone and polysulfone materials are well-known for their high-performance properties. To this day, polysulfones are by far the most widely used sulfur-containing polymer due to a unique combination of thermo-mechanical and chemical stability. These thermoplastics have been employed in a wide range of applications, from membranes for ultrafiltration,[48–50] toughness-modifier

resins,[51] to photoresist for immersion and templated lithography,[52,53] substrate for stretchable electronics,[54] solid polymer electrolytes materials,[37] and organic luminogens in OLEDs.[55] Among specific applications, the key strategy to synthetize high-performance materials seems to be the control over the chemical composition of the final sulfur-containing polymer, in special the oxidation state of the sulfur-centers of the polymer backbone.

The direct synthesis of polysulfones is, however, challenging because it involves stringent reaction conditions, such as limited library of sourced precursors, and solvent-rich formulations. [56,57] This has led to the development of alternative methods based on the oxidation of a parent polysulfide into their desired oxidized derivative, with the advantage of maintaining the structural network in every derivative.

Tuning the degree of oxidation of the sulfur atoms provide another way to control the properties of thiol-ene polymers through post-polymerization modification. The oxidation state of the sulfur-centers present in the polymer network have a strong influence on the thermomechanical behavior of the polymer.[58] The sulfur-centers of polythioethers (SII)) can not only oxidized to fully-oxidized state of polysulfones (S(VI)), but also to an intermediate polysulfoxide (S(IV)) (Figure 2.1.8). Due its challenging direct synthesis, polysulfoxides have been far less explored than polysulfones, and only a limited number of studies are reported on its use, mainly in biomedical field, as oxidation-sensitive degradable materials.[59,60]

The selective oxidation to each species can be controlled by the choice of the oxidant and thus, pure products with well-defined properties are harnessed. It has been demonstrated that both materials present distinctive properties with respect to the parent polysulfide, such as improved wettability for polysulfoxides and thermo-mechanical resistance for polysulfones.[47,61]

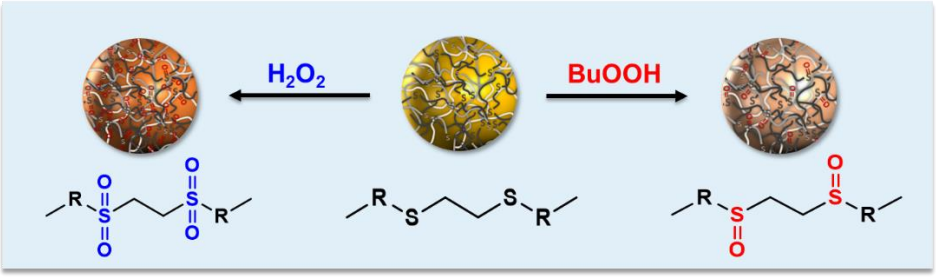

Figure 2.1.8. Selective oxidation of polythioethers (S(II)) with tert-butyl hydroperoxide to the partially oxidized polysulfoxides (S(IV)), and with hydrogen peroxide to the fully oxidized polysulfones (S(VI)).

The oxidation process can overcome common limitations of polysulfides such as limited stiffness and glass transition temperature without lost of the pristine structure.[38] In addition, oxidation increases the hydrophilicity of the polymer network, and polysulfoxides have been shown to reduce the protein-polymer interactions in comparison to the parent polysulfide polymer. Results indicate that polysulfoxide lead to increased in vivo circulation time, similar to the behavior of PEG or polyphosphoesters.[62,63] Furthermore, polysulfone polymers yield polymers with significantly different thermomechanical properties than their parent polysulfide. For example, the oxidation of rubbery sulfide-containing polymers led to the formation of hard and glassy sulfone materials with enhanced glass transition temperatures and toughness (Figure 2.1.9), suitable for applications in rapid prototyping and imprint lithography.[58]

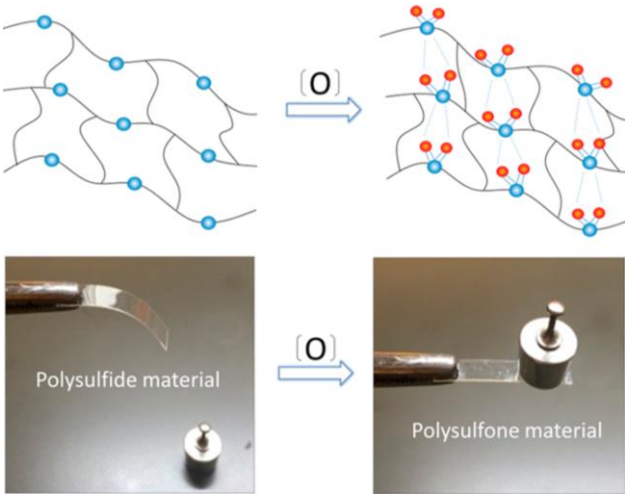

Figure 2.1.9. Schematic of a polysulfide oxidative modification, and illustration of changes observed in the mechanical properties of the material. Reprinted with permission from Chem. Mater. 2016, 28, 5102−5109. Copyright 2016 American Chemical Society.[58]

2.2 Polymer nanoparticles

2.2.1 Polymerization in dispersed media

Polymers can be prepared by a variety of techniques. Some of the more often employed are bulk or solution polymerization, where the monomer(s) and initiators (if any) are all in one phase. However, with the growing need for new nanomaterials and environmental concerns with the use or organic solvents, techniques based on polymerization in dispersed phase have gained popularity. Polymerization in dispersed phase, or heterophase polymerization, make use of the fact that one or more components are partially soluble or insoluble in the continuous phase, typically water-based, and this leads to the formation of colloidal suspensions of polymer nano- or micro- particles, often referred to as latexes. From a practical standpoint, it has considerable advantages over homophase reactions, such as constant viscosity of the mixture throughout the process even at high solid contents, facilitated reaction-heat dissipation, and improving processability and transport in industrial scale.[64,65]

According to the solubility of the main components in the continuous phase, the use of surfactant and costabilizer, the method of emulsification, and size of the droplets of the dispersed phase, these heterophase processes are categorized as precipitation, dispersion, emulsion, microemulsion and miniemulsion polymerization. Among those, emulsion polymerization has become a typical industrial process developed and marked initially for the preparation of synthetic rubber, and its popularity continued to grow to this day with the manufacturing of paints, coatings and resins.[66] However, this processing technique is typically restricted to free-radical reactions, and is not well-suited to other types of polymerization mechanisms. On the other hand, miniemulsion polymerization is a versatile strategy to prepare a wide range of polymer colloids with different chemistries in the confined geometry of the dispersed droplets.[67,68]

2.2.2 Miniemulsion polymerization

Miniemulsions are heterogeneous systems composed of hydrophobic droplets of sub-micrometer sizes dispersed in a waterborne continuous phase, or of hydrophilic droplets in an organic phase in the case of indirect miniemulsion. They are prepared by intense shear processes, such as ultrasonication or high-pressure homogenization. The main components of a miniemulsion polymerization are the monomers, an initiator system, co-stabilizer (also called ultrahydrophobe), surfactant and solvent for the continuous phase. Ideally, the monomers have low solubility in the continuous phase and are constrained to the droplets (Figure 2.2.1). Therefore, assuming that no

effective mass transport occurs between the phases, each one of these droplets act as small reaction locus for the polymerization and become nanoparticles by the end of the process.[69]

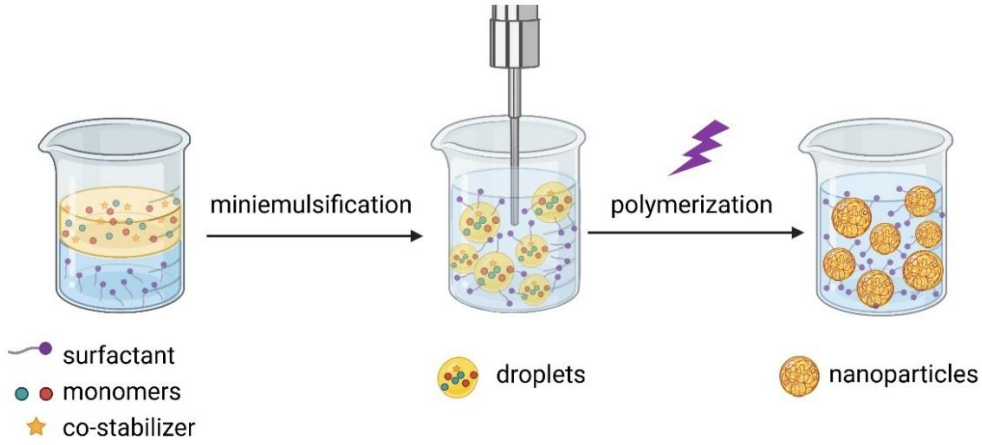

Figure 2.2.1. Principle of the miniemulsion process. Two immiscible phases are subjected to high shear emulsification. Droplets composed by the monomer mixture and co-stabilizer are formed and stabilized in the continuous phase by a surfactant. After polymerization, each droplet becomes a nanoparticle, stabilized by the same system.

Different strategies are put in place to ensure the colloidal stability of the miniemulsion, considering that the dispersion of hydrophobic droplets in a hydrophilic medium is not thermodynamically favorable. There are two major destabilization processes in miniemulsions, which are the growth of droplets due to coalescence and the Ostwald ripening mechanism. To reduce of the excess of interfacial area between the oil and water phases, droplets tend to coalesce, i.e., mutually fuse together through their Brownian motion, and particles tend to aggregate. To avoid that, amphiphilic molecules called surfactants are added to the continuous phase to reduce the interfacial energy.

Surfactant molecules stabilize the formed interface and prevent the fusion of the droplets by creating either electrostatic or steric repulsion between the droplets, or even a combination of both mechanisms. The concentration of these surface-active species directly affects the size of the droplets and thus the size of the final nanoparticles. Figure 2.2.2 exemplifies the influence of the concentration of surfactant on the colloidal stability of a miniemulsion of polystyrene nanoparticles. When the size of droplets or nanoparticles increase, their surface tension also experience an enhancement (Figure 2.2.2A). This is because the surface of the droplets becomes so large that the adsorption of equilibrium ensures a very low concentration of free surfactants. On the other hand, droplets with smaller diameter have higher surface coverage and a higher equilibrium concentration of free surfactant. In overall, the concentration of surfactant in miniemulsions is usually low enough to avoid the presence

of empty micelles in the medium but sufficient to decrease the interfacial tension between the dispersed and continuous phase (Figure 2.2.2 B).[70]

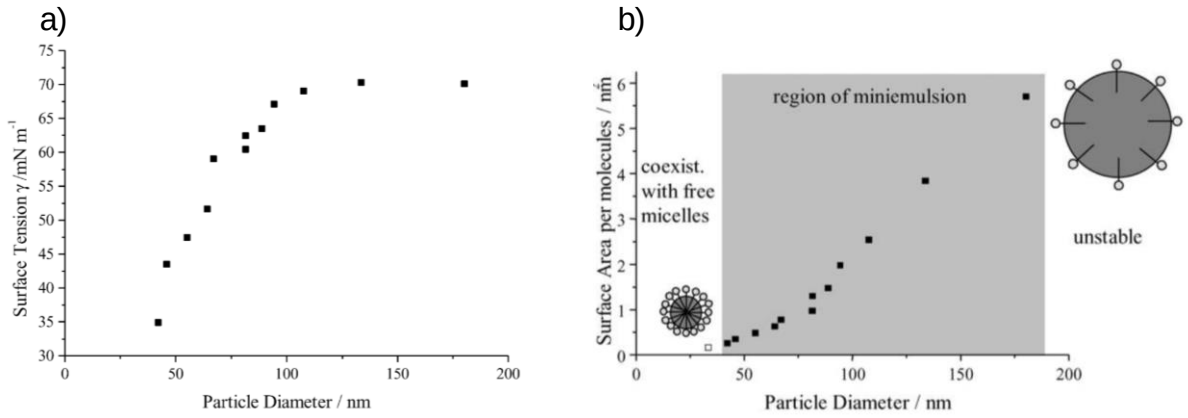

Figure 2.2.2. a) Surface tension of the latexes of polystyrene particles in dependence of size, and c) Relationship between the averaged stabilized oil-water surface area per surfactant molecule and surface tension versus the diameter of the particles. Adapted from Progress in Polymer Science, 27, Markus Antonietti and Katharina Landfester, Polyreactions in miniemulsions, 689-757. Copyright (2002), with permission from Elsevier.[70]

Another phenomenon disturbing the colloidal stability of emulsions in general is the so-called Ostwald ripening of the droplets, where the content of small droplets diffuse into larger droplets to decrease their high surface energy.[71] When droplets have a radius larger than its critical value (r_{cr}), diffusion may occur, with the formation of larger droplets favored to minimize the interfacial energy in the system (γ) (equation 2.2.1). The migration of material from a small droplet to a larger one is mathematically explained by the curvature dependence of the chemical potential (equation 2.2.2). Here μ_0 is the chemical potential of atom/molecule on a flat interface, and κ is the mean interfacial curvature. [72,73]

$$r_{cr} = 2\gamma V_m RT \ln S \qquad \text{(eq. 2.2.1)}$$

$$\mu = \mu_0 + V_m \gamma \kappa \qquad \text{(eq. 2.2.2)}$$

where (S) is the supersaturation of the monomers in solution, (T) is the temperature, (V_m), the volume of the monomer, and the gas constant (R).

In other words, in emulsions with a broad droplet size distribution, the Ostwald ripening induces the growth of larger droplets with lower Laplace pressure in detriment of smaller ones with higher Laplace pressure via the diffusion of encapsulated material from smaller droplets to larger ones. Therefore, If the small droplets in the miniemulsion are not stabilized against this process, they will disappear, and the emulsion will separate in the two immiscible phases. To prevent this, an

osmotic pressure agent of molecular weight *M*, or co-stabilizer, is normally added to the dispersed phase at concentration *c* to partially counteract the effects of the Laplace pressure ($P_{Laplace}$) imposed by the continuous phase, by building up the osmotic pressure (Π_{osm}) within the droplets (equation 2.2.3).

$$\Pi_{osm} = \frac{RTc}{M} \qquad \text{(eq. 2.2.3)}$$

The ideal osmotic pressure agent should be evenly distributed in the dispersed phase and exhibit significantly lower solubility in the continuous phase than the other molecules present in the disperse phase. Consequently, the co-stabilizer has reduced diffusion between droplets or do so much more slowly that the other components of the dispersed phase, it stays virtually entrapped in the droplet. Under these conditions, diffusion of the monomer out of the smaller droplets results in an increase of the concentration of the co-stabilizer molecules in the droplets. The increase in free energy associated with the concentration of the co-stabilizer balances the decrease from the reduced interfacial area afforded by the Ostwald ripening, and, at some point, ripening stops, and the system reaches a steady state (Figure 2.2.3). For direct miniemulsions, often hexadecane or silanes are typical co-stabilizers in direct miniemulsions, whereas salts can be used in inverse miniemulsions.[69,70]

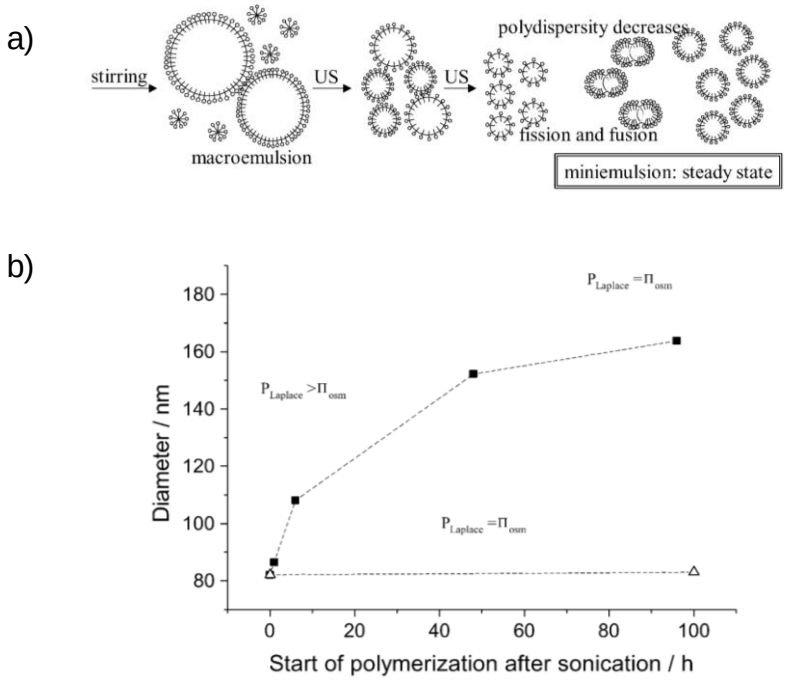

Figure 2.2.3. a) Scheme for the formation of miniemulsion by ultrasonication and b) growth of miniemulsion droplets after steady state ultrasonication with and without osmotic pressure agent. Adapted from Progress in Polymer Science, 27, Markus Antonietti and Katharina Landfester, Polyreactions in miniemulsions, 689-757. Copyright (2002), with permission from Elsevier.[70]

Mechanistic and kinetics considerations of miniemulsion polymerization

An interesting characteristic of miniemulsion polymerization is that the dominant pathway to form nanoparticles is through droplet nucleation. Other mechanisms, such as micellar and homogeneous nucleation, are normally considered absent in miniemulsion polymerization, since the concentration of surfactant in miniemulsions is set below the critical micelle concentration and the miscibility of the selected monomers is low enough to avoid their presence in the continuous phase, respectively.[67]

Ideally, when no colloidal destabilization processes take place and droplet nucleation is the dominant mechanism of nanoparticle formation, each droplet formed by miniemulsion act as an individual nanoreactor. In radical polymerization in miniemulsions for example, the radical entry in each droplet leads to the conversion to a nanoparticle, generating the same number of particles as there were of droplets. Therefore, the overall reaction rate and particle size are independent from the concentration of initiator, and a "zero-one" statistics control the radical entry. This means that at certain point in time, either one or no radicals will enter a given droplet, yielding an average of half-radical per droplet. Otherwise, the concomitant presence of two or more radicals in a small, confined geometry would lead to rapid bimolecular quenching. This effect is also known as segregation effect and is derived from the nanoconfinement promoted by the small sizes of the droplets.[74,75]

The high stability of the nanodroplets and the nearly "one-to-one" copy to particles it affords through a predominant droplet nucleation, places miniemulsion polymerization as a unique technique in preparing a wide range of materials. Some examples are production of high solid content latexes,[76,77] encapsulation of inorganic solids,[68,78] and biomolecules,[79] production of hybrid polymer particles,[80] step-growth polymerization,[81,82] and so on.

To circumvent some challenges of traditional polymerization in miniemulsion, such as high-temperature processes and use of harsh reaction conditions,[1,83] some efforts have been devoted to innovate in using alternative mechanisms that are compatible with lower temperature while potentially being more eco-friendly and energy-effective processes. An option that has been investigated for the past two decades is based on photopolymerization.[84,85] A well-designed photoinitiated polymerization in miniemulsion can provide a number of benefits compared to traditional heat-activated systems, namely higher reaction rates because of the rapid and energy efficient initiation, minor risk of colloidal destabilization as the reaction is carried out at room temperature, the use of milder reaction conditions compatible with sensitive cargoes like proteins and

oligonucleotides, a spatial and temporal control of the polymerization, and additional possibility to implement continuous reactors.[84]

Photopolymerization in dispersed phase can potentially be challenging due to the scattering of light by the droplets in the continuous phase. However, in contrast to macroemulsion, the colloidal sizes in miniemulsion are small enough to reduce light scattering and to allow a larger volume to be irradiated by a light source (Figure 2.2.4).[86] Nonetheless, it is necessary to optimize the conditions of irradiation to achieve comparable results to the ones obtained by thermal initiation.

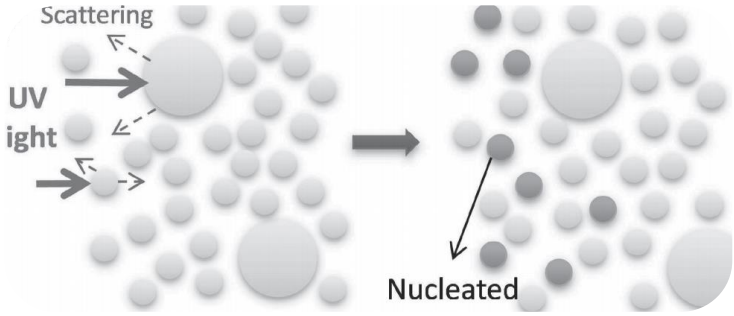

Figure 2.2.4. Schematic representation of the nucleation mechanism of small monomer miniemulsions with an average droplet diameter of 40 nm. To illustrate the polydispersity of this system, the initial distribution is chosen bimodal with most small droplets and a minority of large droplets (120 nm). Larger droplets exhibit light scattering and hinders light penetration, whereas smaller droplets avoid scattering and can be polymerized by light-mediated processes. Reprinted with permission from *Macromol. Chem. Phys*. 2014, 215, 1201−1211. Copyright 2014 John Wiley and Sons.[86]

One important challenge of photopolymerization in miniemulsion is the adjustment of the optical properties of the photoreactor to match the chemical features of the colloidal system. The developments in the technique are still in their infancy but important milestones have already been reached.[85–89] Recent studies used a modular photoreactor and varying reaction conditions (i.e., radiant power, droplet size, solids content, type and concentration of photoinitiators) to evaluate the light penetration in the system (Figure 2.2.5).[88,89] The results indicated that the absorption of light in the droplets were similar to that in solutions, regardless the solids content, as well as demonstrated the possibility of tuning conversion by changing the irradiation parameters.

These findings open the way for more energy-effective and eco-friendly processes. In addition, it can provide a higher spatio-temporal resolution by tuning the irradiation parameters, as well as enable the use of sensitive components, such as biomolecules that would otherwise be degraded during the polymerization reaction at high temperature. Step-growth polymerization such as thiol-ene[39,82,90] have also been demonstrated to adapt well to the technology, profiting from the spatio-temporal control provided.

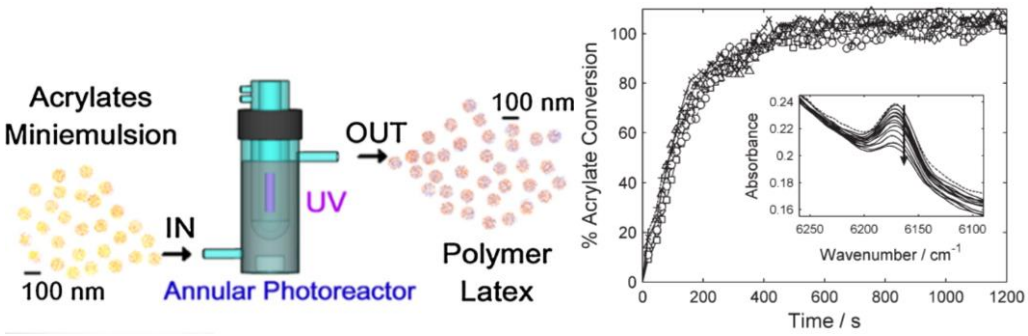

Figure 2.2.5. Scheme of the polymerization of acrylates miniemulsion by an annular photoreactor. To the left, the acrylates conversion kinetics and inset showing the decrease of the fingerprint absorption peak. Full conversions are achieved in less than 2 min of irradiation. Reprinted with the permission from *Macromolecules* 2011, 44, 22, 8727–8738. Copyright 2011 American Chemical Society.[89]

2.2.3 Nanocapsules

Another interesting feature of the polymerization in miniemulsion is the possibility for the encapsulation of different materials, ranging from liquid to solid, from organic to inorganic, and from molecularly dissolved to aggregated species into polymer nanoparticles or nanocapsules.[78] Because of the nucleation mechanism in miniemulsion polymerization, molecules can be encapsulated by simply adding the components with adequate partition coefficients to the pre-polymerization mixture forming the dispersed phase. As diffusion is suppressed in miniemulsion, the concentration of the cargo stays constant and within the boundaries of the nanoreactor throughout the polymerization. Other techniques of polymer processing are often not as effective in doing so since their reactions conditions can be harsh to the cargo and diffusional degradation might takes place.

Several mechanisms based on miniemulsion techniques can be used to create nanocapsules, i.e., a morphology of a shell with hollow cavity: Phase separation within droplets during polymerization, or interfacial reactions on droplets to encapsulate organic liquids or aqueous solutions. Nanoprecipitation is also an option to prepare nanocapsules with pre-formed polymers. In the case of the phase separation, it is important to tune the interfacial tensions of the components between the interfaces formed throughout the polymerization processes to create a polymeric shell, given that the monomers should be soluble in the dispersed droplets but not the polymer formed.[78,79]

Nanocapsules prepared by interfacial reactions require monomers with unpaired miscibility or interfacially active initiators, pushing the reaction locus to take place at the liquid-liquid interface between the continuous and dispersed phase (Figure 2.2.6).[91] For example, the polyaddition reaction between isocyanates and biopolymers in inverse miniemulsion (i.e. water-in-oil) is a typical case of such mechanism of nanocapsule formation, especially for biomedical use. In this case, the hydrophilic

biomolecule, i.e., starch, is in the aqueous dispersed droplets, and the hydrophobic isocyanate is added to the continuous phase after emulsification. The highly reactive isocyanate leads to a fast nucleophilic addition at the interface between the droplets and the continuous phase, forming rather selectively the capsule wall by the precipitation of the polymer formed at the interface. It is important to mention that the encapsulated liquids must be a non-solvent for the generated polymer. If the reaction locus is shifted towards the core of the droplets because of particular reaction conditions, i.e., higher miscibility between the monomers, slow reaction rates, bulky nanoparticles will be formed instead of hollow structures.[78] This platform allows the generation of smart nanocarriers for various application, especially for the biomedical field where active or sensitive molecules, [92] as enzymes, vitamins, DNA, or proteins, can be encapsulate in polymer nanocapsules to be carried and protected.

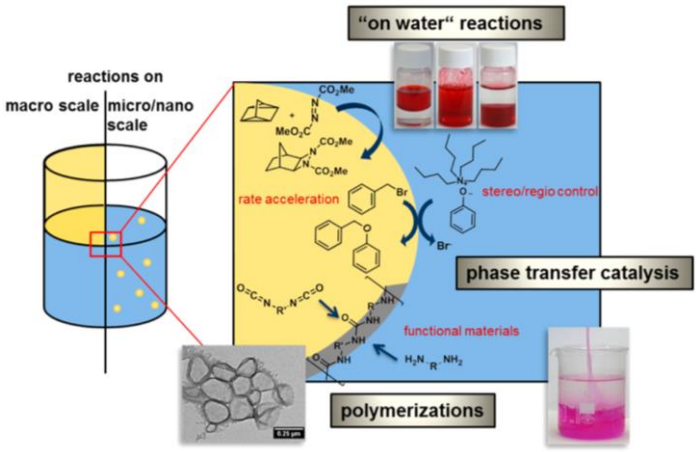

Figure 2.2.6. Schematic representation of reactions at the liquid–liquid interface. Reprinted with the permission from *Chem. Rev.* 2016, 116, 4, 2141–2169. Copyright 2016 American Chemical Society.[91]

Nanocapsules can exhibit different properties as shell thickness and core size according to the conditions of the interfacial reaction, namely concentration of monomers, partition coefficients, and amount of surfactant and initiator system. Interfacial polymerization of amine and isocyanate have shown to produce nanocapsules with varying shell-thickness by tuning the concentration of monomers (Figure 2.2.7).[93] In other applications, for example in drug-delivery applications, parameters such as encapsulation and release capacities need to be well-defined. The nanocarriers should be stable enough to protect and transport the cargo to a specific target and be sufficiently labile to certain external changes in the environment to release it. Therefore, shell-thickness, permeability, swelling capacity as well as compatible shell-degradation mechanisms are important in the development of these materials. Smart nanocarriers for biomedical applications have been prepared and displayed high encapsulation and release efficacy often occurring through variations in pH (Figure 2.2.8) and redox environment,[94–96] two common mechanism in biological media.

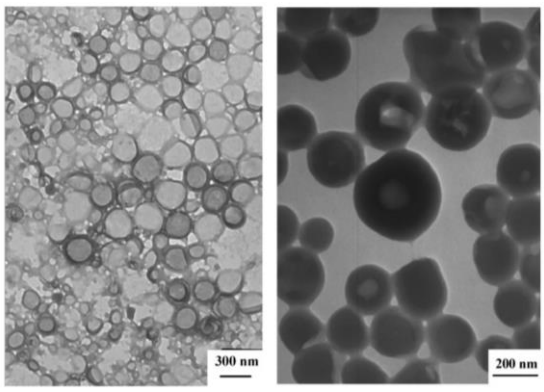

Figure 2.2.7. TEM micrographs of polyurea nanocapsules prepared with different amounts of monomers: a) 0.1 g of diethylenetriamine and 0.26 g of tolylene 2,4-diisocyanate, and b) double the amount: 0.2 g and 0.5 g, respectively. The wall thickness in (b) is much larger and the nanocapsules still keep a spherical shape independently on the number of monomers employed. Reprinted with the permission from *Macromolecules* 2007, 40, 9, 3122-3135. Copyright 2007 American Chemical Society.[93]

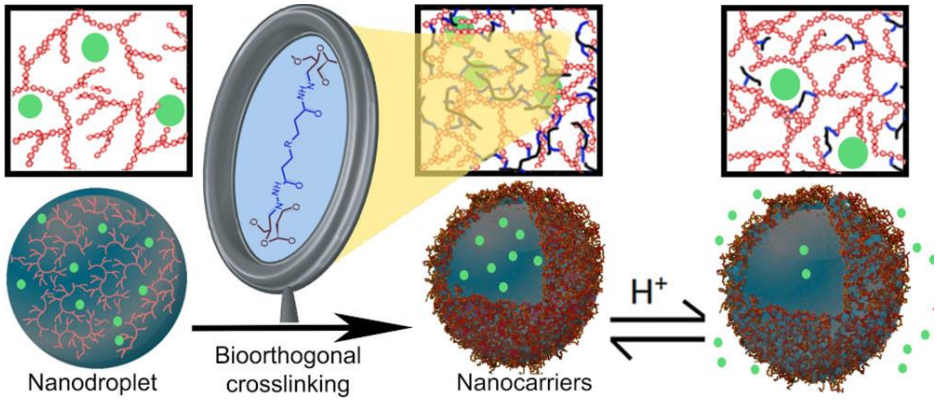

Figure 2.2.8. Schematic of the preparation of pH-responsive nanocarriers using dynamic bio-orthogonal chemistry. The reaction between a poly(hydrazide) crosslinker and functionalized polysaccharides was used to form a pH-responsive hydrazone network. Reprinted with the permission from *Biomacromolecules* 2020, 21, 7, 2764-2771. Copyright 2020 American Chemical Society. [94]

The combination of the thiol-ene step-growth photopolymerization with the miniemulsion technique figures as a promising toolbox in the design of highly tunable nanosystems. On the one hand, the latter could be used to form nanoparticles and nanocapsules with well-defined physicochemical properties by controlling the size, distribution, and composition of the initial droplets. On the other hand, the thiol-ene photopolymerization could, within such well-defined droplets, selectively and quantitatively produce modifiable polymer particles either through oxidation of the sulfur-centers in the polymer chains, or by surface modification through thiol-ene click reaction to optimize the properties of the system for a wide array of specific applications, from non-leaching materials, nanocarriers for biomedical use, high barrier packaging film, and chromatography columns.

2.3 Reactions in nanoconfinement

At the molecular level, confinement occurs when molecules are placed in a sub-micron sized environment excluded from the bulk, geometrically constrained by a physical boundary. This confinement can affect the physicochemical behavior of molecules and reactions. Over the past decades, chemists have investigated the effects of confinement on the dynamics, structure, and kinetics of a variety of molecules and reactions and shown, for example, improved polymerization rates in dispersions,[74,97] thermodynamic changes in the conformation of confined proteins,[98–101] as well as of the manufacturing of materials with high-performance properties[102–104] that would otherwise be rather challenging to achieve in the absence of confinement or interfacial interactions. The reasons for that revolve around a number of phenomena arising both from the restricted spatial disposition that could favor effective collisions between reacting species and from the presence of an interface between the core and the continuous phase, creating a complex structure that communicates with different chemical environments.[91,105]

2.3.1 Reaction in confined systems

Reactions occurring in confined systems or at their interfaces hold great synthetic potential and have been explored in different fields. The interest in interfacial reactions goes back to the seminal work of Schotten and Baumann a century ago.[106,107] Immiscible reaction partners can react at liquid-liquid interfaces and profit from optimal environments for each reactant (Figure 2.3.1), with no detrimental effects on the reaction.[108,109] In addition, when this interface is located between a nanoconfined volume and a continuous phase, it can behave similarly to membranes in cells and organelles,[110,111] controlling the entry and exit of species to/from the confined space, regulating the chemical compositions and crowding density in the compartment. On the one hand, the presence of interfaces allows organic reactions, typically performed in bulk or solvents, to be transferred to a mostly aqueous environment. On the other hand, it also protects sensitive species and products from degradation driven by the chemical incompatibility of media, such as in the case of hydrolysis of certain polymers formed in confinement. Therefore, interfaces create complex nanoreactors, where the thermodynamics and kinetics of molecular interactions are altered with respect to the exterior environment.

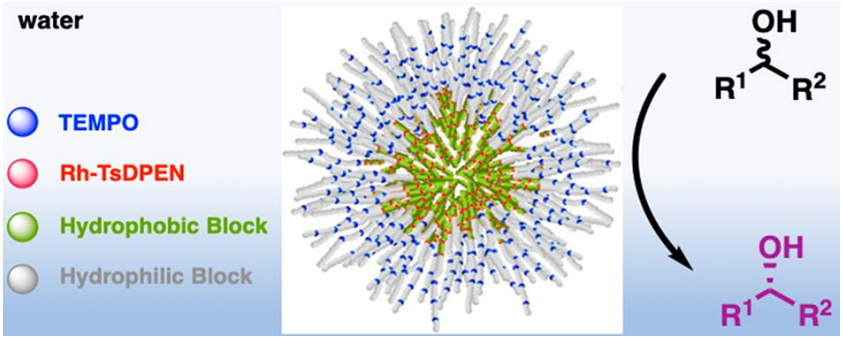

Figure 2.3.1. Schematic representation of a compartmentalized nanoreactor for one-pot redox-driven deracemization of racemic secondary alcohols. The polymer nanoreactor with a hydrophobic core and a hydrophilic corona allows catalysts of contrasting miscibility to co-exist. Here, the organocatalyst TEMPO is used to oxidize racemic mixtures of secondary alcohols into ketone intermediates, followed by asymmetric transfer hydrogenation (ATH) by rhodium N-tosylated 1,2-diphenyl-1,2-ethylenediamine (Rh-TsDPEN), to afford enantioenriched secondary alcohols. Reprinted with the permission from *ACS Catal.* 2019, 9, 4, 2701-2706. Copyright 2019 American Chemical Society.[108]

Until now, a number of natural and synthetic nanoreactors have been used as loci for chemical reactions, such as nanoparticles, nanoholes, nanocapsules, porous templates, micelles, microfluidics, vesicles, as well as protein cages, miniemulsions, and hierarchical nanostructures.[105] The rational design of these structures with a large surface-to-volume ratio creates a synthetic route that can tailor the outcome and the properties of a number of materials. For example, performing reactions in and on nanoreactors is at the core of developments in nanomedicine; the interfaces of nanocarriers can be designed to have different thicknesses, functionalities, and porosity, as well as be used to protect sensitive biomolecules, for optimal drug-delivery at a given target.

Although the main reason for the effect of nanoconfinement and the differences between the chemical environment in bulk and in nanoreactors might differ between specific cases, the effect of confinement and the impact of interfacial reactions can be considered universal and have the potential to dramatically modify the kinetics and dynamics of a range of reactions.[112] Other applications have also highlighted their potential in the understanding of complex processes, such as in the study of single-molecule dynamics,[113] or the study of tandem reactions that would otherwise mutually quench each other in homogeneous environments. [114,115]

2.3.2 Consequences of the nanoconfinement effect

The reduction of the scale of reaction loci has proved to influence the behavior and outcome of reactions. These alterations observed in contrast to bulk or solution media are usually due to a combination of factors that arise from the confinement. Some of these effects are related to conformational constraints,[116,117] proximity effects, partitioning of intermediates,[118] high local concentration and collisional frequency,[104] and protection against termination in free radical polymerization reactions, [119] for example.

In the presence of a physical boundary, different reaction scenarios can occur: 1) all the participants of the reaction are entrapped in the confined volume from the onset of the reaction; or 2) one of the chemicals is already encapsulated, and the other has to diffuse from one medium to the other, reaching the core of the nanoconfined environment or staying closer to the interface, according to its partition coefficient (Figure 2.3.2). The latter is a common strategy to control reactions that involves the use of initiators, where the partition of the reactants across the interface between the phases and the solubility of the initiator can dramatically change the fate of the polymerization. The locus of initiation is expected to have a great influence on the reaction products. For example, in miniemulsion copolymerization, oil-soluble photoinitiators were found to give a higher yield during the copolymerization of acrylamide and methyl methacrylate than water-soluble ones.[120,121] Therefore, by controlling the physicochemical properties of the interface, such as porosity or permeability, shell thickness, and chemical composition, one could tailor the molecular interactions between different media, by effectively gating the entry and exit of species from the nanoconfined environment.

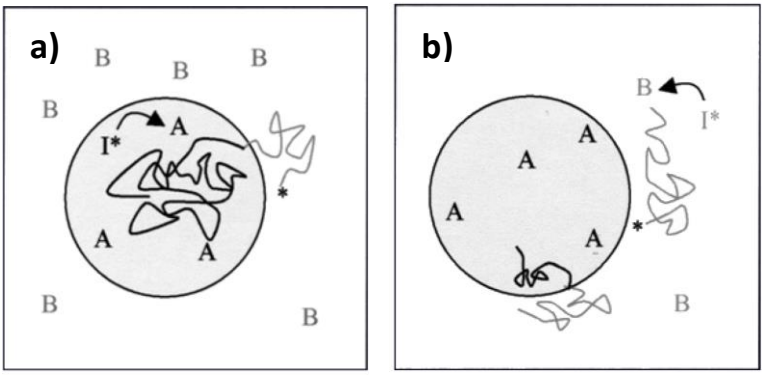

Figure 2.3.2. Copolymerization of 2 monomers A and B with different polarities in direct miniemulsion when the radicals generated by the initiator I* are: a) oil-soluble or b) water-soluble. Adapted with permission from *Macromol. Chem. Phys*. 2002, 203, 5-6, 825-836. Copyright 2002 John Wiley and Sons reference. [121]

This interfacial control of the distribution of different chemical species between the confined nanoreactor and the surrounding environment has been harnessed in different fields. For example, catalytic reactions performed in confined spaces can benefit from an enhancement of selectivity due to a molecular gate-control promoted by a well-tailored interface. The presence of interfaces is also at the core of the design of stimuli-responsive nanocarriers for drug delivery. In this case, the surface of the carrier does not only work as a passive gate that segregates and hinders the uncontrolled distribution of the cargo, but also can be finely tailored to promote the release of the drug only under specific environmental cues (Figure 2.3.3).[122]

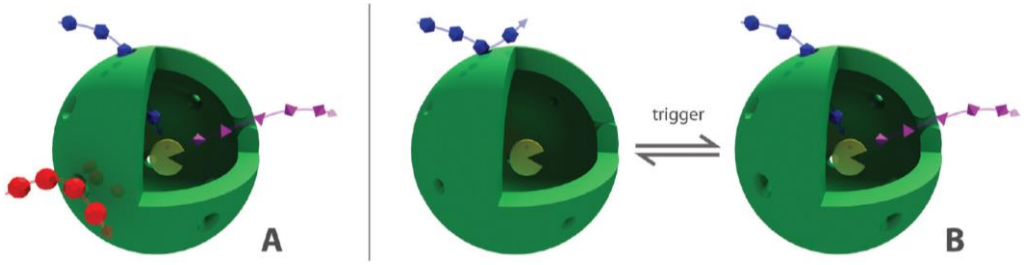

Figure 2.3.3. The concept of selective and responsive nanoreactors. A) Selective nanoreactors allow only specific molecules to enter the inner cavity while others are blocked from entering. Selection criteria can be size, charge, or hydrophobicity of the diffusing molecules, amongst others. B) Responsive or gated nanoreactors possess pores in the membrane that open or close upon a particular trigger, which can be a change in pH, the presence of certain reagents, or a change in the local environment of the pores. Reprinted with permission from *Adv. Funct. Mater.* 2011, 21, 7, 1241-1259. Copyright 2011 John Wiley and Sons.[122]

In addition to the dynamics at the interfaces, the segregated volume itself can act to control the interactions of molecules. Recently, many reports highlighted the effect of spatial confinement in the kinetics of reactions due to the particularly crowded environment the nanoreactor creates. Simulations of bimolecular polymerizations in nanoreactors have shown that competing effects might affect the reaction kinetics: higher density and slower diffusion. Although the former seems to increase the reaction rate, the latter reduces the reaction rate. Consequently, the net result could be either an increase or diminution of the reaction rates, depending on the interactions between the chains themselves and the chains with the interface.[123] In catalysis, the high local concentration and proximity among species offered by the geometrical constraint have reportedly yielded high conversions in shorter reaction times, with improved recyclability of costly materials.[113,124] Examples in synthetic bio-catalysis are also common, and present a more realistic scenario to study bio-interactions than methods based on protein immobilization, once proteins and enzymes can assume different conformations without the constraints of being anchored to a substrate.[125]

These nanometric spaces can also segregate species and promote diffusion from the confined space to the surrounding macroscopic medium. This unique feature offers means to separate toxic intermediates, immiscible products and favor the dynamics of reactions, shifting the equilibrium towards higher yields by removing products from the reaction loci or controlling the concentration of reactants. Radical polymerizations in dispersed media are a well-known example where the effect of confinement favorably enhances the kinetics of polymerization by segregating reactive species. Mathematical models showed that, under the right conditions, each droplet/nanoreactor could statistically contain only one radical or none at a given point in time. The consequence of this radical segregation is a significant decrease of bimolecular termination, enhancing the lifespan of a growing chain and thus leading to higher polymerization rates and molecular weight (Figure 2.3.4).[75]

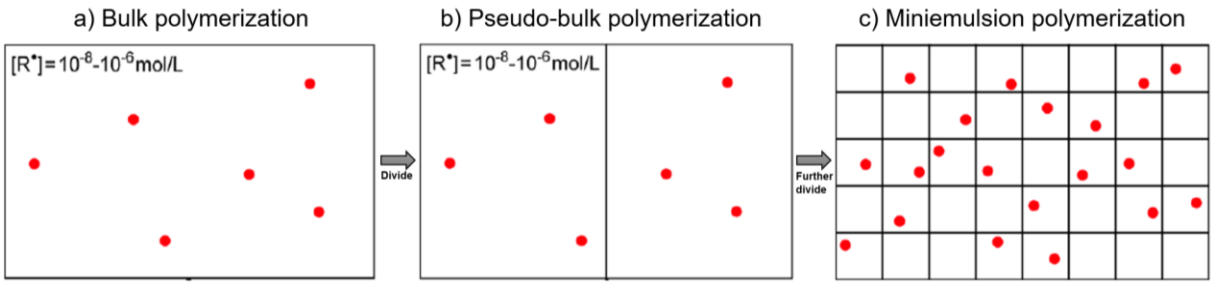

Figure 2.3.4. Schematic representation of the radical concentration in a) bulk, b) pseudo-bulk, and c) miniemulsion polymerization. Each square section in c) represents a droplet in miniemulsion polymerization. The radicals located in other

particles cannot terminate each other. The radical concentration in the reaction locus can become much larger than the corresponding bulk polymerization, leading to a much larger rate of polymerization. Adapted with permission from *Polymers,* 2016, 8, 4, 155. Open Access MDPI journals.[75]

2.3.3 Selected examples of the confinement effect in the synthesis of small molecules and polymers

Figure 2.3.5 illustrates the high local concentration effect and the cooperative interactions of catalyst molecules placed within a cavity. In this example, the researchers studied the catalytic conversion of epoxides. They compared the efficiency of the reaction performed in a nanoconfined system with the one carried in a homogeneous medium, and concluded that the use of nanoreactors leads to significantly higher activity and enantioselectivity in the conversion of epoxides due to the crowded microenvironment of the complexes evoked by the geometrical constraint, that enhances the cooperative activation of species.[126]

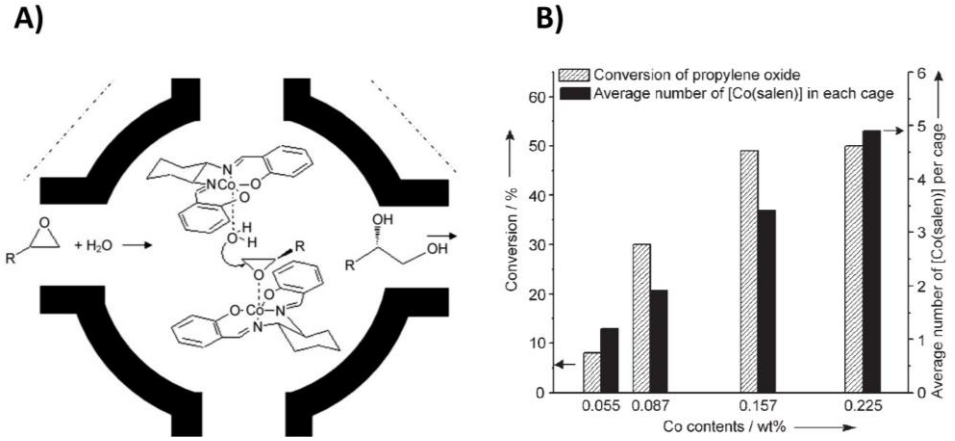

Figure 2.3.5. A) Schematic representation of the Co-complex catalyst trapped in the isolated nanocage of mesoporous materials, which results in enhanced cooperative activation between reactants on two Co-complex molecules for the hydrolytic kinetic resolution of epoxides. B) The conversion of propylene oxide on Co-catalyst/nanocage with different loadings of Co-complexes per cage. Reprinted with permission from *Angew. Chemie – Int. Ed.* 2007, 46, 36, 6861-6865. Copyright 2007 John Wiley and Sons.[126]

Examples like the one depicted in Figure 2.3.5 are also explored in micellar catalytic reactions. Generally, micellar structures create hydrophobic pockets within an aqueous environment, enabling organic reactions to be performed in milder conditions. Catalytic reactions carried out inside micelles not only favor the recyclability of costly catalysts but also notably enhance the catalytic efficiency of the whole

process compared to the equivalent reaction in an aqueous medium. The feature that makes micelles special micro- or nanoreactors is the proximity of extremely polar and nonpolar regions.

Brown et al.[127] described the effect of the micellar environment on the kinetics of reactions as resulting from a combination of mainly three factors: 1) the dielectric constant is lower in the micelles than in water, promoting a solvent effect; 2) stabilization of transition states by interactions with different portions of the micelle; and 3) a high local concentration of reacting species compared the continuous phase, either through interactions with the surface of the micelle or through insertion into the micelle itself, thus leading to an increased rate of bimolecular reactions. In most cases, the increased concentration of species promoted by the presence of spaces with different amphiphilicity within the micelle is the dominant effect determining the acceleration or inhibition of these reactions. [127,128]

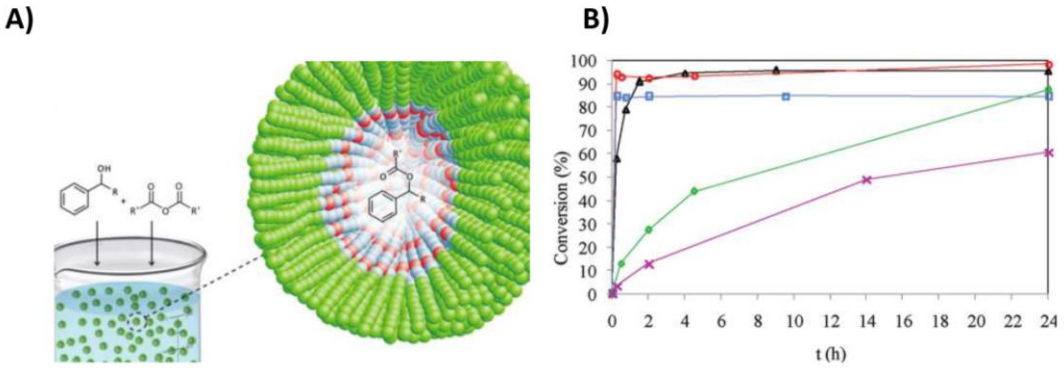

Figure 2.3.6. A) Schematic representation of an acylation reaction performed in amphiphilic micelles on water. B) Conversions vs reaction times for acylation reactions catalyzed by 4-(N-methyl-N-(2-hydroxyethyl)amino)pyridine (DMAP): in THF (◇), hexane (□), bulk (△), micelles on water (○), and polymer-supported DMAP (not self-assembled) in THF (×). Polarity effects and high concentrator effects in micelles are the driving forces altering the reaction rates. Reprinted with permission from *Macromolecules* 2012, 45, 5, 2377-2384. Copyright 2012 American Chemical Society.[114]

O'Reilly and coworkers demonstrated the impact of the micellar hydrophobic pockets on the acylation of 1-phenylpropanol with butyric anhydride, catalyzed by 4-(N-methyl-N-(2-hydroxyethyl)amino)pyridine (DMAP). In this study, the main reacting partners migrate to the core of the nanoreactor where the organocatalyst DMAP is tethered to the micellar structure, with their hydrophobicity as the main driving force for this diffusion step (Figure 2.3.6A). Compared to the reactions carried in water and polar solvents, the equivalent reaction performed in the micelles not only exhibited improved catalytic activity with acylation rates comparable to neat conditions but also enhanced conversions regarding all the tested media. These results seem to stem from the high local catalyst

concentration and the hydrophobic environment created within the nanoreactors, which prevented the protonation and deactivation of DMAP (Figure 2.3.6B).[114] Here, the researchers not only demonstrated an improvement of the catalytic activity but also interesting environmental and economic aspects of the compartmentalization technique. Moreover, this example highlights how nanoreactors can be altered and tuned to yield several different outcomes, from the interplay of the physicochemical properties of the system, such as amphiphilicity and chemical structure.

Polymerization reactions performed in dispersed media are another example of processes influenced by the effect of confinement. In free-radical chain-growth mechanisms, higher conversion rates and improved average molecular weight seem to be favored when the reaction loci move from bulk or solution media into nanoreactors. One of the main factors responsible for that is the so-called segregation effect that occurs between the continuous and confined phases. In this case, active species are generally separated from each other, which reduces the probability of bimolecular termination between them, thus promoting more conversions per active species (Figure 2.3.4).[75,97,129–131]

In contrast to free radical polymerization, there is still a scarcity of studies about the behavior of step-growth polymerization in nanoconfinement medium. However, it has been observed that the effect of confinement in step-growth reactions leads to enhanced rates of polyadditions performed in nanoreactors. This effect was ascribed to two main factors: a higher local concentration of reactants within the confined space than when the reaction is performed in solution, and an interface-mediated shift of the thermodynamic equilibrium occurring when the polymerization product precipitates at the interface (Figure 2.3.7A), leading to higher conversions (Figure 2.3.7B) and average molecular weights.[103]

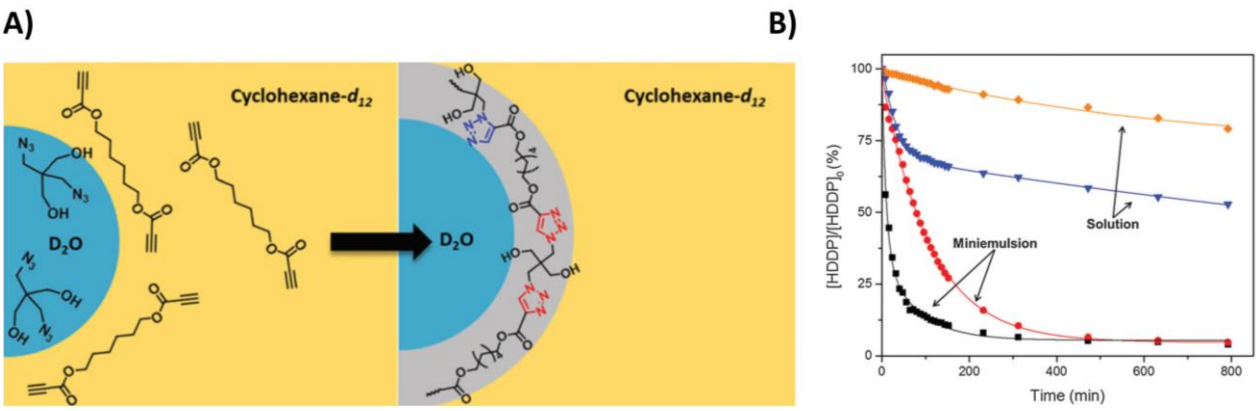

Figure 2.3.7. A) Polyaddition performed at the interface: the system used for evaluating the kinetics of polymerization between a water-soluble azide (2,2-bis-(azidomethyl)propan-1,3-diol, BAP) and an organic soluble alkyne (hexane-1,6-diyil dipropiolate, HDDP) in an inverse miniemulsion (cyclohexane-d_{12}/D_2O). B) Conversion of HDDP for the polyaddition with BAP in miniemulsion (water–cyclohexane) at 323 K (black square) and 298 K (red circles) and in solution (DMSO-d_6) at 323 K (blue inverted triangle) and 298 K (orange rhombus), as determined by ^{1}H-NMR. Reprinted with permission from *Chem. Commun.* 2014, 50, 72, 10495-10498. Copyright 2014 Royal Society of Chemistry.[103]

3 Experimental

Disclaimer: All self-made figures were created either with Microsoft PowerPoint software, PerkinElmer Informatics ChemDraw™ software, or BioRender.com. Graphical figures were created with Origin (Pro), Version 2021b, OriginLab Corporation, Northampton, MA, USA.

3.1 Materials

Diallyl adipate (DAA – 98%), 2,2'-(ethylenedioxy) diethanethiol (EDDT – 95%), triallyl 1,3,5-benzenetricarboxylate (TAP – 98%), (+)-limonene (LIM – 95%), hexadecane (98%), lithium phenyl(2,4,6-trimethylbenzoyl)phosphinate (TPO-Li – 98%), divinyl adipate (DVA – 99%), and tert-butyl hydroperoxide (t-BuOOH – 70% solution) were purchased from TCI Deutschland. Diallyl phthalate (DAP – 98%), divinyl benzene (DVB – 70%), sodium dodecyl sulfate (SDS – 99%), tetrahydrofuran (THF – 99.9%), dimethylformamide (DMF – 99%), chloroform-D ($CDCl_3$ – 99.8%), diphenyl(2,4,6-trimethylbenzoyl)phosphine oxide (TPO – 97%), acetone (99%), 4-methoxyphenol (MEHQ – 99%), and 1,4-butanediol diacrylate (1,4DAc – 87%) were acquired from Sigma-Aldrich. 2,2,2-trifluoroacetophenone (TFAP – 99%) from Acros Organics, and hydrogen peroxide solution (H_2O_2 – 30%) from Merck. Irgacure© 2959 was purchased from BASF. Thio-β-D-glucose tetraacetate (97%), bovine serum albumin (BSA), 5,5'-dithio-bis-(2-nitrobenzoic acid) (DTNB – 98%), dithiothreitol (DTT – 98%), fluorescein-isothiocyanate albumin (FITC-BSA) were acquired from Sigma-Aldrich. Pierce™ 660 nm protein assay reagent 22660 was purchased from Thermo Fisher Scientific. All chemicals were used as received unless noted otherwise. Divinyl benzene, divinyl adipate and 1,4-butanediol diacrylate were purified prior to use with a column of aluminum. Distilled water was used to prepare aqueous samples unless otherwise stated.

3.2 Instrumentation and characterization

The miniemulsions were prepared by the emulsification of biphasic mixtures with a Branson digital sonifier SFX550 cell disruptor, equipped with a standard ½ inch tip (70% amplitude, pulsed mode, 2 min). Section 3.3 details the protocol of sample preparation.

Polymer latexes were synthetized by irradiation of the miniemulsions in a Peschl Ultraviolet GmbH multi-purpose photoreactor platform equipped with four 385 nm LED modules at irradiance of 18 $mW \cdot cm^{-2}$ (Figure 3.4.1 and Figure 3.4.2). The samples of miniemulsion prepared by ultrasonication,

or bulk mixtures of monomers, were placed in the center of the reactor, on top of a magnetic stirrer, and irradiated for 4 h (Section 3.4). Polymerized latexes were generally cleaned-up by centrifugation in a Sigma 3-30k Spincontrol Comfort refrigerated centrifuge at varied conditions (Section 3.5).

Nuclear magnetic resonance spectroscopy, ^{13}C-NMR and ^{1}H-NMR, spectra were recorded in $CDCl_3$ or d_6-DMSO, unless noted otherwise, on a Bruker Avance 300 MHz spectrometer. The general protocol of sample preparation consisted of ca. 20 – 50 mg of polymer dissolved in 600 µL of solvent. For latexes of NPs, the samples were centrifuged down (10,000 – 20,000 × *g*, 10 °C, 15 min) and their pellets were resuspended in deuterated water (ca. 0.05 mg·mL^{-1}). The evaluation of the spectra was made with the aid of the analytical chemistry software MestreNova 8, from MestreLab Research S.L.

Molecular absorption and fluorescence spectroscopy were measured in a Tecan Infinite® M1000 multimode flagship microplate reader. Samples and standards were prepared in aqueous solutions of different concentrations and transferred to wells of a 96-wells flat bottom transparent (for absorbance) or black (for fluorescence) polystyrol microplates. The settings and parameters of the measurements were made through the software Tecan i-control 1.10.4.0.

Fourier-transform infrared (FTIR) measurements were recorded with Perkin Elmer Spectrum BX spectrometer in ATR mode. Polymer samples were directly smeared on the ATR sample window. Miniemulsion samples were analyzed likewise after precipitation with solvents and drying up. The spectra were recorded in absorbance mode, from 400 to 4000 cm^{-1}.

Raman spectra were collected with an Ocean Insight QEPro spectrometer, equipped with a 785 nm laser source and a coupled fiber probe, which was placed at optimal working distance (7.0 mm) from the sample. OceanView software was used to control and evaluate the spectra in online and offline modes. The routine used for the data evaluation was composed by a series of baseline corrections, clean peaks algorithm, integration of the area of the peaks at selected wavenumber ranges. Raw Raman shift data, and the relative abundance of each peak (i.e., ratio between integrated areas of each peak to a reference one) were collected throughout the experiments, with time intervals between scans of 30 s to 1 min. Samples of aqueous latexes of NPs or bulk mixtures of monomers/polymers were analyzed as obtained, i.e., without any further preparation.

Scanning electron microscopy (SEM) was performed by a 1530 Gemini LEO (Zeiss) microscope. Parameters were set at an optimal electron high voltage of 0.121 kV, working distance of 2.0 mm, aperture size of 30.00 µm. For miniemulsions, 10 µL of sample were diluted in 2 mL of distilled water. Then, 10 – 20 µL of this dilution were drop-casted on a silica wafer and allowed to dry at room

temperature. Polymer solutions were prepared likewise using their respective solvents. The software ImageJ was used to process and analyze the images obtained.

Thermogravimetric analyses (TGA) were conducted under N_2 atmosphere between 25 °C to 600 °C at a rate of 10 °C·min^{-1} on a Mettler-Toledo TGA/SDTA-851 thermobalance. Three cycles of differential scanning calorimetry (DSC) were performed between -140 °C to 250 °C at a heating/cooling rate of 10 K·min^{-1} on a 204F1/ASC Phoenix calorimeter. Sample preparation consisted of drying the polymer samples overnight at 60 °C, under reduced pressure. For the measurement, ca. 5 – 15 mg of sample were added to the heating pans.

Gel permeation chromatography (GPC) was performed on a PSS Security of Agilent Technologies 1260 Infinity with THF or DMF as mobile phase with a flow rate of 1.0 mL·min^{-1} at 50 °C, equipped with dual detection by a RI-detector RI-101 from ERC and a UV-detector S-3702 from SOMA (at 270 nm). The GPC was calibrated with a series of poly(methyl methacrylate) (PMMA) provided by the Polymer Standards Service. The software PSS-WinGPC UniChrom (PSS) was used to evaluate the data. For the analysis, samples of miniemulsion were purified by centrifugation cycles, followed by precipitation with solvents, usually THF or DMF in hexane. Following that, the samples were dried overnight at 60 °C under reduced pressure. Then, they were dissolved in pure THF or DMF, with the aid of an ultrasonic bath and/or oil bath, when necessary. Finally, they were filtrated with 0.45 µm syringe filters and injected to the GPC system.

Malvern Zetasizer Nano-S90 dynamic light scattering (DLS) instrument equipped with a detector for a scattering angle of 90° to the incident beam was used to measure the hydrodynamic diameter and size distribution of the nanoparticles in dilute water suspensions at 20 °C. Samples were prepared by diluting ca. 10 – 20 µL of miniemulsion in 2 – 3 mL of distilled water or diluted solution of SDS (0.15%$_{wt}$). Dilutions were made to target attenuation values between 8 – 9, with counts higher than 300 kcps. Polydispersity index (PDI) values were usually maintained below 0.2. Results were averaged from three runs, with ten measurements each.

Malvern Zetasizer NaNo-ZS90 equipped with a module for zeta potential measurements was used for this end. Samples were prepared by diluting ca. 10 – 20 µL of miniemulsion in 2 – 3 mL of a 10^{-3} M potassium chloride solution. Dilutions were made to target attenuation values between 7 and 8. Results were averaged from three runs, with ten measurements each.

The water contact angles were measured on films of polymer spin-casted on glass with a DataPhysics OCA35 telescopic goniometer. DataPhysics software SCA202 version 4.1.10 build 1017 (Copyright 1998 – 2010 DataPhysics Instruments) was used both to control the settings of the

measurement and to retrieve the results after it. To prepare the films used for contact angle measurement, ca. 50 mg of the dried samples of purified polymers were dissolved in 500 µL of $CHCl_3$ or THF. These polymer solutions were then spin-coated on clean glass slides and annealed, i.e., dried at temperature over their glass transition temperature, overnight (ca. 80 °C). Then, the glass slides were placed on the equipment and water droplets were automatically casted at selected positions.

3.3 Preparation of monomer mixtures

Samples for bulk polymerization were prepared by adding the photoinitator (TPO) at a concentration of 0.1%$_{wt}$ compared to the combined monomers used. Samples used during the polymerization in miniemulsions were prepared by the emulsion of the monomers by ultrasonication. In a typical reaction, a biphasic mixture of monomers in water ($C_{monomers}$ = 20%$_{wt}$ to the emulsion). The dispersed phase was composed of the monomers in an equimolar mixture containing hexadecane (4%$_{wt}$ of $C_{monomers}$). The continuous phase was composed of water containing SDS as a surfactant (C_{SDS} = 0.2%$_{wt}$ in water), and the photoinitiator TPO-Li (0.1%$_{wt}$ of $C_{monomers}$). The biphasic mixture was emulsified with a Branson digital sonifier SFX550 cell disruptor (70% amplitude, pulsed mode, 2 min). Experiments with off-stoichiometry ratios employed excesses of 5 or 10% of one of the monomers both in bulk and dispersed media.

3.4 Photopolymerization of the monomer dispersions

All samples were reacted in a multi-purpose photoreactor platform equipped with 385 nm LED modules (Peschl Ultraviolet GmbH - Figure 3.4.1A). The general protocol consisted of miniemulsions of monomer-mixtures being irradiated in quartz vessels of 30 or 60 mL, depending on the volume of the sample, at the center of the reactor, by a constant irradiation-power for 4 h. This basic protocol was used for all samples of miniemulsion prepared in this thesis (Section 4.2 and 4.3), unless stated otherwise (Section 4.1).

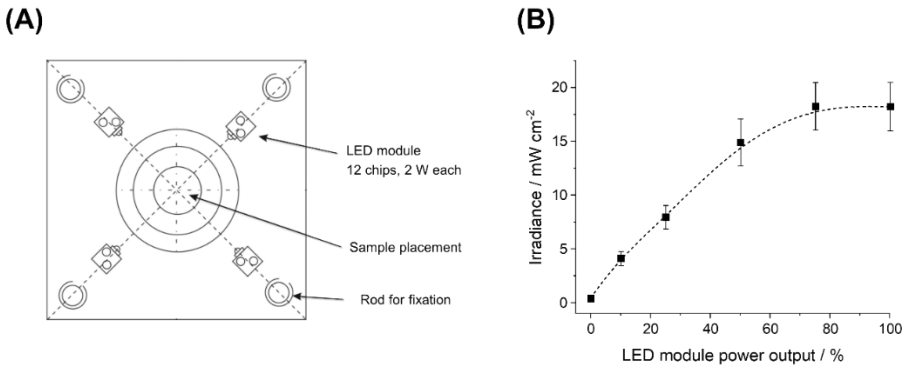

Figure 3.4.1. UV-LED module employed for the photopolymerization of the thiol-ene monomer-mixtures. A) Scheme of the top view of the photoreactor, with 4 LED modules with 12 chips each, and rods for the fixation of reaction vessels. B) UV-irradiance measured at the distance of the sample placement, from 10 to 100% of the total power output. Measured with a ThorLabs S120VC photodiode power sensor.

For experiments that evaluated the kinetic of polymerization (Section 4.1) of samples of miniemulsion or samples prepared in bulk, i.e., solventless mixture of monomers, the general protocol was adapted. In the case of bulk samples, the polymerization was carried out in polystyrene cuvettes placed in the center of the photoreactor (Figure 3.4.2 – 7b). In the case of samples of miniemulsion, the miniemulsion was flown through a 16 cm long tubing ($Ø_{int}$ = 0.08 cm, V = 0.330 mL), coiled around a tube, also located inside the reactor (Figure 3.4.2 – 7a), with a peristaltic pump at flow rates varying from 0.05 to 14 mL·min^{-1}.

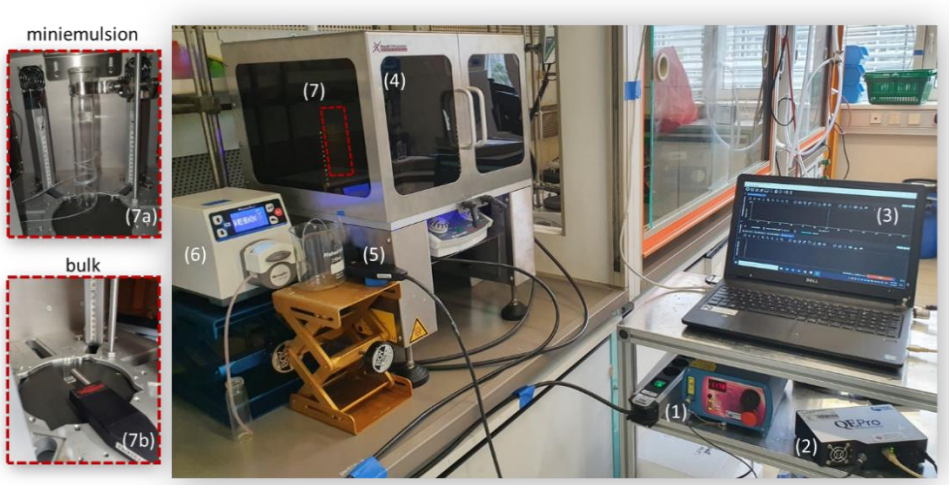

Figure 3.4.2. Photograph of the Raman in-flow spectroscopy setup and components: 1) 785 nm laser source, 2) Detector, 3) Software for online quantification, 4) UV-reactor chamber, 5) External probe, coupled by optical fibers to the (1) and (2), 6) peristaltic pump for miniemulsion experiments, 7) Inside the chamber: a) UV-transparent tubing for miniemulsion, and b) Cuvette for bulk experiments – probe is placed at optimal focal distance from the sample.

3.5 General protocols of purification

After confirming the full conversion of the monomers by ^{1}H-NMR spectroscopy in $CDCl_3$ by the consumption of the allyl (or vinyl) protons, the samples of miniemulsion were purified. The purification was made either through dialysis or centrifugation, depending on the colloidal stability of the sample. Dialysis was usually employed to remove larger molecules such as polyethylene glycol (PEG-SH 2kDa) from the miniemulsion, or to clean latexes with delicate colloidal stability. The membranes used had varying molecular weight-cutoff (MWCO) of 14 or 50 kDa, and dialysis was made against distilled water for 2 – 3 days. Centrifugation cycles were generally performed at acceleration of 10,000 – 20,000 × *g*, 10 °C, for 15 to 30 min. This process was repeated two or three times, with resuspension of the pellets of NPs in their respective clean solvent at each turn. The purified miniemulsions were characterized in terms of hydrodynamic radius size of the NPs, average molecular weight of the polymer chains, chemical composition NMR and FTIR spectroscopy, and thermal analysis when necessary.

3.6 Kinetics of photopolymerization by Raman spectroscopy

To measure the extent of polymerization, Raman spectra were recorded at different intervals of time (or different flow rate) during the reaction, at different UV-irradiance (Figure 3.4.1B). OceanView spectroscopy software with graphical interface was used for data treatment. All the spectra were normalized to the C=O stretching at ca. 1728 cm^{-1}, originating from the carbonyl present in the di-ene monomers.

In general, samples of bulk formulations were aliquoted at 30 s, 1, 2, 5, 10, and 30 min of reaction (end of the monitoring), quenched in liquid N_2, and dissolved in THF containing 200 ppm of MEHQ radical inhibitor for further GPC measurements. In this case, the variation in the chemical composition of the samples over time was monitored using an optical fiber Raman probe placed inside the reactor, at optimal working distance of the cuvette.

After going through the reactor, samples of miniemulsion were flown to an external flow-through cuvette with a quartz window for the detection by a Raman probe inserted in the cuvette holder at optimal working distance (Figure 3.4.2). Samples for GPC were collected at the outlet of the tubing and quenched in N_2 and by the addition of MEHQ. All intervals of time selected to analyze the reactions in bulk were also collected for samples of miniemulsion by the varying of flow rates, and both were probed at varying UV-power, with optical output power of the LED modules varying from 4 to 18 $mW \cdot cm^{-2}$ (Figure 3.4.1B).

3.7 Oxidation of polysulfide nanoparticles in dispersed medium

The oxidation of the latex of polysulfide nanoparticles (NP) was performed by mixing 5 g of a sample of miniemulsion containing 5%$_{wt}$ of NP (ca. 1 mmol of sulfur-centers) with 10.7 mmol of oxidant (1.08 mL of H_2O_2 or 1.47 mL of t-BuOOH), with the addition of TFAP (50 µL, 0.352 mmol). After a predetermined reaction time, a 2 mL aliquot of the reaction mixture was poured in a centrifuge tube containing 10 mL of brine, followed by centrifugation (20,000 × *g*, 8 min, 5 °C). The oxidized NPs were cleaned further by redispersion in 10 mL of aqueous SDS solution (5 – 6%$_{wt}$ NP) followed by precipitation in brine and centrifugation (2×). The final NPs were redispersed in distilled water.

A fraction of the purified suspension was then dried in an oven at 65 °C under reduced pressure overnight. Then, ca. 500 mg of the polymer was dissolved in 1 mL of THF and precipitated in 10 mL of water or brine under stirring, and recovered by centrifugation (20,000 × *g*, 8 min, 5 °C) (2×). The purified polymers were dried overnight in a vacuum oven and used for FTIR, ^{13}C-NMR spectroscopy and contact angle analysis.

3.8 Kinetics of oxidation and oxidation state

To measure the extent of oxidation, FTIR spectra were recorded at different intervals of time during the reaction. The peak at ca. 1030 cm^{-1} corresponds to a stretching of the S=O bound in sulfoxides, and the peak at ca. 1122 cm^{-1} resulting from the stretching of O=S=O was used to monitor the reaction. During the quantification of each species, the integral of the relevant peak was normalized against a peak not involved in the reaction, either the C=O stretching at 1728 cm^{-1} for the polymers containing ester linkages or the peak of the C-H stretching at 2890 cm^{-1} for the other polymers. The composition of the polymer was also quantified by ^{13}C-NMR spectroscopy. Quantitative ^{13}C-NMR spectra were recorded using an inverse-gated pulse sequence. The signals from the C atoms close to the sulfur in alpha and beta positions were chosen as markers of the oxidation state. The chemical shifts of those carbon atoms at 70.9, 29.2, 28.8 ppm (sulfides), 63.5, 52.5, 49.8 ppm (sulfoxides), 53.3, 64.7 and 51.6 ppm (sulfones) enabled the quantification of each species throughout the course of the reaction.

3.9 Surface functionalization of polythioether nanoparticles with polyethylene glycol

Samples of poly(ethylene glycol) methyl ether thiol (PEG-SH 2 kDa) at a concentration range from 10 to 40 mmol·L^{-1} were added to 2%$_{wt}$ suspensions of NPs, with lithium phenyl-2,4,6-trimethylbenzoylphosphinate (TPO-Li) as a photoinitiator. The reaction was carried out for 3 h under UV-light at 385 nm and irradiance of 18 mW·cm^{-2} (Figure 3.4.1). Following the reaction, the reacted

latexes of NPs were dialyzed against a 0.15%$_{wt}$ SDS solution for 2 days in 50 kDa MWCO membranes, with 3 medium changes/day. Then, the samples were transferred to 2 mL centrifugal filters (MWCO 100 kDa) and further washed by 3 cycles of centrifugation and redispersion in a 0.15%$_{wt}$ SDS solution, followed by 2 more cycles with redispersion in deionized water (3,000 × *g*, 30 min, 15 °C), to remove any unreacted PEG-SH.

The detection and quantification of the grafting density were made by ^{1}H-NMR spectroscopy, with the last redispersion after centrifugation made in deuterated water. A tailor-made glass capillary filled with $CDCl_3$ was introduced to the NMR tube containing the sample (400 µL). The quantification of the grafting density of PEG-SH on the NPs was then made by calculating the ratio of the integral of the peak corresponding to the PEG chain at (ca. 3.5 ppm) to the integral of the signal of $CDCl_3$ present inside the capillary. The ratio of the integrals between these two peaks was calibrated with solutions of known concentration of PEG-SH 2 kDa. Therefore, the grafting density values were obtained by interpolating the measured ratios to the calibration curve prepared with standard aqueous solutions of PEG at varied concentrations, using the same capillary filled with $CDCl_3$ throughout the study.

3.10 Bioconjugation of polythioether nanoparticles with carbohydrates and peptides

Thio-β-D-glucose tetraacetate was used as a model for the conjugation of carbohydrates, while Bovine Serum Albumin (BSA) was a model for the conjugation with peptides. Conjugation was realized by reacting ca. 2 g of miniemulsion prepared with a 10%$_{wt}$ excess of diene monomers (ca. 4%$_{wt}$ solid content) with 0.11 mg of thioglucose tetraacetate or 3.35 mg of BSA, with an excess of photoinitiator Irgacure© 2959 (1.5 mg). The samples were then irradiated with UV-light at 385 nm – 18 mW·cm^{-2} (LED modules - Figure 3.4.1) for 3 h. Control samples were prepared by incubating samples of nanoparticles and thioglucose or BSA with the same composition at 37 °C for 20 h. The samples were then purified by five cycles of centrifugation followed by redispersion in water. The solid content of all samples was measured after the reaction.

3.10.1 Quantification of free moieties on the surface of nanoparticles

Number of free-thiols on the surface: After three cycles of centrifugation, the resuspended nanoparticles samples were mixed with the Ellman's reagent (5,5'-dithio-bis-(2-nitrobenzoic acid) (DTNB)). DTNB reacts with free thiols producing a mixed disulfide and the fragment molecule 2-nitro-5-thiobenzoic acid (TNB), which in turn gives a yellow coloration detected at 412 nm (Figure 3.10.1).

The quantification is done by means of interpolation of the absorbance signal of the samples in a calibration curve made with a standard thiol, dithiothreitol (DTT) in this case.

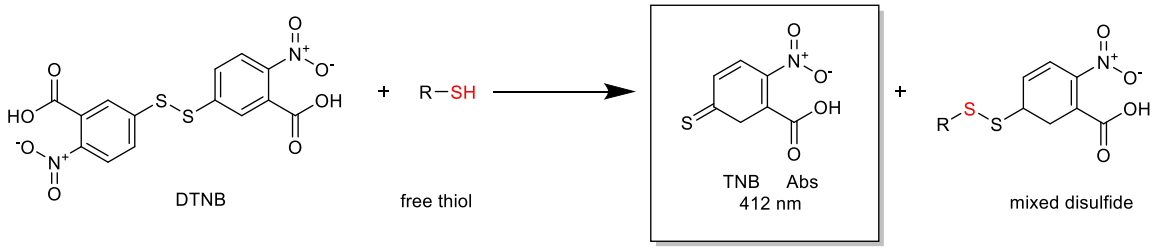

Figure 3.10.1. Schematic representation of the reduction reaction of the Ellman's reagent in the presence of free thiols.

Diluted samples of miniemulsion (ca. 0.1%$_{wt}$) were added (20 µL) to wells of a 96-wells microplate, along with 180 µL of phosphate buffer at pH 7.0, and 4 µL of Ellman's reagent solution (4.5 mg DTNB in 1.0 mL buffer). Standard samples of DTT at different concentrations (20 µL each – 0.025 mM to 0.4 mM) and a blank sample, i.e., only buffer (20 + 180 µL), were prepared likewise. All of them were prepared in triplicates and had their absorbances read at 412 nm.

Total number of free C=C double bonds: After three cycles of centrifugation, the pellet of nanoparticles was dried under reduced pressure, dissolved in $CDCl_3$ (ca. 0.05 mg·mL^{-1}) and placed in NMR tubes. ^{1}H-NMR spectroscopy of each sample was taken, and the quantification of free C=C double bonds was made by means of integration of the respective peaks (5.15 - 5.8 ppm) against the integration of peaks of CH_2 moieties from the thiol-derivative (4.02 ppm) that were not shifted nor consumed during the reaction. The number of accessible C=C double bonds at the surface of the nanoparticle is considered to be 1%$_{mol}$ of the total number of free C=C groups (Figure 3.10.2).

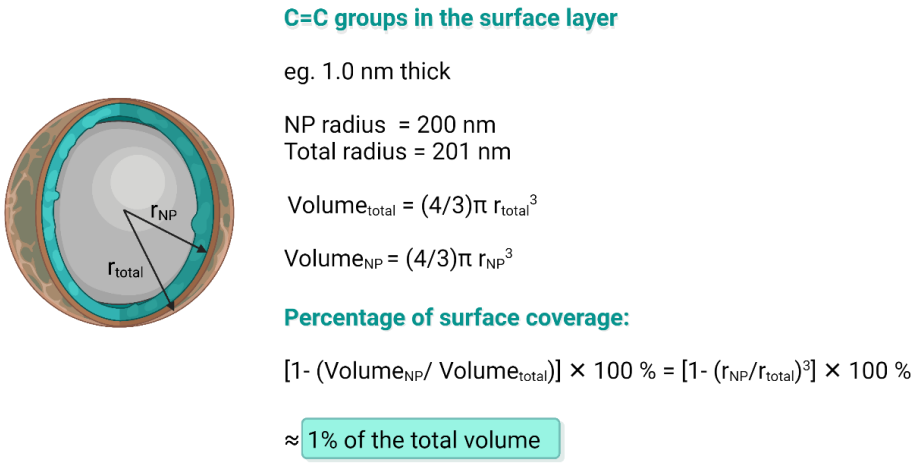

Figure 3.10.2. Scheme of the estimation of the average thickness of a surface layer of C=C double bonds on a nanoparticle.

3.10.2 Glucose quantification enzymatic assay

The principle of this assay is based on the hexokinase (HK)-catalyzed phosphorylation reaction of glucose molecules by adenosine triphosphate (ATP), followed by its oxidation from glucose-6-phosphate (G6P) to 6-phospho-gluconate in the presence of oxidized nicotinamide adenine dinucleotide (NAD), catalyzed by glucose-6-phosphate dehydrogenase (G6PDH), with the reduction of NAD to NADH (Figure 3.10.3). This leads to an increase in the absorbance of the system at 340 nm that is proportional to the initial concentration of glucose.

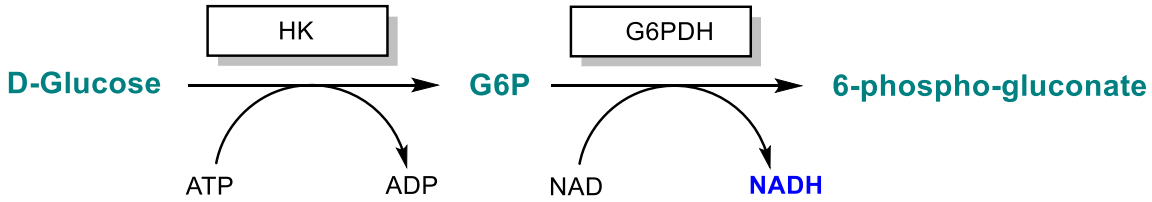

Figure 3.10.3. Schematic representation of the reaction between glucose and Glucose (HK) Assay Reagent (Catalog number G3293). After reconstitution of the reagent 20 mL, the reagent contains 1.5 mM NAD, 1.0 mM ATP, 1.0 unit·mL^{-1} of HK, and 1.0 unit·mL^{-1} of G6PDH.

The concentration of glucose in the suspensions of NPs reacted with thioglucose tetraacetate was determined by a Glucose (HK) Enzymatic Assay (Sigma-Aldrich). To do so, 500 µL of the Glucose (HK) Assay Reagent (Catalog Number G3293) was added to 100 µL of miniemulsion (0.2%$_{wt}$) and incubated at room temperature for 15 min. Then, 100 µL of this solution was transferred in triplicates into wells of a 96-wells transparent microplate to have their absorbance at 340 nm measured against water. Standard solutions in water of Glucose Standard Solution (Catalog Number G3285) of d-glucose (1.0 mg·mL^{-1} in 0.1% benzoic acid) at a concentration range of 1.0 to 0.02 mg·mL^{-1} were used as the calibration set.

3.10.3 Experiments with protein adhesion

The protein adsorption experiments were done by incubating the latexes of NPs with either a solution of fluorescently labeled bovine serum albumin (FITC-BSA), fetal bovine serum, or human citrate plasma.

Fetal bovine serum (FBS) non-USA origin, sterile-filtered, and suitable for cell culture grade was acquired from Sigma-Aldrich. Upon arrival, its total volume was aliquoted and transferred in portions of 10 mL to 15 mL centrifuge tubes. They were then stored at -20 °C and freshly thawed before usage.

Human citrate Plasma (HP) was obtained from ten healthy donors at the Department of Transfusion Medicine from Mainz, after their physical aptitude was verified, which knowingly consent to it, according to the Declaration of Helsinki. The HP samples were pooled and stored at -80 °C. Before each experiment using HP as protein source, aliquots of HP were thawed and centrifuged at 20,000 × *g*, 4 °C, for 30 h to remove any protein aggregates.

The nanoparticles suspensions of polythioether, polysulfoxide, polysulfone, and polythioether functionalized with PEG-SH 2 kDa were diluted to a concentration of 1.0 mg·mL^{-1} of NPs, and added to 1.0 mL of FITC-BSA, FBS or HP in 1.5 mL Eppendorf© test tubes. After that, the tubes were incubated at 37 °C, 300 rpm, for 1 h in an HLC by DITABIS Heating-Thermomixer model MKR 23. Samples incubated with FITC-BSA were directly centrifuged and analyzed straight after the incubation step. The

following steps are dedicated to samples incubated with complex polls of proteins such as FBS and HP. After removed from incubation, the test tubes were centrifuged at 10,000 × *g* at 4 °C for 10 min, followed by pellet resuspension in 1.0 mL of PBS. This step was repeated three times. Following the cleaning, the pellets were resuspended in a desorption buffer (2%$_{wt}$ SDS + 62.5 mM Tris*HCl), and incubated at 95 °C for 5 min. After centrifuging the solutions at 10,000 × *g* at 4 °C for 10 min, the supernatants were transferred into fresh tubes and use for protein quantification (Pierce™ protein assay) or stored at -20 °C for further analysis.

3.10.4 Determination of the concentration of proteins

Fluorescence of FITC-BSA: After incubation at 37 °C, the suspensions with FITC-BSA were centrifuged down. The fluorescence of the supernatants was measured in 96-wells black microplates, at an excitation wavelength of 495 nm and emission at 520 nm. Standard solutions of FITC-BSA in distilled water were used as calibration set, from a concentration range of 0.005 to 0.02 mg·mL^{-1}.

Pierce™ protein assay (Thermo Scientific, Cat. No. 22660): The Pierce™ 660 nm Assay is based on the binding of a dye metal complex to proteins a low pH values, causing a shift in the absorption maximum of the dye to 660 nm. This shift is caused by the deprotonation of the metal complex in the presence of positively charged residues in proteins, such as histidine, arginine, and lysine, and to a lesser extent tyrosine, tryptophan, and phenylalanine.

The supernatants retrieved from the protein adhesion experiments (Section 3.10.3) were used protein quantification. Calibration was made by preparing a dilution series BSA in Milli-Q water in the concentrations of 2000, 1000, 500, 250, 125, 62.5, and 31.3 µg·mL^{-1}. For the analysis, 10 µL of each BSA standard and of each sample was loaded in triplicates into wells in a transparent 96-well microplate. Then, 150 µL of Pierce™ reagent with Ionic Detergent Compatibility Reagent were added to each well. For the measurement, the samples were incubated at RT for 5 min and their absorbance read at 660 nm. The quantification was done by means of interpolation of the absorbance signal of the samples in the calibration curve made with standard solutions of BSA.

3.10.5 SDS polyacrylamide gel electrophoresis (SDS-PAGE)

SDS-PAGE was used to discriminate the proteins absorbed onto the surface of the NPs, according to their respective molecular weights. NuPAGE series from Novex, ThermoFisher was used to perform the experiments. For that, 16.25 µL of the supernatants retrieved from the desorption of proteins from the surface of the NPs (Section 3.10.3) was added to 6.25 µl of LDS sample buffer (4×), with 2.5 µl of sample reducing agent, and then applied onto a bis-tris protein gel (10%). Then, MES SDS running buffer (20×) was added to the gel to carry out the electrophoresis for 1.5 h at 150 V, with the molecular marker Invitrogen SeeBlue Plus2 pre-stained standard marker. After this time interval, the gel was stained using SimplyBlue SafeStain (Thermo Fisher Scientific).

3.10.6 Multiple angles scattering in human citrate plasma

For multi-angle dynamic light scattering experiments, cylindrical quartz cuvettes (Hellma) were cleaned and transferred to a dust free flow box. Light scattering measurements were performed on an ALV spectrometer consisting of a goniometer, and an ALV-5004 multiple-tau digital correlator (320 channels). This setup allows measurements at different angles, ranging from 30° to 150°. The light source was a He-Ne Laser (632.8 nm). The temperature of the systems was maintained by a Julabo. This method was used to investigate the aggregation profile of NPs in human citrate plasma.

To do so, 3 samples were prepared and filtered with a Millipore GS 0.2 µm: 1) 1 µl of solutions of NPs ($1\%_{wt}$) was added to 1 ml of PBS, 2) 1 ml of pure plasma, and 3) 1 µl of solutions of NPs ($1\%_{wt}$) added to 1 ml of plasma. The samples were incubated at 37 °C for 1 h. Then, light scattering measurements were carried out at 37 °C at a range of angles, 30°, 60°, 90°, 120°, and 135°, in five replicates of 30 s each. The protocol of data evaluation described in Rausch et al.[132] was used to interpret the results. The correlation curves of pure plasma samples were fitted to a triexponential decay function, while the samples containing only NPs in PBS were fitted using a sum of two exponentials. Mixtures of plasma and NPs were fitted with a sum of exponential decay functions, with and without additional aggregate term.

4 Results and discussions

Polymerization in dispersed media provides a way to control the design of nanoparticles and materials, and enables different types of polymerization reactions in water, which also appeals to environmental aspects. While the polymerization reaction defines the chemical properties of the nanoparticles, the process in dispersed media creates an environment favorable to the post-modification of these particles, which can tune the physicochemical properties of the final materials. The success of this synthetic platform relies on the careful control of each step of the process, from the kinetics of polymerization inside the droplets that will then become polymer particles, to the post-modification chemistry employed to deliver a set of properties according to a given application.

However, performing reactions in dispersed media adds complexity to the reaction rates, due to confinement effects. Understanding and controlling the kinetics of the polymerization reactions occurring in dispersed media is essential. Raman spectroscopy is a good option to do so in thiol-ene systems since both thiol and ene can be analyzed at the same time. Moreover, this technique can be coupled to a flow-system, allowing an online monitoring of the kinetics of polymerization (Section 4.1).

Another important factor on the design of nanoparticles is the post-modification process. Through such approach, it is possible to modify the composition, structure, or surface coverage of the polymer nanoparticles. One example of post-polymerization modification is the oxidation of latexes (Section 4.2). Upon oxidation, the chemical composition of the polymer chains is changed, at the same time as their structure is kept. In such way, the properties gained by the polymerization process can be further tuned, without compromising the initial network. Thiol-ene allows such modification by the interplay of oxidation states of the sulfur-centers present in the main chains of the polymer.

In addition, thiol-ene click reactions are employed to attach other functionalities to the surface of the nanoparticles. Polymerizations of off-stoichiometry mixtures of monomers provide networks with unreacted moieties, either thiols or enes according to the function in excess. Consequently, these appending chains are used as anchors for new molecules through thiol-ene click chemistry (Section 4.3). Such reactions are particularly suitable in the design of biorelevant particles since thiols are abundant in biomolecules.

In this thesis, the potentialities of thiol-ene chemistry as a smart platform for developing highly tunable materials was analyzed. It allowed for nanoparticles to be tailored from core to surface for specific applications.

4.1 Nanoconfinement increases reaction rates and yields high molecular weights polymers during thiol-ene photopolymerization in miniemulsion*

The first step in the design of tunable thiol-ene nanoparticles is their synthesis. To preserve unreacted thiol or enes functions on the surface of the nanoparticles for further modification, it is crucial to control the polymerization reaction. To do so, two strategies can be considered, either stop the reaction before the full conversion of the functionalities or perform the reaction with an excess of either dienes or dithiols. Both strategies are challenging because they have the potential to yield materials with low degree of polymerization and poor thermomechanical properties. Consequently, understanding the kinetics of monomer conversion become essential to produce polymer nanoparticles with enough unreacted ene (or thiol) to allow post modification of the surface but having a high enough conversion to ensure adequate polymer performance.

Thiol-ene polymerization is a powerful synthetic platform for the preparation of a variety of polymer materials but is often plagued by the formation of low molecular weight polymers. This is typical of step-growth polymerization, where high molecular weights are achieved only at nearly complete monomer conversions. However, experimental results suggest that it is possible to produce step-growth polymers with a high degree of polymerization by performing the reaction in miniemulsion, where the dispersed droplets act as nanoreactors. Here, we investigate the effect of confinement arising from the reduction of the reaction loci from the bulk to a nanoreactor and how it affects the thiol-ene reaction and the resulting polymers. The polymerization rates observed for the reaction in miniemulsion were up to 100-fold higher than the rates observed in bulk. Different monomer pairs were evaluated using either a diallyl, divinyl, or diacrylate monomers as dienes. The reaction was followed by Raman spectroscopy to simultaneously quantify the conversion of thiols and enes in the system, which enabled the detection of side-reactions, such as homopolymerization. Mixtures with a non-stoichiometric ratio of dithiol and diene monomer also benefited from the polymerization in nanoconfinement. In such cases, the polymerizations in bulk were limited to very low degree of polymerization. However, when the polymerization was performed in the confinement of the miniemulsion droplets, high molecular weights polymers were produced (Figure 4.1.1).

* This section is based on the article: " Nanoconfinement increases reaction rates and yields high molecular weights polymers during thiol-ene photopolymerization in miniemulsion " by L. Infante Teixeira, H. Thérien-Aubin, K. Landfester submitted for publication in Macromolecules.

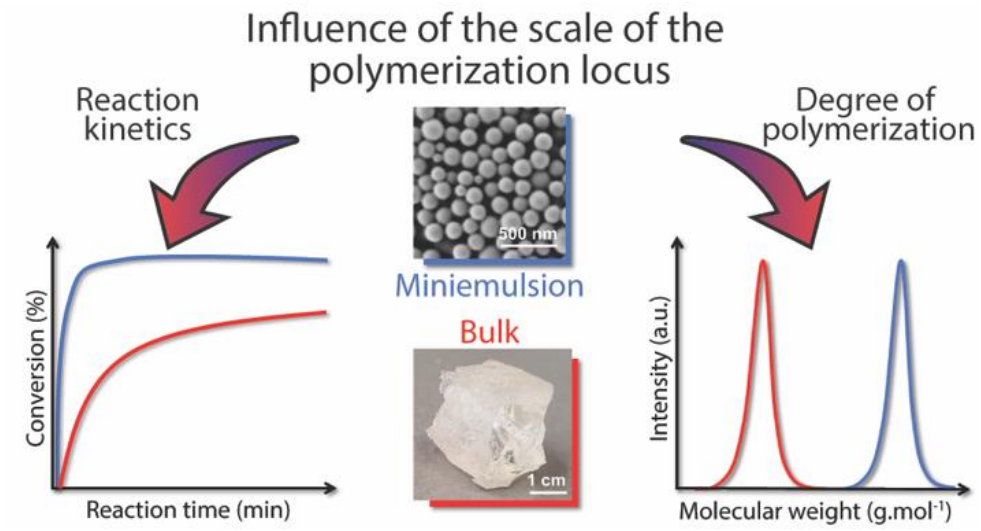

Figure 4.1.1. Graphical summary of the influence of the scale of the polymerization locus on the polymerization kinetics and on the degree of polymerization of a thiol-ene step-growth reaction.

4.1.1 Introduction

Thiol-ene polymerization is a popular synthetic platform due to its versatility and synthetic simplicity,[11,13,82,133] but is often plagued by the formation of low molecular weight polymers. This limitation impacts the thermomechanical properties of the resulting polythioethers and prevents their applications where high-performance polymers are required.[35,36,134] Because of the step-growth character of thiol-ene polymerization, high molecular weights are achieved only at nearly complete monomer conversions, which is challenging to accomplish in practice.[6,135,136] However, recent studies showed the formation of polymers with improved degrees of polymerization for thiol-ene products prepared in miniemulsion.[38,82,90,137] Such a behavior could potentially be ascribed to a confinement effect similar to that observed during free-radical polymerization carried out in nanodispersed media, which leads to higher conversion rates of the monomers yield polymers with higher degrees of polymerization.[130] These observations demonstrate the need to investigate the mechanism of thiol-ene polymerization in nanoconfined systems to rationally design high molecular weight polythioethers and expand the range of applications of the resulting thiol-ene systems.

Reactions in colloidal suspensions can take advantage of the compartmentalization of the reactants to increase the rate of conversion. During a polymerization performed in droplets created by miniemulsion, the monomers-containing droplets act as nanoreactors and become the final polymer particles.[68] Typical free-radical polymerization and controlled-living radical polymerization in such dispersed systems have shown improved reaction kinetics. Primarily due to the segregation of radicals in different compartments, which reduces termination events.[75,130] Most of the current understanding of the effect of confinement on polymerization reactions comes from the study of those chain-growth polymerization,[97,102,129,138,139] and confinement effect on step-growth polymerization remains ambiguous.[81,92,140] However, we need to address the effect of confinement on the rate and yield of step-growth reactions, like thiol-ene polymerization, to harness this effect to design new polymers.

Understanding the kinetic of the thiol-ene polymerization in miniemulsion is crucial to reach high monomer conversion and produce high molecular weight polymer materials. Typically, thiol-ene polymerization reactions are studied by monitoring the conversion with ^{1}H-NMR or FTIR spectroscopy.[82,136,141] However, the detection of thiol moieties can be difficult due to intermolecular interactions or intrinsic low analytical sensitivity; thus, quantification usually relies only on the conversion of the enes alone.[142,143] Furthermore, during thiol-ene polymerization, two conversion mechanisms can compete.[7,144] On the one hand, there is the step-growth controlled thiol-ene coupling, where a thiyl attacks an ene moiety producing a thiol-ene adduct. On the other hand, some

commonly used enes can concomitantly undergo radical homopolymerization through a chain-growth process; hence the sole detection of the conversion of the carbon-carbon double bonds might be misleading to characterize the thiol-ene reaction. In systems where allyl ethers are used, the reaction can be relatively well described by overlooking any chain-growth mechanism since their ene-centered radicals show greater selectivity to thiyl radicals than homopolymerization.[145,146] However, for monomer systems using (meth)acrylates or vinylic enes, this approximation can no longer hold since homopolymerization can occur at a rate faster than the addition of thiol to the double bonds.[5,141,147] To study such systems, the simultaneous detection of both functionalities thiol and ene could provide a better view of the reaction. In addition, it can also provide strategies to control polymerizations performed with off-stoichiometric ratios of thiols and enes, which is a strategy used to synthesize polymers that can readily undergo post-polymerization modifications.[8,13,148]

Although it has been shown that thiol-ene polymerization performed in dispersed media yields polythioethers with high degrees of polymerization,[39,137] the origin of this effect remains ambiguous. However, harnessing the effect of confinement during thiol-ene polymerizations performed in dispersed media would be an efficient method to produce high-quality polythioethers. Here we report a systematic study comparing the reaction in bulk and miniemulsion systems of thiol-ene polymerization. Monomer pairs bearing thiol and allyl/vinyl functionalities were prepared in both types of environments. The polymerization reaction was followed by Raman spectroscopy to characterize the conversion of thiols and enes during the reaction. In conjunction with the evolution of the polymer molecular weight, those results can provide insights into the thiol-ene polymerization mechanism in confined systems. Furthermore, the effect of the off-stoichiometric ratios of monomers, which would bring more flexibility in the design of new thiol-ene polymers, has been investigated. Our results pave the way for the broader use of polythioethers in applications where not only their functional versatility and reduced shrinkage stress are needed,[11,42,149] but also the improved thermomechanical properties[145,146] associated with higher molecular weight,[41] such as in scratch-resistant coatings,[36] dental restorative materials,[150] fibers manufacturing,[151] microfluidics scaffolds,[13,152] and even in industrial-scale molding processes.[153]

4.1.2 Results and discussions

We selected a model monomer-pair composed of diallyl adipate (DAA) as the di-ene, and 2,2'-(ethylenedioxy) diethanethiol (EDDT) as its di-thiol counterpart to study the kinetics of the thiol-ene polymerization. Raman spectroscopy was employed to perform the detection and quantification of the moieties throughout the experiments in a flow-through setup (Figure 4.1.2). The choice of this monomer system stemmed from the well-resolved peaks of the monomer couple, without any overlaps between vibrations in the thiol and ene region. Furthermore, those monomers also are not absorbent in the UV-range (385 nm) used to initiate the polymerization. In addition, DAA contains an ester linkage, allowing the normalization of the spectra using the carbonyl vibration (ca. 1735 cm^{-1}) as an internal standard (Figure 4.1.3A). In addition, Raman spectroscopy, in comparison to FTIR for example, enables the simultaneous analysis of both thiols and enes functionalities with sufficient accuracy to follow the conversion kinetics. Furthermore, Raman spectroscopy is also well-suited to waterborne media since the water vibrations are not a significant concern in the spectral window of interest.

Also, the use of a flow system allowed to probe a large variety of reaction conditions by conveniently changing the flow rate, using the same miniemulsion for a given set of experiments. By fixing the volume, i.e., the tubing length and diameter, of miniemulsion inside the reactor, the reaction time was calculated for each flow rate as:

$$t = \frac{V}{Q} \qquad \text{(eq. 4.1.1)}$$

where t is the reaction time, V the volume of the irradiated tubing and Q, the flow rate of the liquid through the tubing. Moreover, the use of a flow-through system also enables the easy collection of aliquots for further analysis (e.g., GPC) without the need to stop the reaction. While miniemulsion samples could be readily processed using this flow-through system, bulk samples were unsuitable because the increase in viscosity during the polymerization precluded the unobstructed flow of the monomer/polymer mixture. Therefore, irradiation and detection of bulk samples were made in cuvettes placed inside the reactor.

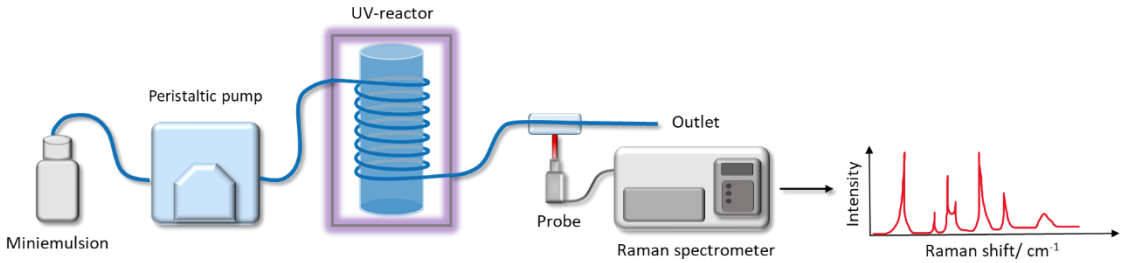

Figure 4.1.2. Scheme of the experimental setup.

For both the miniemulsion samples and the bulk samples, the evolution of the chemical composition of the reaction mixture was evaluated over time using the Raman spectra collected. As the reaction occurred, the peak of thiol from the EDDT (ca. 2570 cm^{-1}) and ene from the DAA (ca. 1650 cm^{-1}) were consumed, while the peak belonging to the C=O stretching mode of the ester group in DAA was not involved in the reaction and remained constant. The conversion of each monomer was calculated using the variation in the integration of the thiol or ene peaks over time (Figure 4.1.3B, C).

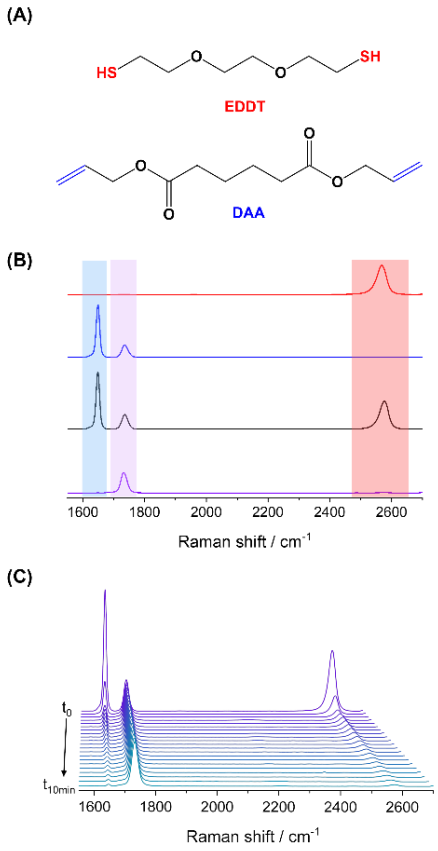

Figure 4.1.3. Model system used to study the kinetics of the thiol-ene polymerization. A) Chemical structure of the monomers 2,2'-(ethylenedioxy) diethanethiol (EDDT) and diallyl adipate (DAA), and B) Raman spectra of EDDT-DAA monomer-pair before and after polymerization in bulk. From top to bottom: EDDT (red), DAA (blue), EDDT-DAA 0% conversion – before UV irradiation (black), and EDDT-DAA 100% conversion – after UV irradiation (violet). Shaded areas highlight the vibrations of

the functional groups analyzed: S-H (red); C=C (blue); C=O (violet). C) Evolution of the Raman spectra of the monomer mixture during a bulk polymerization from t = 0 (back) to 10 min (front) under UV irradiation.

Generally, the kinetics of thiol-ene photopolymerization in bulk is chemically controlled by the interplay of the rate of reaction of the thiyl radical with the C=C double bond and the rate of chain transfer from the carbon-center radical to unreacted S-H group to generate a new thiyl radical (Figure 4.1.4), which in turn is highly dependent of the chemical structures of the monomers involved. Typically, systems composed of thiol and allyl ethers, have shown to be "chain-transfer limited", i.e., the overall rate varies as a first order reaction only with respect to the thiol concentration, and is unaffected (zero-order) by the concentration of available C=C double bonds, at least, under stoichiometric conditions.[154]

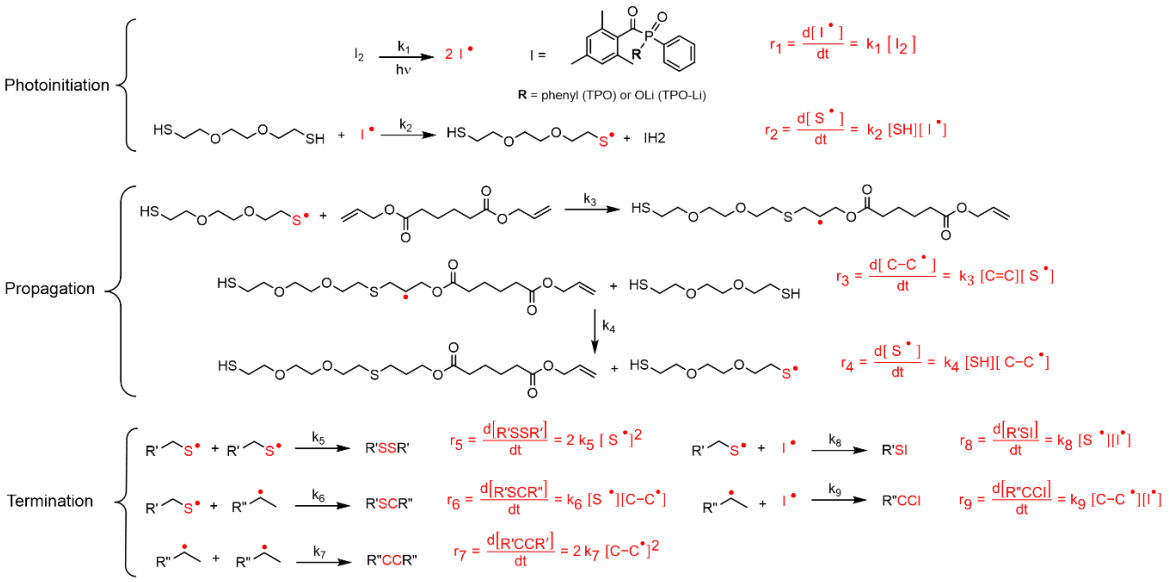

Figure 4.1.4. Mechanism of thiol-ene reaction of the system EDDT-DAA. The following approximations were used to analyze the kinetics: (1) Both radicals formed from the homolysis of TPO are equally reactive ≈ 2 I*, (2) Pseudo-steady-state assumption $\frac{d[S^{\bullet}]}{dt} = \frac{d[C^{\bullet}]}{dt} = 0$, (3) $r_3 = r_4$, and (4) all termination steps are equally likely to occur.[154]

Figure 4.1.5 shows the kinetics of conversion of both C=C ene bonds and S-H thiol bonds in bulk and in miniemulsion. In both bulk and miniemulsion, there is an initial rapid conversion of the functionalities, followed by a slower conversion at longer reaction times. Such conversion profile is characteristic of step-growth polymerizations, such as thiol-ene, where monomers are rapidly consumed to form dimers and then oligomers, with increasing chain lengths. Over time, the presence of larger chains slows down the additions due to the combined effect of the reduction in the local concentration of reactive sites, and slower diffusion caused by the increased of viscosity resulting from the formation of larger and larger oligo/polymers.

However, the conversion curves obtained for the reaction in miniemulsion show a much faster monomer conversion than the bulk reaction with an increase in the initial rate of conversion of ca. 15 times. Such behavior is in keeping with the increased reaction rate observed in other dispersed systems.[75,129,139] This phenomenon can be ascribed to the confinement effect, provided by the formation of droplets of monomer phase that act as individual nanoreactors, and to the mechanism of initiation of the thiol-ene reaction. This confinement can influence the polymerization reaction in different ways. The presence of the interface can force the molecules present in the droplets to adopt a reactive conformation and restrict the diffusion of the monomers and oligomers to the nanodroplets; the interface also regulates the entry of the thiyl radicals in the droplets. Both leading to the increased reaction rate observed. Although every thiol group reacting in a thiol-ene polymerization need to be first converted into a thiyl radical, the thiol-ene coupling is generally considered as self-sustaining, i.e., the external initiation process is essential to generate the first thiyl radical, but then following the coupling between the thiyl and the ene, a chain-transfer reaction occurs to transfer the radical from the reacted ene to an unreacted thiol present in the reaction environment. Thus, one thiyl radical entering the monomer droplet can lead to the formation of long polymer chains through the efficient propagation of the initial radical, while in bulk, the presence of a large number of thiyl and TPO-Li radicals lead to competition between termination and propagation steps.

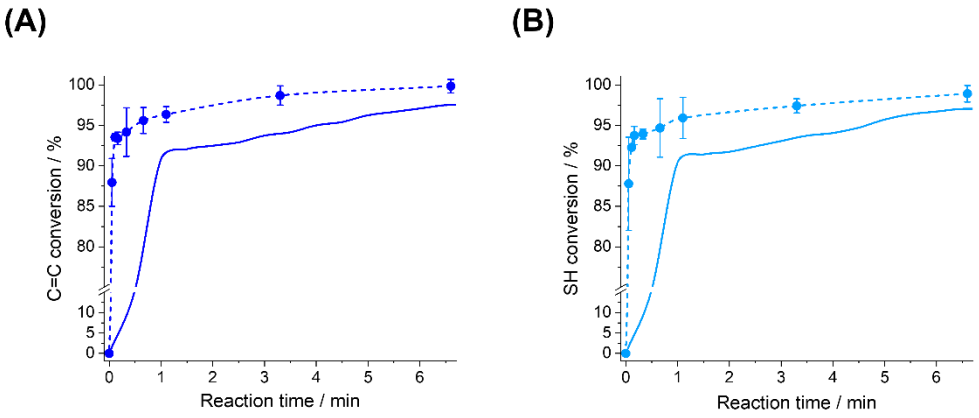

Figure 4.1.5. Effect of the nanoconfinement on the conversion kinetics of A) ene and B) thiol moieties for the EDDT-DAA monomer pair for polymerization carried out in bulk (solid line) and in miniemulsion (dashed line).

The presence of an interface between the confined and continuous spaces influences the reaction kinetics by modifying the interactions between reactants,[91,152] and control the concentration of radicals within the droplets. Although the rate limiting step of the thiol-allyl reaction is typically the chain transfer of the radical from the ene-radical to an unreacted thiol, the reaction rate is also affected on the amount of radical initiator used (Figure 4.1.4 and Figure 4.1.6). Experimental results

(Figure 4.1.6) show that increasing the concentration of radicals generated by the UV-irradiation of bulk samples led, after a threshold concentration, to a reduction in the apparent polymerization rate.

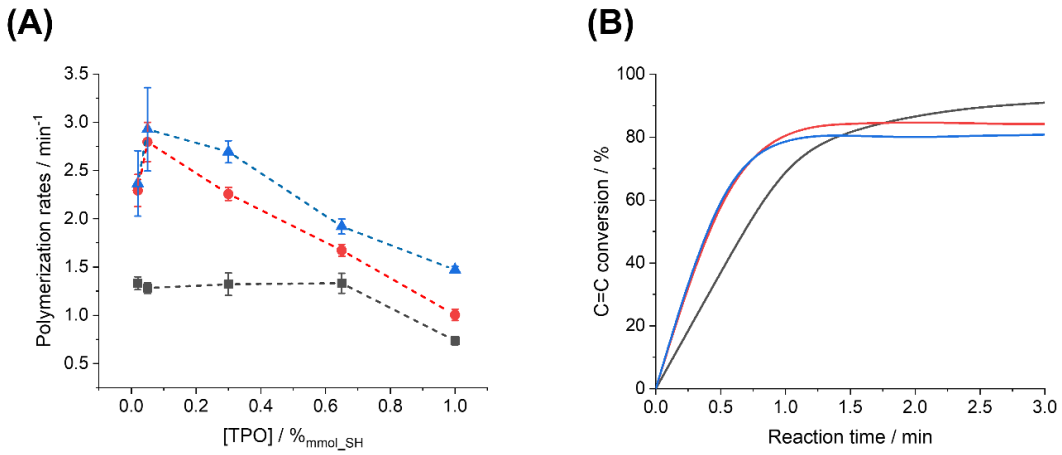

Figure 4.1.6. Effect of the concentration of photoinitiator and irradiance in the reaction of the system EDDT-DAA in **bulk**: A) Polymerization rates as a function of [TPO] at different UV-irradiance: 4 mW·cm^{-2} (gray squares and dashed line), 7 mW·cm^{-2} (red circles and dashed line), 15 mW·cm^{-2} (blue triangles and dashed line). B) Conversion of C=C double bonds over time at different UV-irradiance for [TPO] = 0.05%$_{mmol\_SH}$: 4 mW·cm^{-2} (gray line), 7 mW·cm^{-2} (red line), 15 mW·cm^{-2} (blue line). Polymerization rates of the system EDDT-DAA in bulk.

This phenomenon can be attributed to recombination involving free radical species generated by the degradation of the photoinitiator. Thus, the acceleration observed in the confinement of the nanodroplets can potentially be ascribed to the beneficial distribution of radical species in the system between the droplets and the continuous phase. In the miniemulsion studied here, the radical photoinitiator was water-soluble while the monomers were confined to the hydrophobic droplets. However, the two monomers, EDDT and DAA, present different partition coefficients, with the EDDT, the di-thiol, exhibiting a higher water solubility (15 g·L^{-1} at 25 °C).[82] Consequently, EDDT can likely diffuse between the monomer droplet through the continuous aqueous phase. Furthermore, the radicals were formed during the photoconversion of the initiator TPO-Li in the continuous phase and were unlikely to enter the monomer droplets directly due to their high hydrophilicity. The most probable reaction mechanism consists of the reaction between the TPO-Li radicals and the EDDT molecules present in the continuous phase. The reaction forms a thiyl radical, which has a lower hydrophilicity than the TPO-Li radicals and can then reenter the monomer droplet to initiate the polymerization. The reentry of the thiyl radical into the droplets is controlled by the interface between the oil droplet and the continuous phase. Such gate control provided by the droplet interface is inexistent in bulk formulations, with all species, monomers, and radicals, being present in the medium from the onset of the irradiation and can lead to an increased termination rate. Consequently, the

generation of thiyl radicals in the continuous phase of the miniemulsion and their controlled reentry in the monomer droplets limited the probability of termination reaction through disproportionation or recombination in the droplets and led to the increased apparent polymerization rate observed.

The diene, DAA, was then substituted by other enes to analyze the effect of different chemical structures, more specifically electron-density and radical stability, on the polymerization kinetics. The ene groups in DAA are allylic double-bonds, and their reactivity was compared to that of divinyl adipate (DVA) bearing vinylic double-bond and 1,4-butanediol diacrylate (1,4Dac) containing acrylic double bonds. Figure 4.1.7 clearly shows that the use of different dienes yielded different polymerization. For the systems composed of DAA and DVA, the conversions of thiols and enes occurred at a similar rate. In contrast, the polymerization of 1,4Dac and EDDT led to a much faster conversion of the enes compared to the conversion of the thiols. This result suggests that, when using acrylates as the ene-component, the monomer pair did not react through a purely thiol-ene addition, but that the thiol-ene reaction competed with a free-radical chain-growth polymerization, leading to the formation of a heavily crosslinked network, as confirmed by NMR spectroscopy (Figure 4.1.8). Monomers and radials from (meth)acrylates usually present high polarity values and resonance structures, as evidenced by their Q-e values (butyl acrylate: Q 0.38/e 0.85),[155] which favor their homopolymerization. On the other hand, vinylic radicals (vinyl acetate: Q 0.026/e -0.88)[155] and even more so allylic radicals (allyl acetate: Q 0.24/e -1.07)[155] have lower polarity values, and their homopolymerization through free radical polymerization will be disadvantaged compared to that of (meth)acrylates.[156]

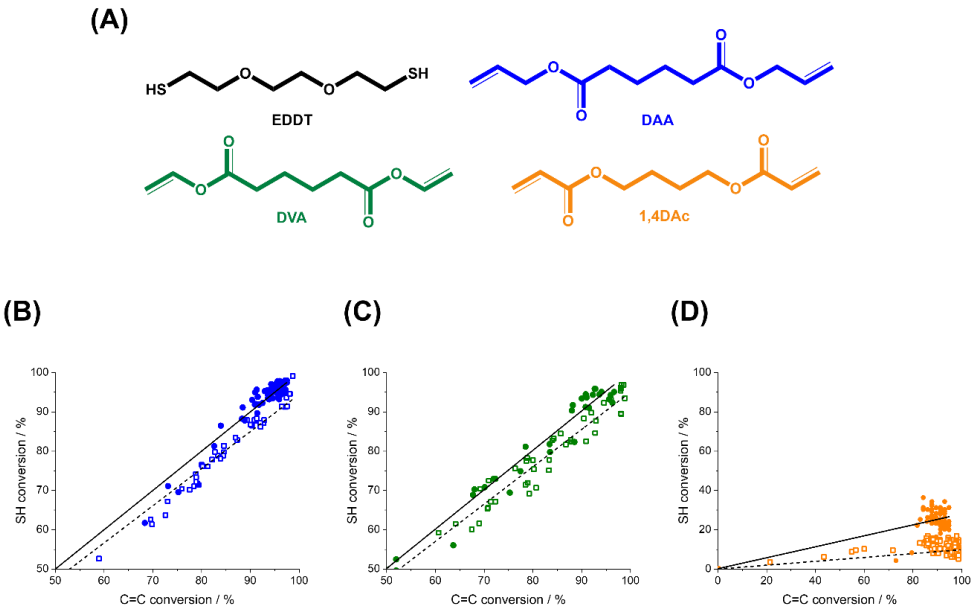

Figure 4.1.7. Monomer conversion during thiol-ene polymerization of different monomer pairs. A) Chemical structures of the monomer systems. 2,2' –(ethylenedioxy)diethanethiol (EDDT) (black) was used as the di-thiol for the polymerization with diallyl adipate (DAA) (blue), divinyl adipate (DVA) (green), and 1,4-butanediol diacrylate (1,4DAc) (orange). B-D) Comparison of the conversion of thiols and carbon double bonds in each system for polymerization carried out in miniemulsion (solid circle) and in bulk (open squares). B) EDDT-DAA (blue), C) EDDT-DVA (green) and D) EDDT-1,4Dac (orange).

Interestingly, Figure 4.1.7 also show a difference between the conversion during the polymerization in bulk and in miniemulsion. In miniemulsion, the conversion of both enes and thiols occurred at an identical rate for the polymerization of DAA and DVA with EDDT. However, in bulk, the conversion of enes occurred moderately faster than the conversion of the thiols. The reaction in miniemulsion likely led to fewer side reactions and better heat exchange,[1,66] which could affect the conversion of the enes in bulk. The same phenomenon was also observed for the polymerization of the monomer pair EDDT-1,4Dac in miniemulsion, although the polymerization of the enes was still highly favored compared to the conversion of the thiols.

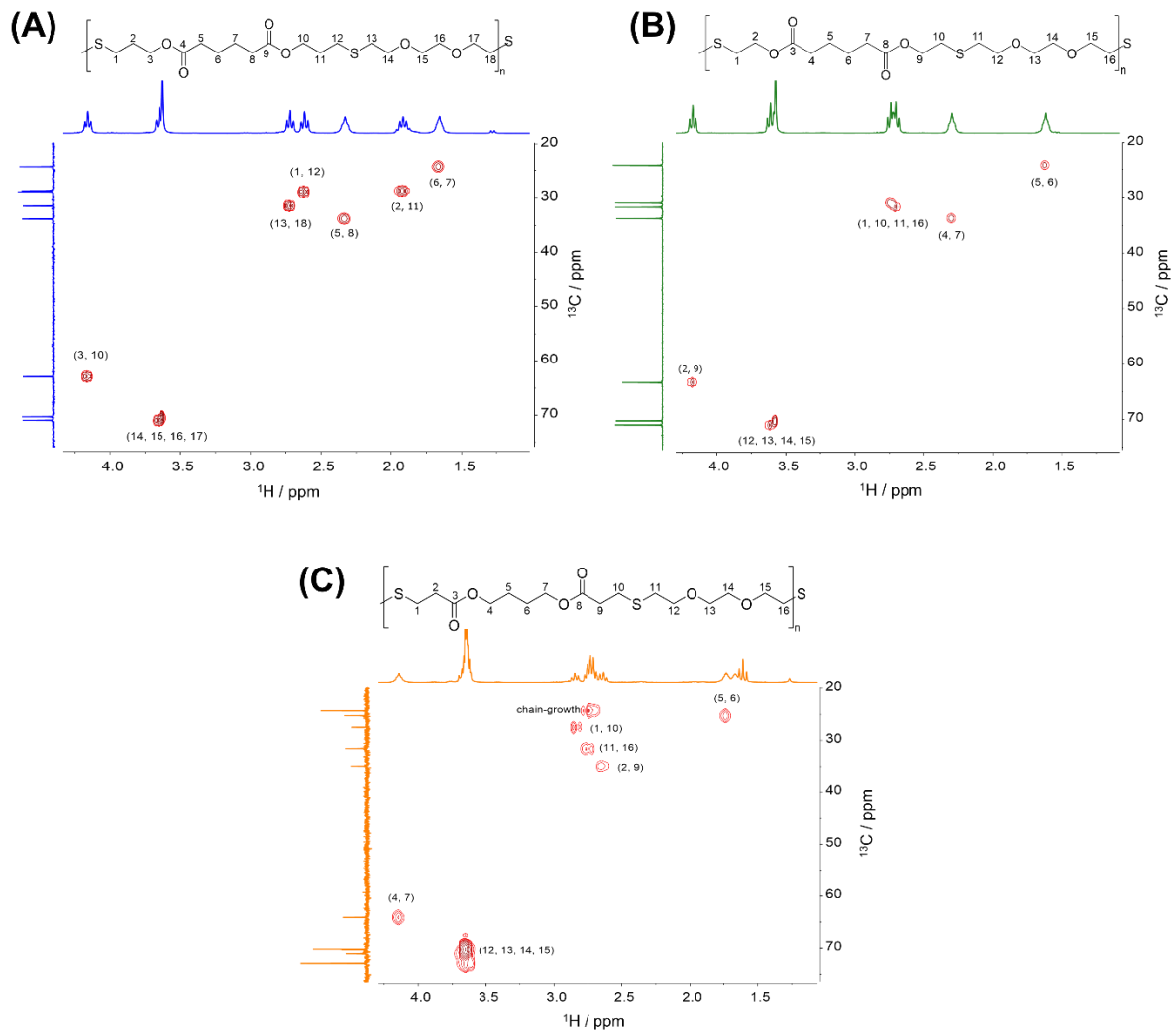

Figure 4.1.8. HSQC spectra of the polymers obtained by thiol-ene photopolymerization in bulk of A) EDDT-DAA, B) EDDT-DVA, and C) EDDT-1,4DAc. A) and B) exhibit no detectable signs of homopolymerization, whereas C) exhibits peaks originating from the chain-growth homopolymerization of the acrylic moieties.

In general, the conversion of both enes and thiols occurred more rapidly in the miniemulsion nanodroplets than in the bulk (Figure 4.1.5). This increase in the polymerization rate was observed for both the monomer pair EDDT-DAA and EDDT-DVA. Figure 4.1.9 compares the polymerization rates of EDDT-DAA and EDDT-DVA prepared in bulk and miniemulsion. The results indicate that the polymerization rate of the reaction performed in miniemulsion increased up to 100-fold compared to the same reaction performed in bulk. This result was observed for both monomer pairs and was likely due to the lower concentration of radicals present in the monomer droplets in comparison to the bulk.

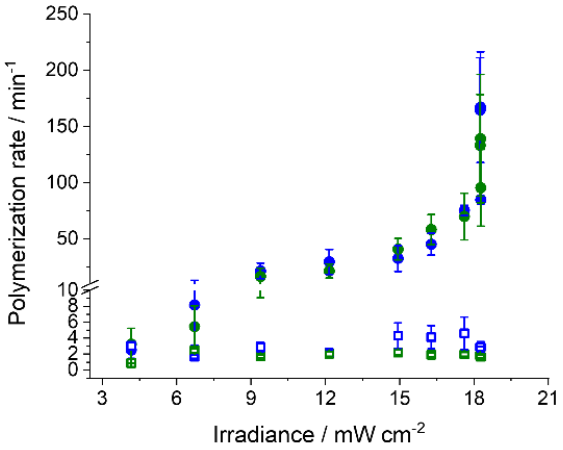

Figure 4.1.9. Effect of nanoconfinement in the rate of thiol-ene polymerization for EDDT-DAA (blue), and EDDT-DVA (green) performed in bulk (open squares) and miniemulsion (solid circles). The polymerization rates (*k*) were obtained from fits of the conversion kinetics with $[C=C]_t = [C=C]_0 (1 + e^{-kt})$, where $[C=C]_t$ and $[C=C]_0$ is the concentration of carbon double bonds at time *t* and time 0.

Furthermore, the polymerization rate increased when the UV dose was increased, likely due to a faster generation of radicals from the photoinitiator, inducing the formation of the thiyl radicals, which in turn initiated the thiol-ene addition. This effect was weaker for reactions performed in bulk in comparison to reactions performed in miniemulsion. In bulk, when the concentration of the initiator was increased over a certain threshold (Figure 4.1.6A), a decrease in the polymerization rate was observed. Similarly, when the UV dose was increased over a certain point, only marginal variations in the kinetics of conversion were observed (Figure 4.1.6B). These results suggest that a higher concentration of initiating radicals induced rapid termination side reactions competing and hindering the thiol-ene coupling. In addition, the increased viscosity observed at the early stages of the reaction in bulk can also play a role in hindering diffusion and mass exchange. However, in miniemulsion, the presence of the interface controlling the diffusion of the radicals and their entry within the nanoreactor prevented the termination of the growing polymer chains. However, when increasing the irradiance, more radicals were formed, and while this may lead to more recombination and termination in the aqueous phase, this also increased the gradient of concentration across the interface and acted as a driving force to promote the entry of radicals in the droplets. These factors led to the enhancement of the polymerization rate observed in miniemulsion for higher UV doses.

We also examined the evolution of the average molecular weight ($\overline{M}_n$) of the polymer during the reaction (Figure 4.1.10). The results show that as the reaction time increased, the conversion of the monomers increased, and so did the molecular weight of the polymer isolated (Figure 4.1.10A, C) both in bulk and in miniemulsion. Interestingly, $\overline{M}_n$ did not increased in a similar manner with the

monomer conversion when the reaction was performed in bulk or in miniemulsion (Figure 4.1.10B, D). The polymers obtained from both EDDT-DAA and EDDT-DVA in miniemulsion medium not only show higher degrees of conversions after a given reaction time, but also much larger $\bar{M}_n$, even at lower monomer conversions. Typically, the variation of $\bar{M}_n$ in a step-growth polymerization, such as thiol-ene polyaddition, is highly dependent on the conversion of the polymerizable groups,[137,157] and high $\bar{M}_n$ can only be achieved at near complete conversions as described by:

$$\bar{M}_n = M_{rp} \times \bar{X}_n = M_{rp} \left(\frac{1}{1-p}\right) \qquad \text{(eq. 4.1.2)}$$

where $\bar{X}_n$ is the number-average of the degree of polymerization at a monomer conversion p and M_{rp} is the molecular weight of the repetition unit.[158]

Systematically, the $\bar{M}_n$ obtained in bulk mostly followed the trend expected from equation 4.1.2, although minimal deviations were observed at high conversions, likely due to the limited Raman signal from the monomer functionalities at high conversion, affecting the precise quantification of the conversion and potentially the presence of other side-reactions. However, the polymers obtained by the polymerization in miniemulsion had larger $\bar{M}_n$ than what could be expected from equation 4.1.2 for a given monomer conversion.

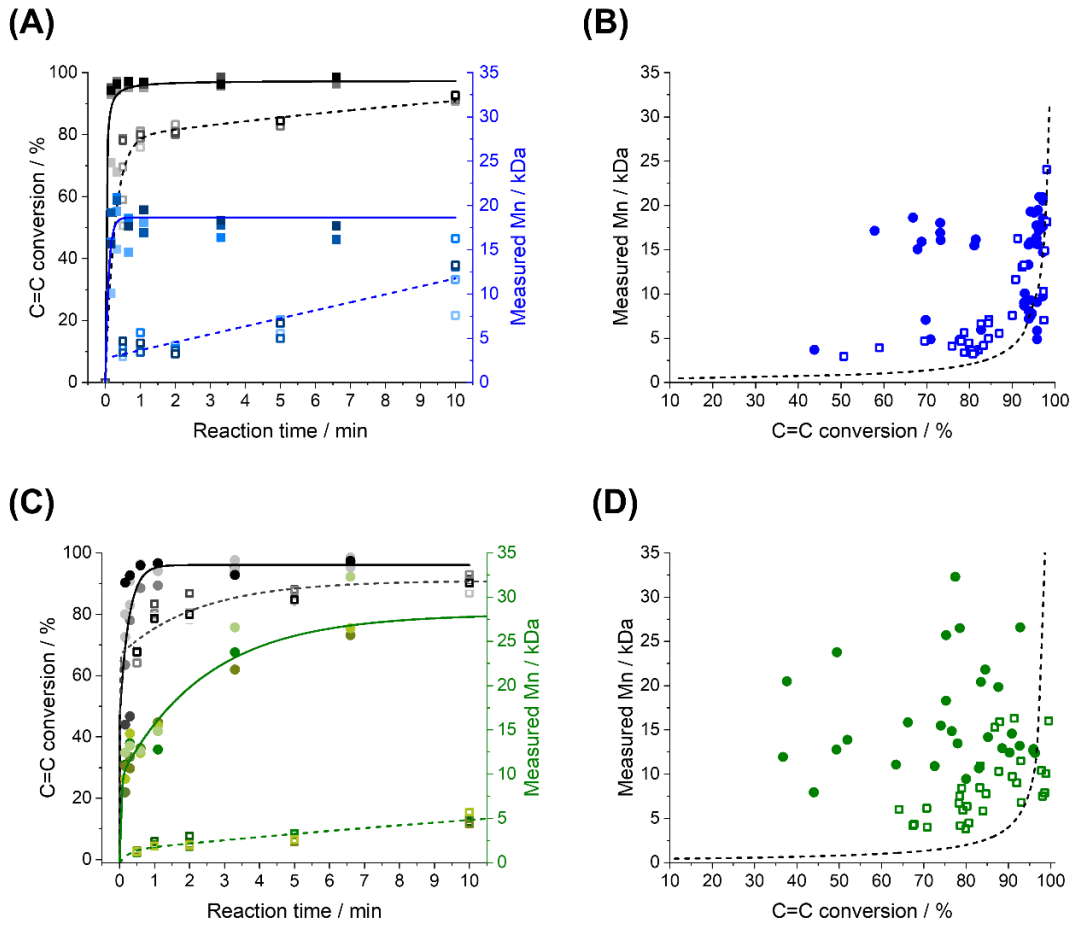

Figure 4.1.10. Effect of the nanoconfinement on the average molecular weight of the polymer ($\bar{M}_n$) for (A, B) EDDT-DAA (blue) and (C, D) EDDT-DVA (green). (A, C) Kinetics of the conversion of enes (left axis, black) and $\bar{M}_n$ of the resulting polymer (right axis, blue) in bulk (dashed line, opened symbols) and in miniemulsion (solid line, closed symbols). (B, D) Influence of the monomer conversion on the $\bar{M}_n$ of the resulting polymers for polymerization performed in miniemulsion (closed circles) and bulk (open squares). The black curve represents a fit to equation 4.1.2.

The molecular weight of polymers synthesized by step-growth polymerization is strongly influenced by the monomer conversion, but also the presence of impurities and stoichiometric imbalance between the reactive functionalities. Figure 4.1.11A shows that the polymerization in miniemulsion was more tolerant to the presence of an off-stochiometric mixture of monomers than the polymerization in bulk. In the presence of a stochiometric excess of one of the monomers, equation 4.1.2 can be rewritten as:

$$\bar{M}_n = M_{rp} \times \bar{X}_n = M_{rp} \left(\frac{(1+E)}{(1+E-2E \cdot p)} \right) \qquad \text{(eq. 4.1.3)}$$

where E is the excess of one monomer ($E = n_{limiting}/n_{excess}$).

Generally, the molecular weights obtained during the polymerization in miniemulsion were larger (15-25 kDa) than those obtained during the polymerization in bulk (4-8 kDa). These results confirmed that the confinement effect promoted by the polymerization in a heterophase system yields high $\bar{M}_n$ polymers, even in off-stoichiometric conditions. Interestingly, mixtures with an excess of enes yielded polymers with higher $\bar{M}_n$, and higher dispersity index (*Đ*), than the ones prepared with an excess of thiols, both in miniemulsion and bulk. This result could stem from side reactions or impurities occurring in the diene rich monomer mixtures in addition to the thiol-ene polymerization, which could lead to mildly crosslinked polymer samples and increasing the dispersity index in off-stoichiometry mixtures, and NMR signals ascribed to the enes homopolymerization were observed for the samples prepared in bulk or in miniemulsion in presence of an excess of dienes (Figure 4.1.12).

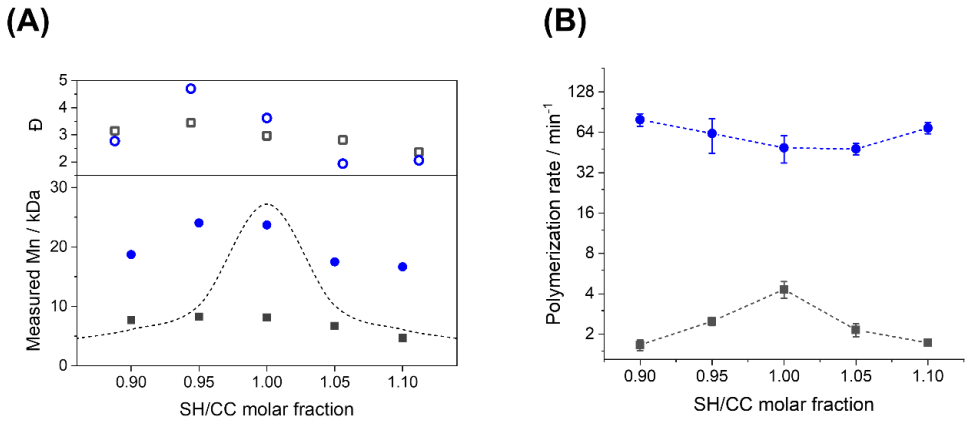

Figure 4.1.11. Effect of excess of di-ene or di-thiol on the polymerization performed in miniemulsion (blue circles) and in bulk (black squares) for the EDDT-DAA monomer mixture. A) Measured $\bar{M}_n$ (close symbols) and dispersity index (*Đ*) (open symbols). The curve represents a fit to equation 4.1.3 for p = 98% of the limiting monomer. B) Reaction rates for polymerizations in bulk and in miniemulsion at different stoichiometry ratios of thiol and ene-monomers. The polymerization rates (*k*) were obtained from fits of the conversion kinetics with $[C=C]_t = [C=C]_0 (1 + e^{-kt})$, where [C=C]t and $[C=C]_0$ are the concentration of carbon double bonds at time *t* and time 0.

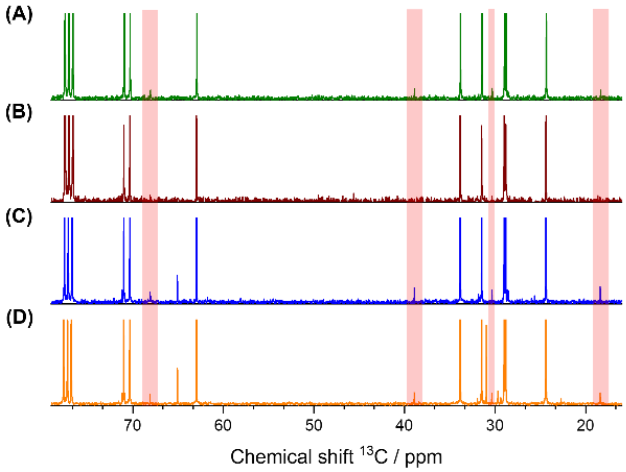

Figure 4.1.12. ^{13}C-NMR spectra of the polymers obtained by photopolymerization of the system EDDT-DAA at (A-B) stoichiometry ratio of monomers in (A) bulk (green) and (B) miniemulsion (brown), and at (C-D) off-stoichiometry ratio of monomers in (C) bulk (blue) and (D) miniemulsion (orange). Shaded areas highlight peaks originating from side-reactions.

The polymerization rates calculated for each stoichiometry also showed the influence of nanoconfinement on the thiol-ene polymerization (Figure 4.1.11B). While the rate of the reactions performed in bulk decreased as the excess of one or the other monomer increased, such a trend was absent for reactions carried out in miniemulsion. In addition to the enhancement of the polymerization rate observed for stoichiometric mixtures of monomer (Figure 4.1.9), the effect of confinement in miniemulsion formulations prevented the decrease in the polymerization rate, even when the reaction was performed with an off-stoichiometric ratio of monomers. This result suggests that in addition to the control entry of thiyl radicals in the miniemulsion droplets, the thiol-ene step-growth polymerization performed in miniemulsion also benefited from the limited diffusion of the monomers, promoted by the interface of the droplets, increasing the rate of favorable collisions, regardless of the presence of 5 or 10% of stoichiometric excess.

4.1.3 Conclusion

The kinetics of the photopolymerization of thiol-ene systems in bulk and miniemulsion conditions was analyzed by Raman spectroscopy. This allowed for the simultaneous detection and quantification of both thiols and ene moieties. The analysis of the polymerization kinetics using Raman spectroscopy allowed us to detect the coexistence of different polymerization mechanisms. This situation was more pronounced in monomer-pairs prone to homopolymerization, such as (meth)acrylates.

Polymerizations performed in miniemulsion showed much higher reaction rates than the ones carried in bulk because of the confinement effect. Each droplet of the miniemulsion contained the two monomers and acted as nanoreactors, promoting higher conversions and yielded polymers with higher molecular weight than what was achieved in bulk. The presence of the interface between the monomer droplet and the continuous aqueous phase regulated the entry of radicals into the nanoreactor, reducing the probability of termination. Moreover, the reduced reaction locus created an environment that restricted the diffusion of the monomers and oligomers by sequestering them within the droplets and could also induce changes in the molecule conformations, both factors leading to an increase in the number of efficient collisions between reacting species. Systematically, higher molecular weights were observed in miniemulsion in comparison to the same polymerization performed in bulk. This phenomenon was even more pronounced when the polymerization was performed with non-stoichiometric mixtures of monomers.

The polymerization of thiol-ene pairs in confinement produced well-defined polymer nanoparticles, with high average molecular weights, larger than what could typically be expected for step-growth polymers produced with the degree of conversion achieved. In addition, the effect of confinement seems not only to enhance the total rate of polymerization, but also to limit the effects associated with the presence of one of the monomers in stoichiometric excess. This is an interesting effect, which can be harnessed to design high molecular weight polymers with well-defined end-group that can be further used for post-polymerization functionalization with an additional thiol-ene coupling reaction.

4.2 Selective oxidation of polysulfide latexes to produce polysulfoxide and polysulfone in a waterborne environment[†]

The previous section described how the effect of confinement affects not only the rates of the thiol-ene polymerization, but also in the properties of the material. Understanding the mechanisms of the reaction in miniemulsion is the first step in the designing of nanoparticles. After the synthetic platform is defined and the basic nanoparticles are prepared, post-polymerization modifications are performed, to tailor the material to a given purpose. Polysulfides are a special type of tunable material. Different from many other polymer platforms, it allows the modification of the core chemistry of the network by the oxidation of the sulfur-centers in the main chains of the polymer. A new range of properties arises from it and these findings are described in the following section. Here, polythioethers are referred as polysulfides to keep the nomenclature used in the paper.

Polymers containing sulfur-centers with high oxidation states in the main chain, polysulfoxide and polysulfone, display desirable properties such as thermo-mechanical and chemical stability. To circumvent their challenging direct synthesis, methods based on the oxidation of a parent polysulfide have been developed but are plagued by uncontrolled reactions, leading either to ill-defined mixtures of polysulfoxides and polysulfones or to polysulfones with reduced degrees of polymerization due to over-oxidation of the polymer. We developed an alternative method to produce well-defined polysulfoxide and polysulfone in waterborne colloidal emulsion using different oxidants to control the oxidation state of the sulfur in the final materials (Figure 4.2.1).

The direct oxidation of water-based polysulfide latexes avoided the use of volatile organic solvents and allowed for the control of the oxidation state of the sulfur atoms. Oxidation of parent polysulfides by tert-butyl hydroperoxide led to the production of pure polysulfoxides, even after 70 days of reaction time. Additionally, hydrogen peroxide produced both species through the course of the reaction but yielded fully converted polysulfones after 24 h. By employing mild oxidants, our approach controlled the oxidation state of the sulfur atoms in the final sulfur-containing polymer and prevented any over-oxidation, thus ensuring the integrity of the polymer chains and colloidal stability of the system. We also verified the selectivity, versatility, and robustness of the method by applying it with polysulfides of different chemical compositions and structures. The universality demonstrated by this method makes it a powerful yet simple platform for the design of sulfur-containing polymers and nanoparticles.

[†] This section is based on the article: "Selective oxidation of polysulfide latexes to produce polysulfoxide and polysulfone in a waterborne environment" by L. Infante Teixeira, H. Thérien-Aubin, K. Landfester. Macromolecules, DOI: 10.1021/acs.macromol.1c00382. Reproduced permission from copyright 2021 Macromolecules. *Macromolecules* 2021, 54, 8, 3659–3667.

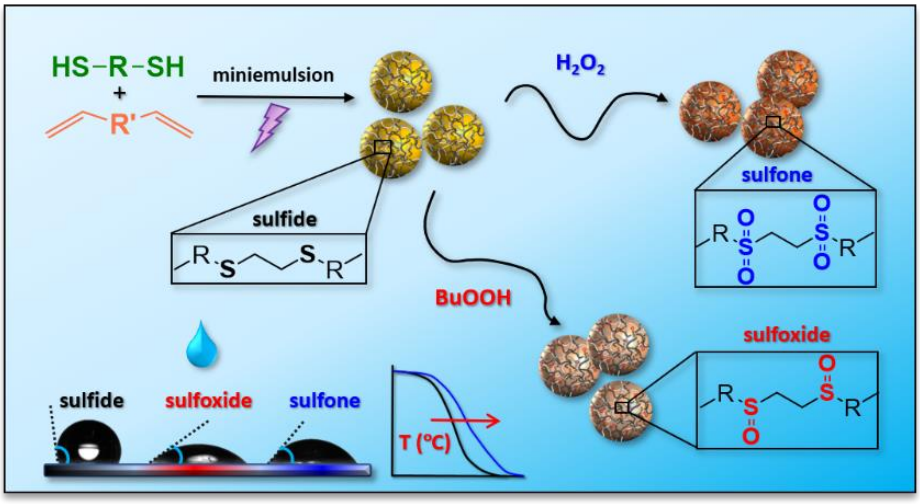

Figure 4.2.1. Schematic representation of the one-pot synthesis of polysulfides, followed by the oxidation with H_2O_2 and tert-BuOOH, producing polysulfones and polysulfoxides, respectively. Results are represented at the bottom. Reproduced from reference [38], with the permission of American Chemical Society.

4.2.1 Introduction

Sulfur-containing polymers are a class of high-performance materials and have been instrumental in the development of specialty applications. While polysulfide (PSR) can be prepared directly from polycondensation,[159,160] the direct synthesis of polysulfoxide and polysulfone is challenging.[50,161] However, the polymers containing sulfur-centers with higher oxidation states, polysulfoxide (PSO) and polysulfone (PSO2), display desirable properties, such as thermo-mechanical and chemical stability.[162,163] Other polymers such as those containing phosphorous are also good examples of how the oxidation state of the main chain heteroatom can influence the properties of the polymer.[164]

To circumvent the synthetic challenge involved in the direct production of PSOs and PSO2s, for example, by Friedel-Crafts polysulfonylation process or a nucleophilic substitution of activated aromatic halides,[165–167] alternative methods based on the oxidation of a parent PSR have been developed.[55,59] This strategy leads to a second drawback: the oxidation is often plagued by uncontrolled reactions, leading to the coexistence of PSO and PSO2 or the depolymerization of the chains due to the over oxidation of the sulfur-centers.[39,58] However, it is of critical importance to produce these oxidized derivatives as pure species to understand and harness the full potential of these PSOs and PSO2s. This critical challenge has been tackled using different approaches, and the selective oxidation of polysulfide materials to either PSO or PSO2 by controlling the oxidation conditions has been achieved for selected polysulfides.[37,59,62] For example, methods based on a delicate balance of the ratio between oxidant and sulfur (II) center have been successful in producing pure oxidized species.[37,62] Alternative methodologies, like selective oxidation based on the use of selenium catalyst, could also be a solution.[168] However, most of these strategies require the use of organic solvents and are incompatible with some polymer systems. To address these limitations, we need to develop an approach based on the use of mild oxidation conditions to yield pure PSOs and PSO2s in polysulfide latex suspensions.

The synthesis of PSO and PSO2 by the oxidation of a parent PSR creates a platform that enables chemical modification of the polymer chains.[169] Such an approach offers a simple and straightforward synthetic method, with unmatched potential in structural versatility as it solely relies on the previously synthesized PSR network. Furthermore, the use of thiol-ene polymerization allows the production of a broad range of parent PSR, bearing various functional groups using suitable monomers.[58,170,171] Previous studies have demonstrated the convenience of the oxidation of parent PSR in different oxidative environments, reporting the synthesis of PSO2s or mixtures of both PSO and PSO2 from a parent PSR in solution, in bulk, of following the immersion of PSR films or 3D objects.[58,172–

[174] Although those processes yield high oxidation-state sulfur-containing polymers, they remain deficient for the production of high-quality PSO and PSO2 in terms of processability, use of volatile organic solvents, but mostly in the poor quantitative control of the composition of either pure PSO or PSO2.

Alternatively, it is possible to use water-based dispersions of PSR as starting material.[39,169,175] From a practical standpoint, the oxidation conditions required for the formation of PSO and PSO2 from a parent PSR are compatible with water-based suspensions, due to the hydrophilic nature of commonly used oxidants. Also, such a method could offer improved processability by circumventing the excessive use of organic solvents and the production of toxic volatile organic compounds (VOC) common to other approaches,[173,174] and by enabling the use of high solid content suspensions without significant variation of the viscosity of the system. Consequently, it is highly beneficial for the large-scale production of PSO and PSO2. However, from the chemical point of view, uncontrolled oxidation or over-oxidation usually follows the synthesis of oxidized derivatives of PSRs, regardless of the medium in which it occurs. Therefore, the resulting oxidized sulfur-containing polymers are either ill-defined mixtures of PSOs and PSO2s or pure PSO2s with reduced molecular weight due to chain scission.[39,176]

To address these issues, a milder and more selective synthetic method is necessary. We propose an approach based on the controlled oxidation of parent PSRs using mild oxidants, such as hydrogen peroxide (H_2O_2) and tert-butyl hydroperoxide (t-BuOOH) in an aqueous environment, to control the oxidation state of the sulfur atoms in the final polymer. The oxidation reaction happens directly in waterborne suspension, avoiding the use of volatile organic solvents during the reaction, as well as taking advantage of the high surface-to-volume ratio of the nanoparticles in suspension for improved reaction kinetics when compared to the same reaction in bulk.[39,175] By employing mild oxidants, our approach provides control over the oxidation state of the final sulfur-containing derivative and prevents any over-oxidation, thus ensuring the integrity of the polymer backbone. Due to this newly gained control, polymers with intermediate oxidation state, PSO, can be synthesized as pure compounds and exploited for potential applications. Here, we also show that the control over the degree of oxidation of the sulfur centers provides a way to tune the properties of the sulfur-containing polymers, such as hydrophilicity and glass transition temperature. Our approach provides unmatched potential in developing a new VOCs-free platform for polymer design with on-demand properties with the simplicity of a one-pot process.

4.2.2 Results and discussions

Miniemulsion photoinitiated thiol-ene polymerization of five PSR NPs was carried out to address the structure-properties relationship of the final NPs and their oxidized derivatives using different monomers mixtures. The different thiol-ene couples investigated were 2,2'-(ethylenedioxy) diethanethiol with diallyl adipate (EDDT-DAA), EDDT with diallyl phthalate (EDDT-DAP), EDDT with limonene (EDDT-LIM), 1,4-dithiol benzene with divinyl benzene (1,4DTB-DVB), and 1,3-dithiol benzene with divinyl benzene (1,3DTB-DVB). Following the irradiation of the miniemulsion with UV light at 385 nm, ^{1}H-NMR spectroscopy was used to quantify the conversion of the allyl or vinyl protons of the di-ene. The characterization of the suspension and the resulting polymers was performed with a combination of GPC, DLS, SEM, TGA, and DSC.

Table 4.2.1. Characterization of the parent polysulfides synthetized. Average molecular weight and dispersion coefficient were obtained by GPC. The conversion was measured by 1H-NMR spectroscopy from the integration of remaining allyl/vinyl protons.

HS/C=C	Conversion (%)	M_n (kg·mol^{-1})	$Đ$
EDDT-DAA	> 99[a]	5020 (125)[c]	2.4 (0.1)
EDDT-DAP	> 99[a]	15000 (200)	2.8 (0.1)
EDDT-LIM	97[a]	5800 (1000)	2.7 (0.3)
1,3DTB-DVB	91[a]	2330 (20)	7.1 (0.3)
1,4DTB-DVB[2]	90[b]	2300 (50)	2.1 (0.4)

[a] Measured in $CDCl_3$
[b] Measured in d_6-DMSO
[c] The numbers in parenthesis are the standard deviations

The colloidal properties of the PSR NPs (size and polydispersity index) were largely independent of the monomer mixture used, while the polymer chains composing the PSR NPs displayed distinct properties. The number-average molecular weight ($\overline{M}_n$) of the polymer prepared varied significantly for the different thiol-ene couples (Table 4.2.1). The final $\overline{M}_n$ of the PSR polymers was highly dependent on the degree of conversion of the monomers, a direct consequence of the step-growth mechanism of the thiol-ene polycondensation reaction. The conversion was more limited for the less reactive dienes,[4,177] like limonene. Additionally, certain dithiols, like the dithiol benzene, contained up to 4% of impurities in the form of monothiol derivatives influencing the stoichiometry of the reaction and the extent of conversion of the monomers. Those thiol-ene couples resulted in lower conversions, as measured by NMR spectroscopy, and yielded polymers with lower $\overline{M}_n$.

The conversion of those parent PSR NPs suspensions, through oxidation, yielded the targeted polysulfone (PSO2) and polysulfoxide (PSO) NPs (Figure 4.2.2). The oxidation of sulfur-containing polymer NPs has been used to trigger the release of payloads.[176,178–181] However, such an approach relies on the over-oxidation of the sulfur centers to initiate the degradation of the polymer network leading to the release of the encapsulated payload, but has been incompatible in isolating pure PSO and PSO2 NPs. Consequently, one of the main challenges faced when using oxidants in the presence of PSR to PSO or PSO2 is the uncontrolled oxidation leading to the formation of a mixture of PSR, PSO, and PSO2 or even to the complete degradation of the main chain due to the over-oxidation of the sulfur center in the backbone.[39,182] To gain more control over the oxidation reaction, we analyzed the kinetics of the conversion of aqueous suspensions of PSR NPs in the presence of low concentrations of two different oxidizing agents (Figure 4.2.3).

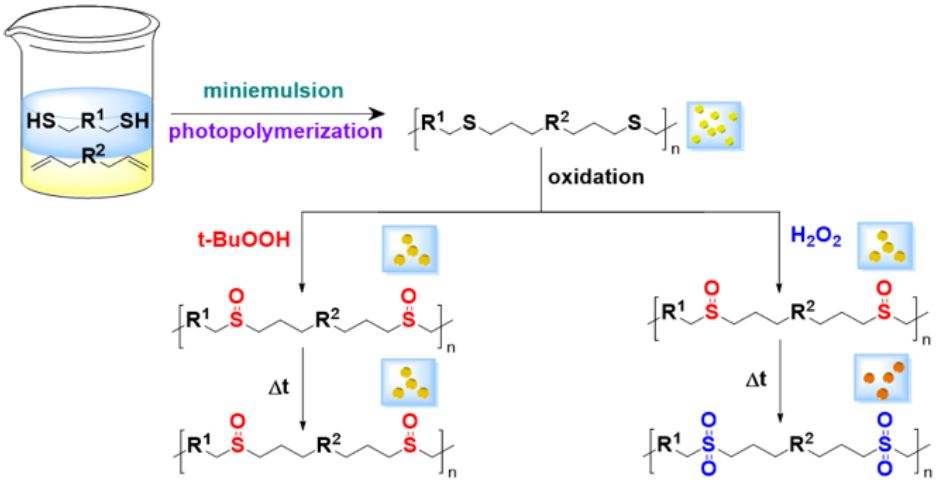

Figure 4.2.2. Scheme of the synthesis and oxidation of polysulfide nanoparticles in water-based suspension. Different oxidants and reaction conditions can yield nanoparticles with different degrees of oxidation.

The NPs prepared with EDDT-DAA were used as a model PSR to study the different oxidation conditions. The kinetics of the oxidation with H_2O_2 was monitored by FTIR and ^{13}C-NMR spectroscopy (Figure 4.2.3 and Figure 4.2.4). H_2O_2-mediated oxidation is known to promote a stepwise type of oxidation of the sulfur-centers, going from sulfur (II) to sulfur (IV) in a matter of minutes, and then to sulfur (VI) in a later stage of the reaction.[174,179,183] Figure 4.2.3 shows the formation of PSO and PSO2 over time as monitored by FTIR spectroscopy. As the reaction progressed, a peak at ca. 1030 cm^{-1} appeared within the first 15 min of the reaction; this peak belonged to the stretching mode of the SO bond and was characteristic of the presence of sulfoxide groups. Then, after 2 h of reaction, a peak characteristic of SO_2 stretching at ca. 1122 cm^{-1} appeared, indicating the formation of sulfone groups. After 48 h of reaction, only the SO_2 peak had a detectable signal. The results suggest the concomitant

formation of PSO and PSO2. However, the vibration of the C-S bonds was very weak in FTIR, and it was challenging to ascertain the complete oxidation of the parent sulfide using this method.

Using ^{13}C-NMR spectroscopy, it was possible to track the progress of the reaction by following the signal from the carbon atoms in α and β of the sulfur centers in the EDDT-DAA PSR and analyzing the conversion of the PSR network. Figure 4.2.4A shows the NMR spectra of EDDT-DAA PSR NPs after different reaction times. During the reaction, there were clear changes in the chemical environment within the polymer, the β -carbons shifting upfield while the α-carbons shifted downfield. Figure 4.2.4B shows that all the S(II) centers were rapidly converted in a mixture of S(IV) and S(VI), as a result of the autocatalytic nature of the reaction with H_2O_2.[173,184,185] After 30 min of reaction, all the sulfur(II) atoms of the parent PSR were converted in a mixture of ca. 77%$_{mol}$ of PSO and 23%$_{mol}$ of PSO2. As the reaction progressed further, all the PSO were converted in PSO2 after 48h. Consequently, a strong oxidizing agent, like H_2O_2, even in a dispersed media, is not adapted for producing pure PSO. Milder reaction conditions were necessary to isolate the pure PSO NPs.

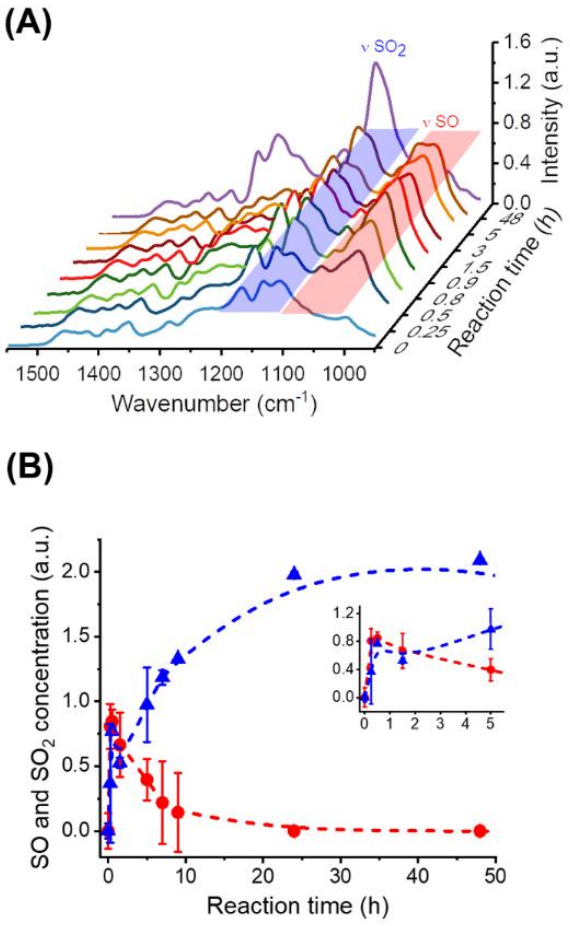

Figure 4.2.3. Oxidation kinetics of polysulfide NPs by H_2O_2 measured by FTIR spectroscopy. A) FTIR spectra over time, showing the appearance of both SO and SO2 species, B) Relative concentration of SO (red) and SO2 (blue) in the polymer nanoparticles. The inset shows the initial 5 h of the reaction kinetics.

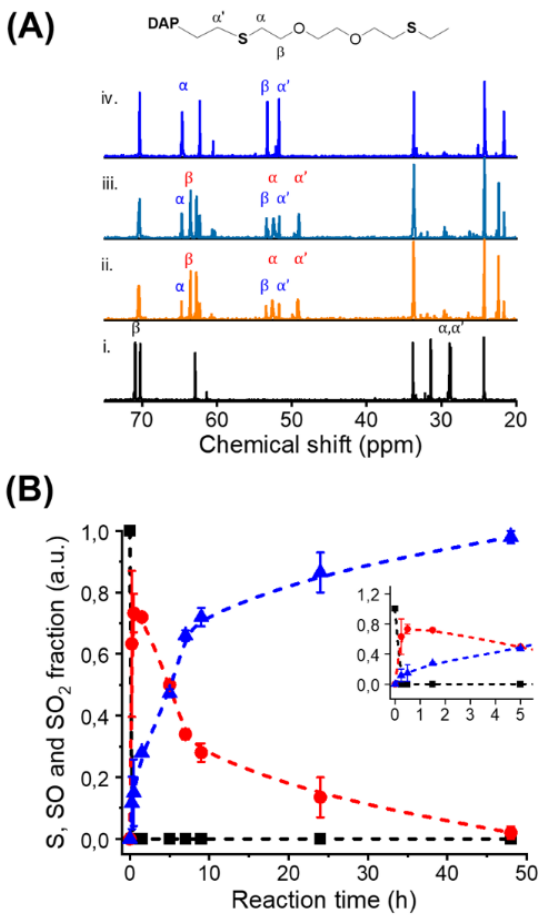

Figure 4.2.4. Oxidation kinetics of polysulfide NPs by H_2O_2 measured by ^{13}C-NMR spectroscopy. A) ^{13}C-NMR spectra of the polymer NPs, after i. 0 h, ii. 5 h, iii. 10 h, and iv. 24 h of oxidation, showing the formation of SO (red) and SO2 (blue) species, and the disappearance of parent sulfide (black). B) Concentration of S (black), SO (red) and SO2 (blue) in the polymer nanoparticles. The inset shows the initial 5 h of the reaction kinetics.

To promote the formation of PSO, the aqueous suspensions of PSR NPs of EDDT-DAA were reacted using t-BuOOH instead of H_2O_2 as the oxidizing agent, since alkyl peroxides provide milder reaction conditions than hydrogen peroxide.[186,187] Figure 4.2.5 shows the variation of the oxidation state of the PSR NPs after 24 h of reaction with H_2O_2 and t-BuOOH. The ^{13}C spectra of the polymer NPs obtained after 24 h of reaction with either H_2O_2 or t-BuOOH clearly showed that the composition of the polymer changed during the reaction. When treated with H_2O_2, the sample transitioned from PSR to PSO and then to PSO2, and after 24 h of reaction, only PSO2 was visible on the NMR spectra.

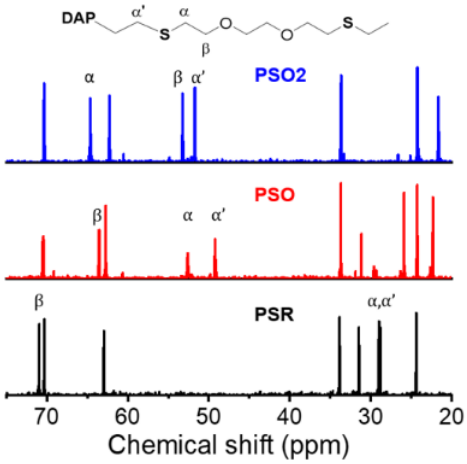

Figure 4.2.5. Selective and controlled reaction with different oxidants. ^{13}C-NMR spectra of pure polysulfide (black), polysulfoxide (red) and polysulfone (blue). The polysulfoxide was produced by the oxidation of the parent PSR with t-butyl hydroperoxide, and the polysulfone with hydrogen peroxide.

After the same reaction time, only the samples reacted with t-BuOOH displayed PSO groups, characterized by the carbons in the vicinity of the sulfur at 49.2 and 52.6 ppm. The results obtained both by ^{13}C-NMR (Figure 4.2.5) and by FTIR spectroscopy (Figure 4.2.6) confirmed this result. Using a mild oxidant like t-BuOOH, we successfully realized the selective synthesis of the intermediate oxidation state PSO. The results showed that using the right oxidizing agent could lead to the quantitative conversion of the PSR in either the PSO or the PSO2.

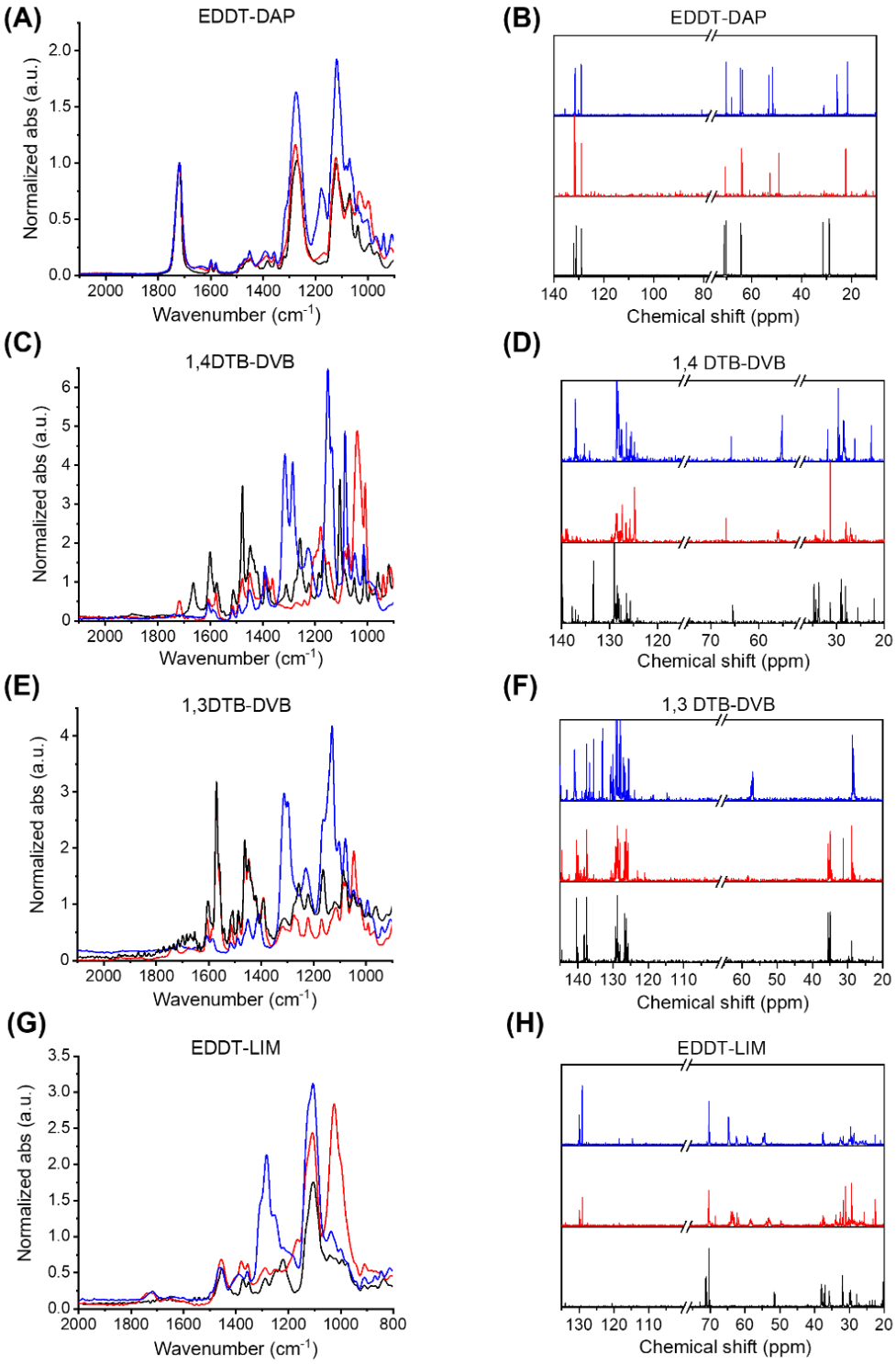

Figure 4.2.6 - Characterization of the selective oxidation of polysulfides by H_2O_2 and t-BuOOH. FTIR and ^{13}C-NMR spectra taken from each polysulfide (black), and their oxidated derivatives, polysulfoxide (red) and polysulfone (blue). Spectra were gathered in A-B) for EDDT-LIM, C-D) EDDT-DAP, E-F) 1,3DTB-DVB, and G-H) for 1,4DTB-DVB group of sulfur-containing polymers.

The selectivity of the reaction observed can be attributed to the redox potential of the oxidant,[188] and to the fact that the transition from PSO to PSO2 requires a stronger oxidizing power than the potential involved in the formation of PSO from PSR.[186,189,190] Secondary radicals such as alkyl peroxides are less reactive and thus more selective, offering milder options to control redox processes.[186,187,191–193] The present results show that the alkyl peroxide was not a strong enough oxidant to oxidize PSO to PSO2. Moreover, experiments carried out for 70 days with samples reacted with t-BuOOH showed no formation of PSO2 by FTIR and ^{13}C-NMR spectroscopy.

A common challenge observed during the oxidation of PSRs is their over-oxidation leading to the depolymerization of the polymer chains or the degradation of colloids.[39,176] In addition, when the reaction is occurring in suspension, the addition of reagent to the continuous phase has the potential to destabilize the colloids.[194] Figure 4.2.7 shows that the colloidal stability and the polymer integrity were preserved during the oxidation of PSR NPs to PSO and PSO2 NPs. Characterization of the $\overline{M}_n$ of the polymers (EDDT-DAA and EDDT-DAP) by GPC after 24 h of oxidation with either H_2O_2 or t-BuOOH displayed no variation in $\overline{M}_n$ that would indicate the occurrence of chain scission events during the oxidation reaction (Figure 4.2.8).

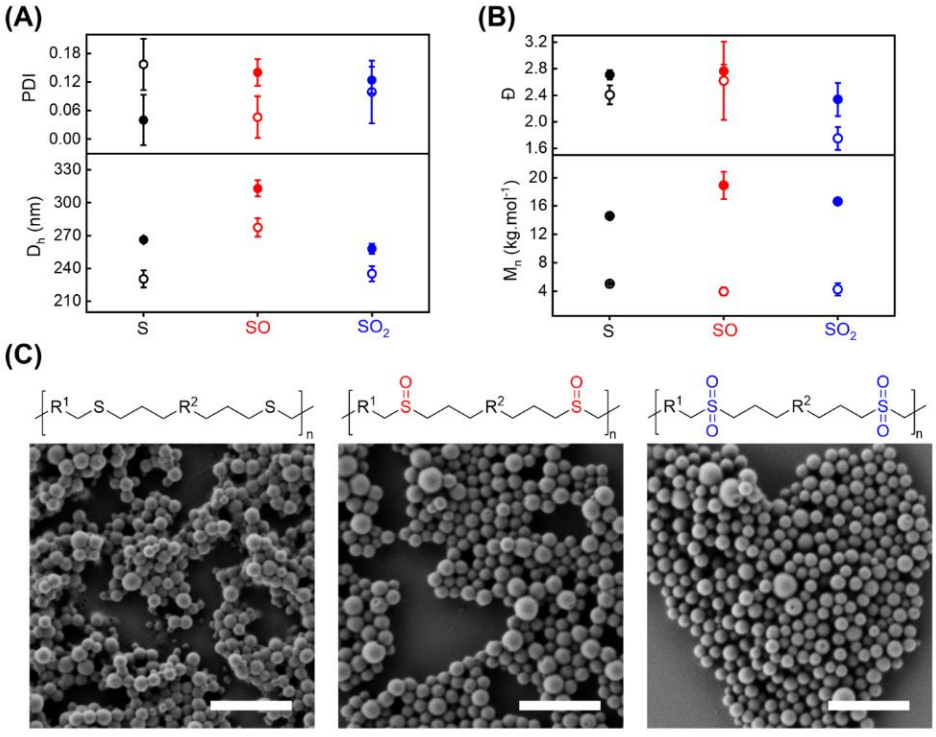

Figure 4.2.7. Colloidal stability and integrity of the polymer chains and NPs during oxidation for the parent polysulfide produced by the photoinitiated thiol-ene emulsion polymerization of 2,2'-(ethylenedioxy)diethanethiol and diallyl phthalate (solid symbols) or diallyl adipate (open symbols) in their original polysulfide (black), polysulfoxide (red) or polysulfone (blue) oxidation state. A) Hydrodynamic size and polydispersity index of the NPs measured by DLS indicating an increase in size for the polysulfoxide NPs. B) $\overline{M}_n$ and dispersity of the polymer's chains with different degrees of oxidation measured by GPC in

DMF. C) Scanning electronic microscopy pictures of the NPs. These NPs were cross-linked using triallyl phthalate to prevent the deformation of the soft and rubbery non-cross-linked NPs. Scale bars in SEM pictures stand for 500 nm.

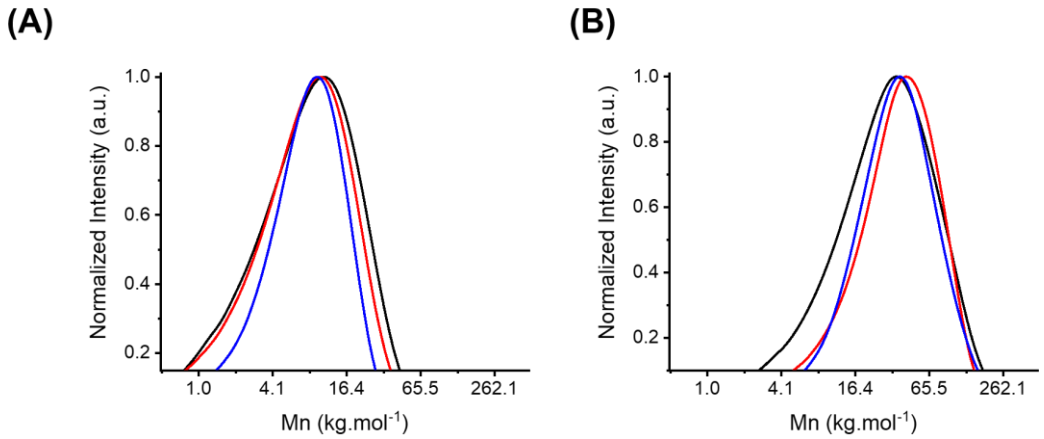

Figure 4.2.8. GPC traces of polysulfide (black), polysulfoxide (red), and polysulfone (blue) of (A) EDDT-DAA, and B) EDDT-DAP systems.

The size of the NPs measured by DLS during the reaction also did not show signs of degradation. First, during the formation of the PSO NPs a limited swelling (ca. 20%) of the NPs was observed. This phenomenon resulted from an increase in the hydrophilicity of the network, leading to an increased influx of medium into the core of the NPs.[182,195] However, when the NPs were fully oxidized to PSO2 NPs, the size of the oxidized NPs was similar to the size of the parent PSR NPs, suggesting that the PSO2 NPs were either less hydrophilic than the PSO NPs or that the interchain interactions were stronger in the PSO2 NPs than in the PSO NPs. Furthermore, the SEM images of the dry NPs showed no difference in the size of the NPs containing sulfur atoms with different oxidation states (Figure 4.2.7 and Figure 4.2.9). This observation indicates that the increase in size observed for the PSO NPs in suspension was likely the result of stronger intermolecular interactions with water molecules in PSOs than in PSO2 case, leading to the preferential swelling of the PSO in keeping with the higher H-bonding of SOs derivatives observed previously.[196–198] The analysis of the NPs by SEM before and after oxidation did not show any detrimental effects of the reaction on the size nor the morphology of the NPs, corroborating the results obtained by GPC. We observed the same behavior during the oxidation of every parent PSR NPs (Figure 4.2.10).

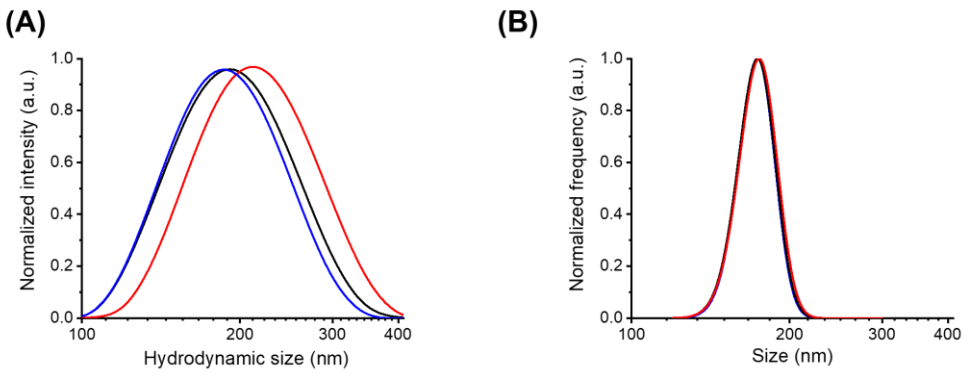

Figure 4.2.9. Comparison of the sizes of TAP-EDDT cross-linked NPs at different degrees of oxidation measured A) in suspension by DLS, and B) as dried particles by SEM imaging for the polysulfide (black), polysulfoxide (red), and polysulfone (blue). The data indicate a preferential swelling of PSO NPs when in suspensions (A), which was not observed in dried state (B).

Different parent PSR NPs were prepared and oxidized with both H_2O_2 and t-BuOOH (Figure 4.2.10A). Every case resulted in NPs with preserved colloidal stability and degree of polymerization, with a controlled oxidation state of the sulfur atoms, from S (II) to either fully S (IV) or fully S (VI) (Figure 4.2.6). For every parent PSR NPs used, a similar swelling (ca. 20%) of the NPs was observed after oxidation to PSO but the swelling decrease to only ca. 3% for the PSO2 (Figure 4.2.10B), as observed with EDDT-DAA (Figure 4.2.7). Although the oxidation reaction of the PSR network did not significantly influence the size and stability of the polymer NPs in suspension, the properties of the resulting oxidized polymers were. Films cast from the polymers after oxidation showed an increase in hydrophilicity for the oxidized derivatives (Figure 4.2.10C and Figure 4.2.11), resulting in a lower water contact angle on the films prepared with PSO and PSO2 in comparison to those made with PSR. However, the difference between the wetting of PSO and PSO2 was limited. The increased hydrophilicity of the oxidized derivatives was due to dipolar interactions between the polymer chains and the solvent and can potentially be harnessed in the design of biomaterials for *in vivo* applications.[62,199–201]

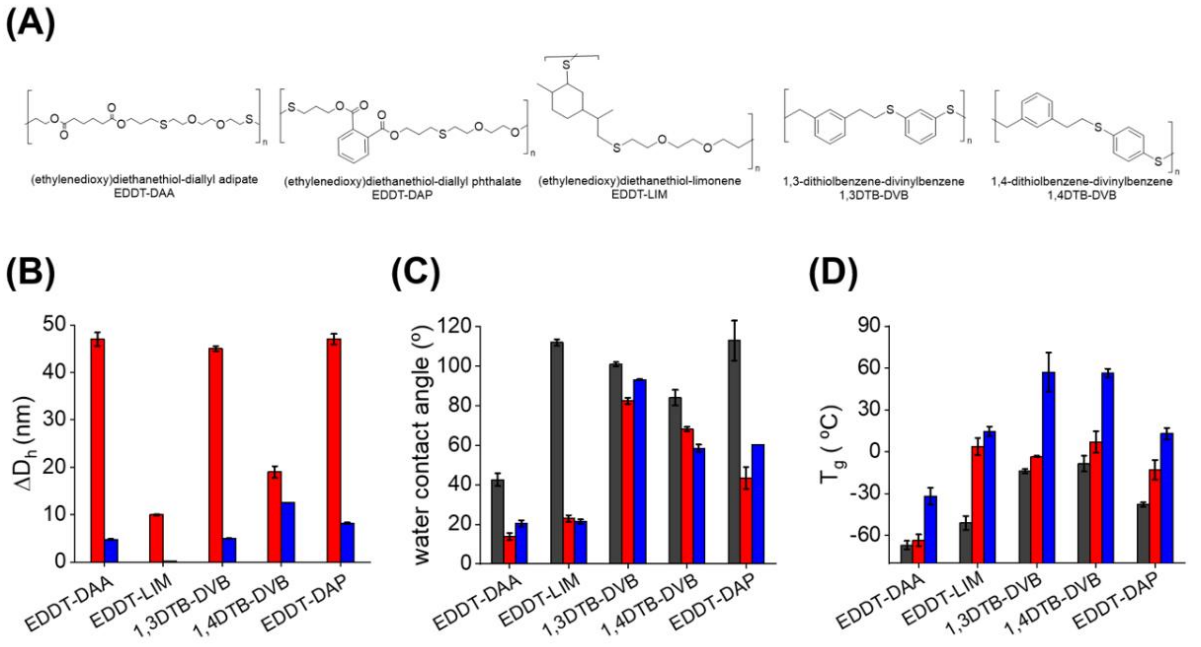

Figure 4.2.10. Properties of a library of sulfur-containing polymers. A) Structures of the thiol-ene couple used as parent polysulfides. B) Variation of the hydrodynamic diameter of the nanoparticles in suspension, C) Water contact angle, and D) glass transition temperatures of the parent polysulfides (black) and their oxidized derivatives polysulfoxides (red) and polysulfones (blue).

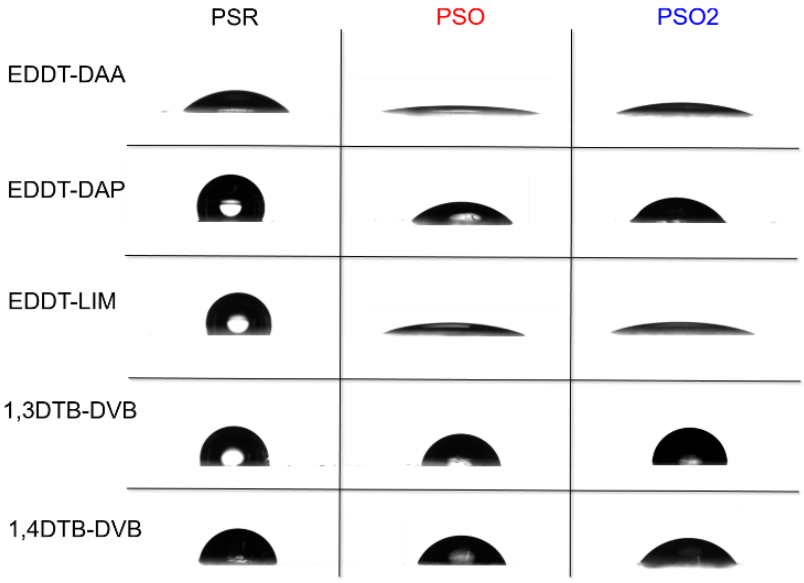

Figure 4.2.11. Photography of water droplets on the surface of glass slides covered with film of polymers. The contact angle of the water droplets, i.e., hydrophilicity, on the surfaces of the films decrease after oxidation, and was the lowest for the polysulfoxides.

The oxidation state of the sulfur centers also influenced the thermomechanical properties of the polymers. As the oxidation state increased, the glass transition temperatures (T_g) of the polymer also increased (Figure 4.2.10D). In the case of the parent PSRs containing aromatic moieties, the polymers prepared with the cyclic monomers dithiol benzene and divinyl benzene, yielded the polymers with higher T_g in comparison to the polymer prepared with aliphatic structures due to the strong interchain interactions created by π-π stacking.

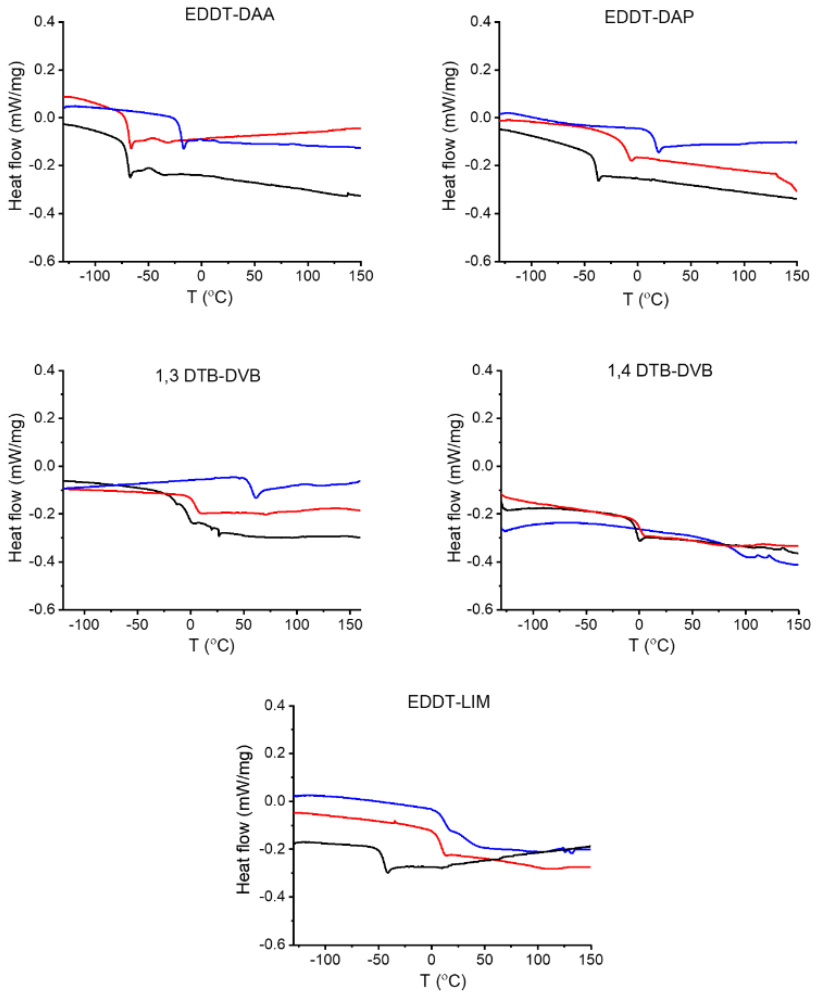

Figure 4.2.12. DSC traces of polysulfide (black), polysulfoxide (red), and polysulfone (blue) of all systems.

The oxidation reaction of PSR to PSO resulted in only a limited increase in T_g. However, after the formation of fully oxidized PSO2, the T_g steeply increased, possibly due to the loss in flexibility caused by the interchain dipolar interactions between the sulfone groups (Figure 4.2.12).[37,58] Furthermore, the oxidation state of the sulfur atoms also influenced the thermal degradation of the polymers (Figure 4.2.13 and Table 4.2.2). The thermal stability of the network decreased upon the formation of PSOs. For most polymers, the onset of degradation decreased by ca. 120 °C, but only by

ca. 10 – 20 °C for the polymers prepared with the aromatic dithiol. In general, the formation of SO groups in the polymer backbone destabilized the polymer network and led to an early decomposition. This effect likely occurred due to a Pummerer elimination in the sulfoxide-containing polymers, in which the rearrangement of the SO groups within the chains led to the rapid degradation of the polymer scaffold.[37,179,202] As the oxidation is pushed further and the fully PSO2s polymers were formed, the thermal stability increased. While some poly(olefin sulfone)s can show self-immolative properties,[203,204] the backbone of the PSO2s formed by thiol-ene addition followed by oxidation yielded thermally stable polymer materials. However, the thermal stability of the PSO2s was the highest in comparison to PSOs and similar to PSRs.

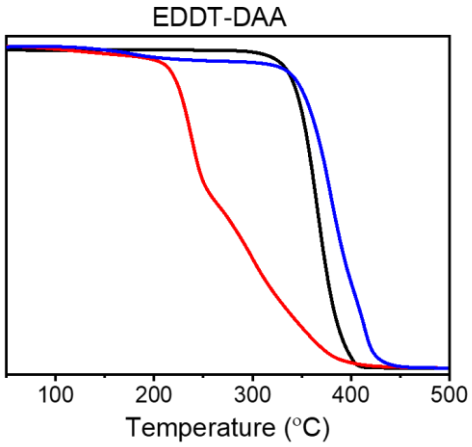

Figure 4.2.13. TGA curves of polysulfide (black), polysulfoxide (red), and polysulfone (blue) of EDDT-DAA system.

Table 4.2.2. Degradation temperature of the polymers before and after oxidation measured by TGA.

HS/C=C	PSR	PSO	PSO2
EDDT-DAA	368 (3)	244 (3)	382 (2)
EDDT-DAP	362 (2)	246	340 (1)
EDDT-LIM	355 (5)	236 (6)/ 295 (9)	353 (2)
1,3DTB-DVB	350 (14)	333 (8)	340 (3)
1,4DTB-DVB	335 (5)	327 (4)	347 (3)

The numbers in parenthesis are the standard deviations

The characterization of the polymers produced from the different parent PSRs showed that the oxidation reaction increased the polarity of the polymer backbone, regardless of the parent polysulfide backbone without adverse effects on the colloidal suspension. However, only the presence of SO_2 groups increased the thermal stability of the polymer, while the intermediate SO groups induced a decrease in thermal stability but provided the polymer with a higher wettability. The production of well-defined PSRs, PSOs and PSO2s with distinct physicochemical properties paves the

way to use those new materials in an array of applications, from control drug delivery systems to smart coatings.

4.2.3 Conclusion

Controlled oxidation of parent polysulfides nanoparticles in waterborne suspensions yielded either pure polysulfoxides or pure polysulfones latexes. Photoinitiated thiol-ene emulsion polymerization was used to generate a library of parent polysulfide nanoparticles. Then, employing two distinct oxidants, tert-butyl hydroperoxide, and hydrogen peroxide, the reactions were effective in both controlling the oxidation state of the sulfur atoms, as well as keeping the colloidal stability of the nanoparticles and the integrity of the polymer chains within the nanoparticles.

Oxidation of polysulfides by H_2O_2 led to the formation of polysulfones after 24 h long reaction time. Kinetics studies of the oxidation via H_2O_2 showed the coexistence of sulfone and sulfoxide throughout the reaction until the full conversion into polysulfone, highlighting the need for a method based on the selective control of the reaction to produce pure polysulfoxide. Conversely, the reaction with tert-butyl hydroperoxide, a milder oxidant, allowed for the selective production of polysulfoxides.

In addition, the oxidation process was robust and versatile, yielding fully oxidized polysulfoxide or polysulfone using a variety of parent polysulfides. With control over the conversion of the pure oxidized species, we analyzed the unique physicochemical properties of the polysulfoxides and polysulfones. The polysulfones displayed better thermal stability and a higher glass transition temperature than the parent polysulfides and the polysulfoxides, while the polysulfoxides displayed higher hydrophilicity than the polysulfides and the polysulfones. The synthetic process introduced here provides a robust synthetic platform to control the design of sulfur-containing polymers with a wide range of finely tuned physicochemical properties, and the resulting materials can find applications as controlled release systems with enhanced “stealth effect” or as the next generation of packaging materials.

4.3 Surface functionalization of polythioether nanoparticles by thiol-ene coupling

Different strategies can be used to control the properties of polymer nanoparticles and their interaction with their environment. The previous section showed how oxidation could be employed to tune the properties of the polymer nanoparticles prepared by thiol-ene photopolymerization in miniemulsion. The chemical composition of the core was modified to obtain either polysulfoxide or polysulfone latexes from the oxidation of a parent suspension of polythioether nanoparticle suspension. The modification of the oxidation state of the sulfur-centers in the polymer chains promoted changes in the properties of the materials, from their thermo-mechanical behavior to their hydrophilicity. An alternative method to tune the properties and behavior of a polymer nanoparticle consists in the functionalization of the surface of the NPs. In this section, the post-polymerization coupling is used to covalently attach different molecules on the surface of the NPs by thiol-ene click chemistry.

4.3.1 Introduction

Polymer nanoparticles are increasingly used in the biomedical field.[79,205] Some of the key advantages of using polymer nanoparticles in the design of drug delivery systems are that they are more stable and more tunable than other nano-delivery systems. For example, they can be used for the controlled transport and delivery of drugs in vivo, where they display improved properties, especially in terms of stability, in comparison with traditional nano-drug delivery systems like liposomes.

One important hurdle in using polymer nanoparticles for the design of drug delivery vehicles is to predict and control their behavior in vivo. For example, after systemic injection, the fate of the nanoparticles is influenced by an array of factors, with one of the most important being the circulation time of the particles.[206] The circulation time of a nanoparticle in vivo and its stability in biological media are influenced by its size and shape, its chemical composition, and its surface chemistry.[207]

A common method to control the properties of nanocarriers, in terms of their circulation time in vivo, relies on their surface functionalization using highly hydrophilic coatings, like a shell of grafted poly(ethylene glycol) chains that will prevent the adhesion of proteins and biomolecules,[25] which is the first step in the removal of foreign entities from a biological system.

The design of biologically active nanomaterials requires a robust platform for efficient nanoparticle synthesis, cellular targeting, and controlled drug release. Strategies based on the post-polymerization modifications of polymer latexes are used to provide specific functionalities to the nanocarriers that can control their behavior in vivo. With that goal in mind, thiol-ene systems offer an unmatched potential for both polymer synthesis and surface modification.

Thiol-ene systems prepared with dithiol and diene monomers present at a non-stoichiometry ratio yield polymers with well-defined end groups, with the functionality in excess as the preferential end-group. When off-stochiometric monomer mixtures are used to prepare NPs thiol-ene polymerization, the surface of the NPs will present an excess of either thiol or ene, which can be further functionalized to tailor the properties of the nanoparticle (Figure 4.3.1). One key advantage of thiol-ene chemistry is the ubiquitous presence of thiol-moieties in biomolecules, enabling the covalent attachment of those biomolecules to the surface and introducing new functionalities relevant for biomedical purposes. The strategy relies on manipulating the thiol-ene polymerization (Section 4.1) and understanding how off-stoichiometric ratios of monomers can be used with no detrimental impact on the stability and performance of the colloidal suspensions.

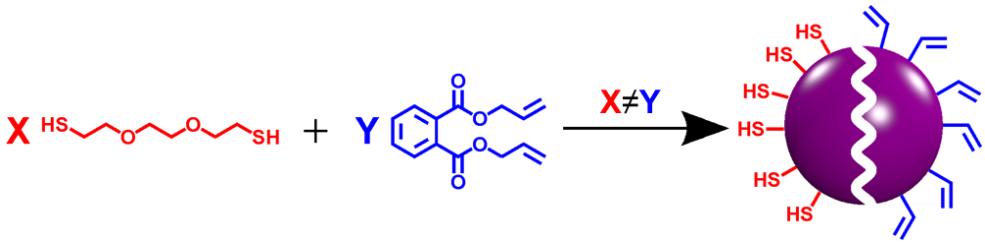

Figure 4.3.1. Scheme of the synthesis of polythioether nanoparticles with remaining unreacted functionalities for further functionalization. According to the monomer in excess, the surface of the nanoparticles can present enes or thiols for post-polymerization reactions.

Here we evaluated the feasibility of the functionalization of nanoparticles (NPs) prepared with off-stoichiometric ratios of monomers by thiol-ene chemistry. Biomolecules of different hydrodynamic sizes were employed to investigate the influence of steric hindrance and grafting density on the reaction in waterborne colloidal suspensions of polythioether nanoparticles (Figure 4.3.2).

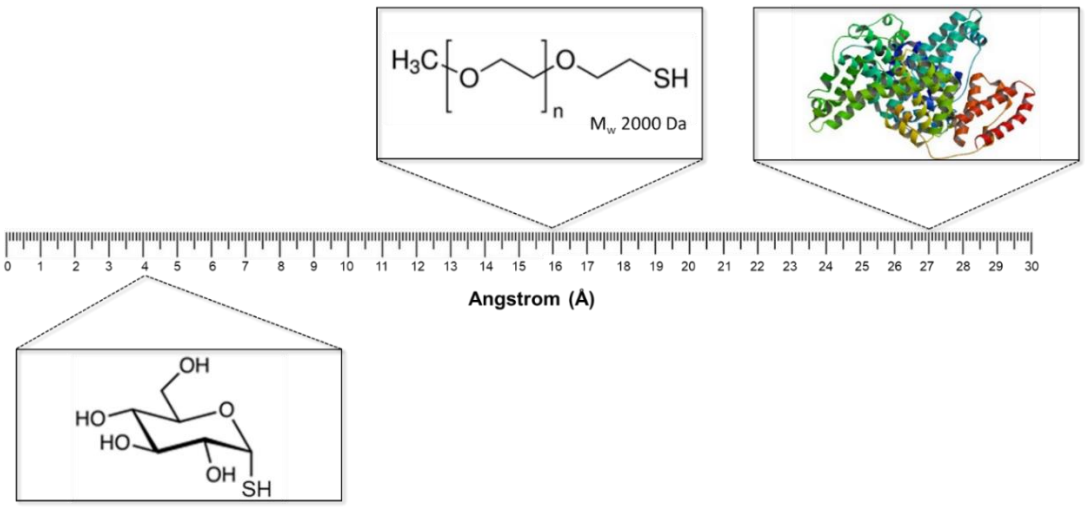

Figure 4.3.2. Schematic representation of the chemical structures of molecules used to modify the surface of the nanoparticles and a qualitative scale of their gyration (R_G) or hydrodynamic radius (R_H): Thioglucose (R_H = 4 Å),[26] PEG-SH 2 kDa (R_G ≈ 16 Å),[208] and Bovine Serum Albumin (BSA – R_G ≈ 27.6 Å).[209] The structure of the BSA was obtained from RCSB PDB (public domain).

4.3.2 Results and discussions

I. Free functionalities for post-polymerization modification

Polythioether nanoparticles were prepared by photopolymerization in miniemulsion. Mixtures of a diene and a dithiol with an excess of either moiety of up to 25%$_{mol}$ were used in the preparation of the nanoparticles. The variation of the monomer feed did not influence the formation of the polythioether nanoparticles, and the size and size distribution of the NPs remained stable for all the monomer mixtures (Figure 4.3.3A). The range of off-stoichiometric ratios used did not affect the colloidal suspension, since the diameter of the nanoparticles depends mainly on the emulsion conditions.

After the synthesis of the polythioether nanoparticles, the samples were purified to remove any unreacted monomers. The number of functionalities available after the polymerization process was assessed either by ^{1}H-NMR spectroscopy for ene-rich samples by integrating the signal of the protons on the unsaturated carbons, or in the case of the thiols, by the Ellman's test, a colorimetric assay specific to sulfhydryl groups. The quantification of the unreacted ene or thiol present in the system yielded the number of functions per surface area of the nanoparticle (Section 3.10.1). Figure 4.3.3B shows that the polymerization in the presence of an excess of diene or dithiol monomers was efficient in providing accessible functions on the surface of the particles.

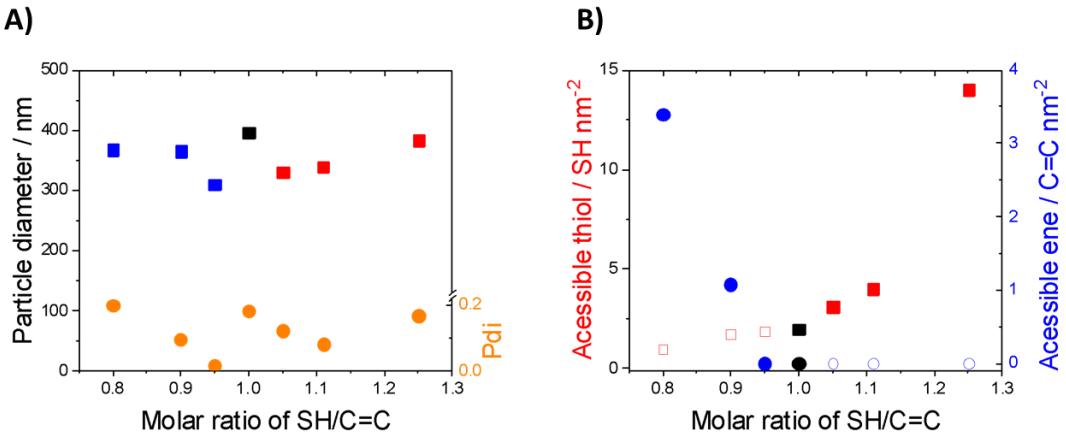

Figure 4.3.3. Nanoparticles prepared with off-stoichiometry ratios between thiol and ene-moieties. A) Hydrodynamic sizes of these nanoparticles at each molar ratio between the functions. B) Number of accessible thiols per surface area (nm^2) in red, and number of accessible C=C double bonds per surface area (nm^2) in blue. Conditions: the number of accessible enes at the surface of the NPs was calculated as 1% of the total number of enes obtained by $CDCl_3$ ^{1}H-NMR spectroscopy.

II. Grafting of polyethylene glycol derivatives

Post-functionalization of the polythioether nanoparticles prepared by photopolymerization in miniemulsion was realized using the thiol-ene conjugation. The nanoparticles prepared with an excess of either ene or thiol on their surface can react with either thiol-functionalized or ene-functionalized molecules (Figure 4.3.4). Here, NPs of polythioether with an excess of ene end-groups were preferably prepared, owing to a wide range of naturally occurring thiolated biomolecules available.

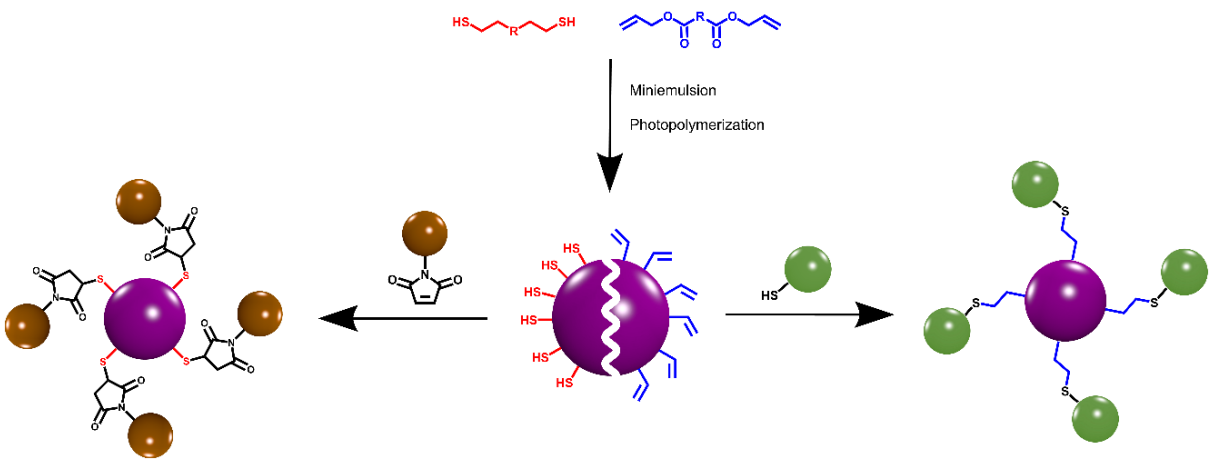

Figure 4.3.4. Schematic representation of the synthesis of polythioether NPs with thiol or ene end-groups and their functionalization with generic molecules through a thiol-ene reaction with their respective counterpart moieties.

Firstly, the polythioether NPs with an excess of ene-moieties were reacted with thiolated polymers. Polyethylene glycol (PEG) is a well-known polymer used to tailor the properties of nanoparticles with respect to their interaction with proteins. Here, thiol-PEG (PEG-SH 2 kDa) was used in the functionalization of the surface of ene-rich nanoparticles (Figure 4.3.4). Latexes of polythioether NPs with different feed concentrations of PEG-SH were prepared and reacted in the presence of a photoinitiator (Section 3.9).

Figure 4.3.5 shows the relationship between the resulting grafting density on the surface of the NPs and the feed concentrations of PEG-SH 2 kDa in the initial suspensions. The grafting density of the PEG chains increased by increasing the amount of PEG in the feed. The maximal grafting density observed was of 1.2 chains/nm^2, and at this density the PEG chains are considered to be in the conformational transition regime between mushroom and brush.[26] The gyration radius of the PEG-SH 2 kDa molecule is ca. 1.6 nm.[208] Consequently, the footprint of a coiled PEG chain will be ca. 8 nm^2, which would correspond to a grafting density of 0.125 chain/nm^2. However, the footprint of a PEG

chain in a pure brush conformation would be ca. 0.3 nm^2 corresponding to a grafting density of 3.3 chains/nm^2.

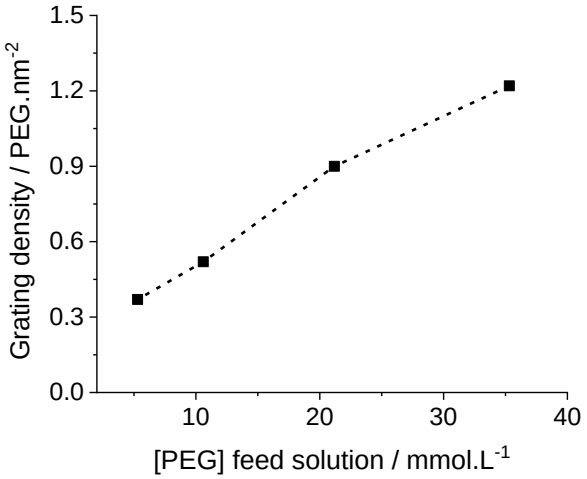

Figure 4.3.5. Number of grafted PEG-SH 2 kDa molecules per surface area of polythioether NPs for different feed concentrations.

Using the thiol-ene coupling described here, the grafting density of PEG chains achieved on the surface of the polythioether NPs is in the same range as the grafting density of PEG on nanocarriers used in drug-delivery studies, which have already shown improved stealth effect, i.e., longer blood half -lives due to a suppression of non-specific protein adhesion, after the PEGylation process.[26] Therefore, these results highlight the versatility and fine control of the thiol-ene coupling of macromolecules onto the surface of nanoparticles.

III. Glycopolymer and peptide-conjugated polythioether latex

A wide array of molecules can be covalently bond to the NPs using the thiol-ene coupling. The polythioether NPs can also be functionalized with biomolecules, such as carbohydrates and peptides. The functionalization of nanoparticles with polypeptides like RGD sequences,[28] lecithin[29] or transferrin,[210] or carbohydrates like galactose[30] and mannose[31] is a frequently employed strategy targeting specific cell lines. After preparing the samples with extra ene functionalities, the accessible, functional groups were further reacted with thiolated molecules (Figure 4.3.6). Here, as a model reaction, ene-functionalized nanoparticles were reacted with the thiol groups of thioglucose or bovine serum albuminn (Section 3.10).

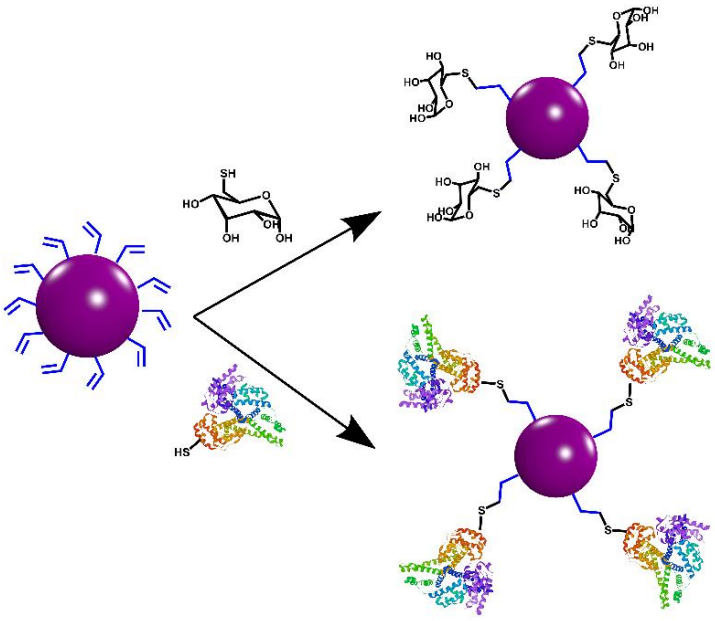

Figure 4.3.6. Scheme of surface functionalization of ene-rich polythioether NPs with biomolecules such as thioglucose and bovine serum albumin (BSA) through click thiol-ene reaction. The structure of the BSA was obtained from RCSB PDB (public domain).

Thioglucose tetraacetate was used as a model carbohydrate in the bioconjugation of ene-rich polythioether nanoparticles. The photoreaction was performed by the addition of this carbohydrate into a latex of polythioether NPs prepared with a 10%$_{mol}$ excess of diene monomers, in the presence of a photoinitiator (Section 3.10). In parallel, control samples were prepared with the same amount of thioglucose and NPs but without photoinitiator nor UV-irradiation. Following the reaction, the NPs were washed by centrifugation cycles to remove unreacted thioglucose. Finally, the concentration of glucose on the nanoparticles was measured with a glucose enzymatic assay.

Figure 4.3.7 shows the results of the functionalization of the nanoparticles with thioglucose tetraacetate. The results show the presence of a minimal amount of glucose molecules in the control samples prepared by the simple incubation of the thioglucose with the NPs, in contrast with the samples submitted to photoreaction. The grafting density of thioglucose of 2 molecules/nm^2 is fitting to the footprint of a glucose molecule (ca. 1 nm^2), and the grafting density of double bonds on the surface of the nanoparticles (ca. 3 C=C/nm^2). The small hydrodynamic radius of this molecule enabled its highly effective covalent addition to the double bonds available on the surface of the NPs.

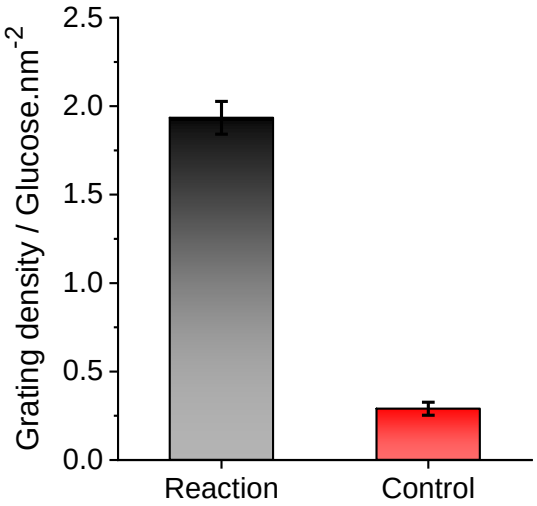

Figure 4.3.7. Thiol-ene conjugation of polythioether nanoparticles with thioglucose. The control sample consisted of the mixture of nanoparticles with thioglucose incubated at room temperature, with no addition of photoinitiators nor irradiation with UV light.

Alternatively, bovine serum albumin (BSA) was used as a model for the covalent attachment of polypeptides. BSA is composed 583 amino acid units, including 6 cysteine residues. Each cysteine are themselves bearing a thiol group that could undergo thiol-ene addition. Nanoparticles with remaining ene groups and further reacted with BSA showed a significant increase in the presence of BSA in comparison to the control samples (Figure 4.3.8). Here, the control experiment consisted of the same NPs incubated with BSA molecules in the absence of photoinitiators nor UV-irradiation, to suppress any attachment besides physisorption.

After the reaction or incubation time, both samples were centrifuged and the recovered pellets of NPs were redispersed in a desorption solution and incubated at high temperature, to ensure that unreacted BSA molecules were efficiently washed away (Section 3.10.3). Then, these samples were centrifuged, and the supernatants were used to access the concentration of BSA present covalently attached to the NPs.

The grafting density of BSA on the surface of the polythioether NPs was determined by a Pierce™ 660 nm protein assay (Section 3.10.4). Figure 4.3.8 shows grafting values of 0.03 BSA molecules/nm^2. This means that an area of 28 nm^2 would be necessary to accommodate 1 BSA molecule. This finding is aligned with the footprint of the molecule calculated by its gyration radius (27 nm^2), indicating the effective bioconjugation of the protein onto the surface of the nanoparticles. Furthermore, the 6 cysteine residues in one BSA molecule could also promote more than a single

covalent attachment per molecule, leading the protein to undergo conformational changes and "wrap around" the nanoparticle to reduce steric hindrance.

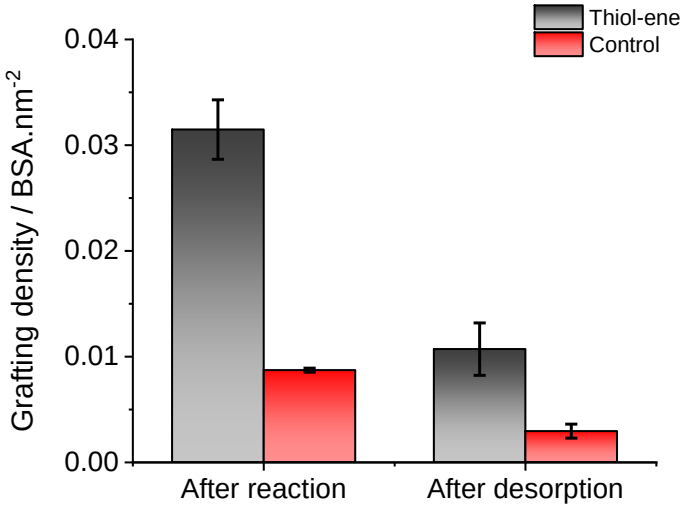

Figure 4.3.8. Conjugation of polythioether nanoparticles with BSA. The control sample consisted of the mixture of nanoparticles with BSA at room temperature, with no addition of photoinitiators nor irradiation with UV-light.

IV. Influence of surface modification on the behavior of the nanoparticle in suspension

One of the main reasons for the widespread use of PEG in the surface modification of nanoparticles for biomedical use is rooted in its ability to tune the solvation layer of the nanocarriers and, with that, their protein adhesion pattern.[25] Here, the efficiency of the PEGylation of the nanoparticles to modulate the interaction between the NPs and their environment was compared to the effect of the oxidation of the nanoparticles (Section 4.2). Given the increased hydrophilicity observed for the polysulfoxide and polysulfone NPs compared to the as-prepared nanoparticles resulting from thiol-ene photopolymerization in miniemulsion, it is possible that the oxidized NPs would display similar properties. Therefore, samples of "naked", i.e., free surface with no grafted molecules, nanoparticles of polythioether and its oxidized-derivatives were prepared and compared in terms of their protein adhesion profile to nanoparticles of polythioether grafted with PEG-SH 2 kDa (Figure 4.3.9).

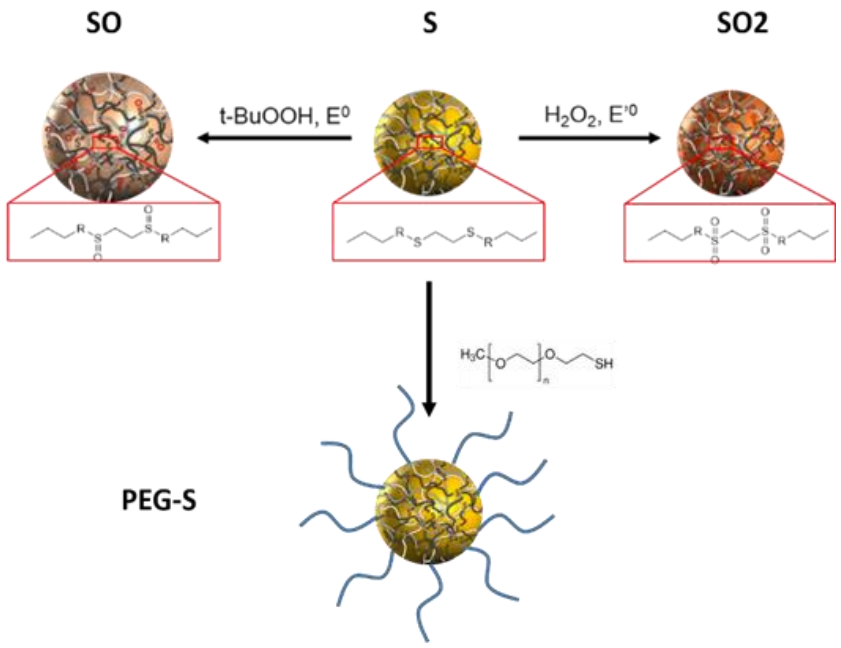

Figure 4.3.9. Preparation of biologically active nanoparticles by the modification of the core of polythioether NPs (S) by controlled oxidation to poly(sulfoxide) NPs (SO) and poly(sulfone) NPs (SO2) or the functionalization of the surface of S NPs with poly(ethylene glycol) (PEG-S).

Prior to using complex polls of proteins, some preliminary adsorption experiments using fluorescently tagged BSA (FTIC-BSA) were performed. Figure 4.3.10 shows the results found for the physisorption of BSA on the different NPs. The NPs with polysulfoxide composition seem to prevent protein adhesion when compared to its analogs polythioethers and polysulfones.

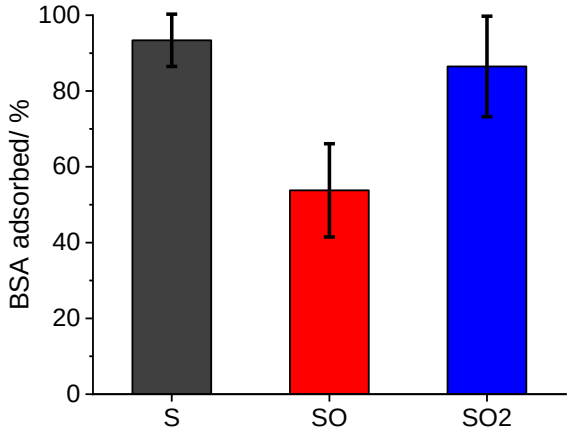

Figure 4.3.10. Fraction of the BSA initially in the suspension adsorbed on the surface of the NP after one hour of incubation of the suspensions of polythioether (S), polysulfoxide (SO), and polysulfone (SO2) at 1 mg·mL^{-1} with BSA at a concentration of 0.01 mg·mL^{-1}.

However, the suppression of the adhesion of one type of protein, e.g., BSA, on a surface or an NP does not necessarily indicate the same performance in more complex media. After verifying the different interactions between the NPs and BSA for each system, we moved forward to more complex protein systems, such as those found in human citrate plasma (HP) and fetal bovine serum (FBS) (Section 3.10.3). Initially, FBS was used as the incubation medium to test the different NP suspensions (Figure 4.3.11). To compare the efficiency of the oxidation of the core of the polythioether NPs on the suppression of protein adhesion, the PEGylated NPs were used as a standard. PEGylation is the typical benchmark to which most new strategies to reduce protein adsorption and enhance the circulation time of NP *in vivo* are usually compared.[25]

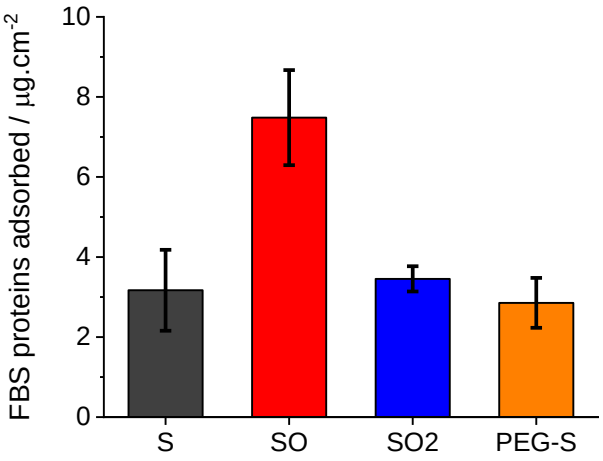

Figure 4.3.11. Adsorption of fetal bovine serum (FBS) proteins on the surface of the nanoparticles of polythioether (S), polysulfoxide (SO), polysulfone (SO2), and polythioether functionalized with PEG-SH.

Surprisingly, Figure 4.3.11 shows that polysulfoxide NPs adsorbed more proteins than the native polythioether NPs, and even PEGylation only marginally affected the performance of the NPs. Some factors could be at the root of this difference, such as the concentration of surfactant and zeta potential of the NPs. Measurements of the zeta potentials of the systems used for the incubation with FBS resulted in largely negative values, indicating the presence of the negatively charged species possibly coming from the surfactant (sodium dodecyl sulfate (SDS)) used during synthesis to provide the NPs with colloidal stability. Protein adhesion onto surfaces and NPs depends on their surface chemistry. The presence of surfactant could be masking the real effects of the NP composition but controlling the surfactant concentration while preserving the colloidal stability of the NPs suspension was challenging.

Following that, the behavior of thoroughly cleaned NPs was investigated in the presence of Human citrate Plasma. Multi-angle dynamic light scattering, protein quantification, and gel electrophoresis (SDS-page) were used to evaluate the interaction between the NPs and the plasma proteins in each system.[132] Using multiangle dynamic light scattering (Section 3.10.6), we can compare the portion of light scattered by the NPs with and without the incubation with HP. The variation in the light scattering is then correlated to the formation of aggregates of the NPs caused by the proteins present in the plasma.

In general, none of the 4 samples present macroscopic aggregation, although some differences are still detected (Figure 4.3.12A-E). These aggregates can just be seen at low angles (30°) because the contribution of big sizes to the total scattering intensity is higher at lower angles. Here, the experimental data points showed relaxation times fitted by two or three exponential correlation models. The shift from the fitting curve to slower or faster relaxation times is attributed to the formation of aggregates caused by the adsorption of proteins onto the surfaces of the NPs.

Therefore, the results indicate that latexes of polysulfoxide NPs were the most colloidally stable in plasma, whereas some aggregation was detected in the other NP systems. For the as-prepared polythioether NPs, aggregates roughly 3-fold larger than the original NPs were found in suspension (Figure 4.3.12E). The PEGylation moderately reduced the fraction of NPs in the aggregates and reduced the size of these aggregates. However, the oxidation of the NPs to polysulfoxide completely prevented the aggregation induced by adsorption of the proteins present in the plasma.

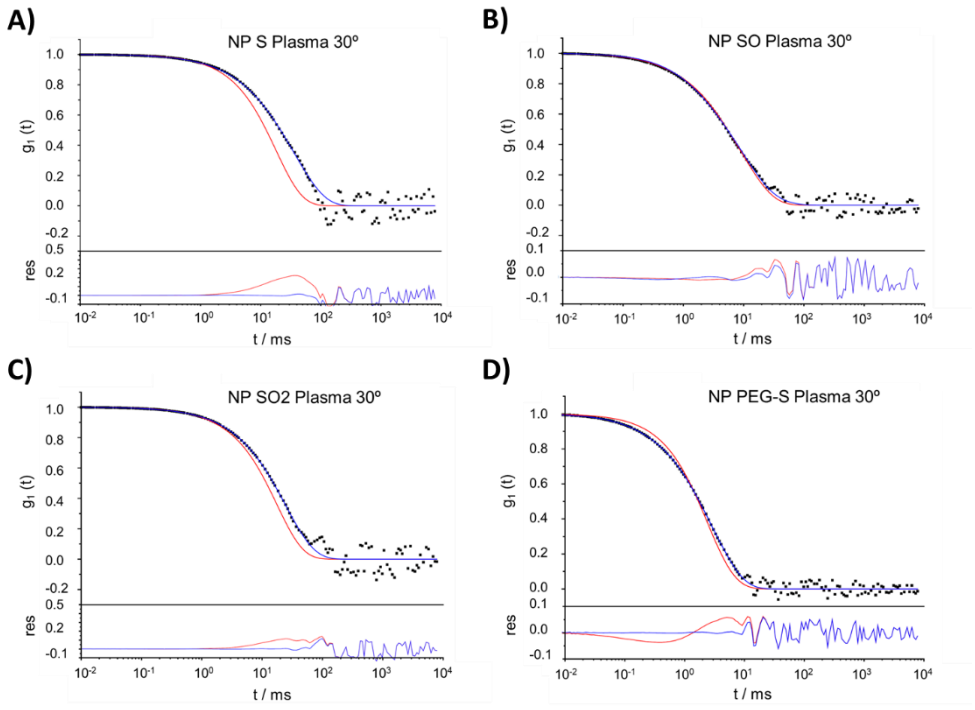

E)

Angle (°)	Fraction of light scattered by aggregates (%)			
	S	SO	SO2	PEG-S
30	58.7	10.2	63.3	29.5
60	18.6	9.2	13.1	13.0
90	24.9	3.6	11.3	22.1
120	15.2	4.8	3.6	16.5
135	14.2	3.7	10.9	11.7
$R_{h,agg}$ / $R_{h,NP}$ (nm)[a]	716 / 234	-	448 / 196	472 / 189

Figure 4.3.12. Multi-angle DLS of suspensions of NPs of a) polythioether (S), b) polysulfoxide (SO), c) polysulfone (SO_2), and d) PEGylated-polythioether (PEG-S) in human citrate plasma. The autocorrelation function $g_1(t)$ for the measurements made at 30° are shown, together with the fitting with (blue line), and without (red line) additional aggregate term, and their corresponding residuals. E) Summary of the results: most of the scattered light is detected at 30°, where the contribution of larger aggregates can be seen. Evidence of aggregation due to protein adhesion is also observed in the hydrodynamic radius of the aggregates, $R_{h,agg}$, when compared to the original radius of the nanoparticles, $R_{h,NP}$. [a] Measured at 30°.

Another important factor in the study of the interactions between proteins and nanomaterials is the discrimination of the type of proteins that interact strongly with each type of surface chemistry. Therefore, the adsorbed protein patterns were further visualized using SDS–polyacrylamide gel electrophoresis (SDS-PAGE) (Section 3.10.5).

Figure 4.3.13 depicts the quantification and the SDS-PAGE of the plasma proteins adsorbed on the surface of the NPs after incubation in HP. Here, the adsorption density of proteins (Figure 4.3.13A) followed the same pattern as the one observed in the adhesion of the single molecule FITC-

BSA (Figure 4.3.10), where NPs with polysulfoxide composition also presented suppression of the protein adsorption. The oxidized derivatives of polythioether, polysulfoxide, and polysulfone, exhibited different profiles of protein adsorption in both assays. Figure 4.3.13B shows a preferential adhesion of albumin on the polysulfoxide NPs, while the other NPs had captured a larger variety of proteins from the media.

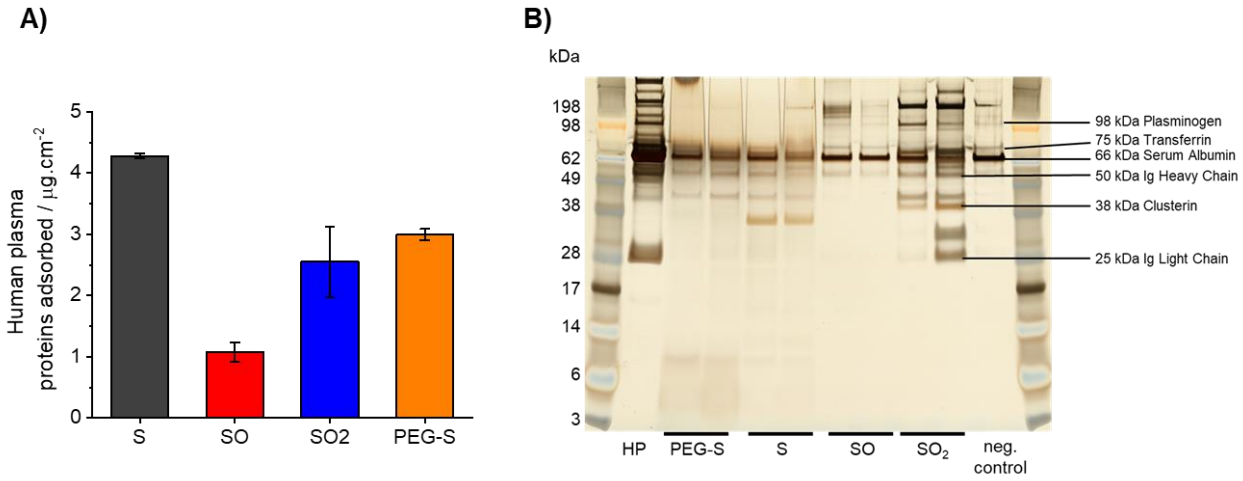

Figure 4.3.13. Protein adhesion following the incubation of the NPs in citrate human plasma: A) Pierce™ protein assay quantification of proteins on the surface of NPs of as prepared polythioether (S), oxidized polysulfoxide (SO), and polysulfone (SO2) and the polythioether functionalized with PEG-SH (PEG-S). B) SDS-page analysis of the proteins adsorbed on the NPs (duplicates), pure plasma as a reference, and negative control. A scale of molecular weight of proteins is shown in the first and last columns.

These series of experiments highlight the great potential of nanoparticles composed of polythioether and oxidized derivatives be employed as nanocarriers in drug-delivery applications. The explanation for the observed stealth effect of such systems could be rooted in the same features that make the PEGylation the gold standard for non-specific protein adhesion and cellular uptake, it is, the high level of hydration of the hydrophilic polyether backbone, preventing protein adsorption on otherwise hydrophobic polymer surfaces by means of steric repulsion.[26,62] This reasoning is also supported by the results obtained in Section 4.2, where films formed from the suspensions of polysulfoxides and polysulfones nanoparticles presented reduced water contact angle and therefore improved hydrophilicity towards the parent polythioether. Consequently, these oxidized nanomaterials could be promising candidates to suppression unspecific cellular uptake, replacing the PEGylation technique altogether, preventing side-effects related to accumulation of PEG-derivatives in the body.[211]

4.3.3 Conclusion

We show that the surface of the polythioether NP prepared with an excess of diene monomer can readily be functionalized with thiolated molecules. Ene-rich NPs were the preferred system, owing to their orthogonality towards other biochemistries and the ubiquitous presence of thiol-moieties in biomolecules. Molecules of different sizes and conformations were functionalized to the surface of the NPs at varying grafting densities, thus highlighting the versatility and control of the thiol-ene coupling. Moreover, we demonstrated the unmatched power of thiol-ene chemistry as a synthetic platform, from the preparation of NPs to their functionalization.

In addition, we also investigated the modified NPs in terms of their interactions in a complex protein environment. NPs with oxidized cores chemistries, polysulfoxides, and polysulfones, were also evaluated in terms of protein adhesion behavior since they had shown improved hydrophilicity with respect to the parent polythioether NPs (Section 4.2). The protein adhesion on different NPs (polythioether, polysulfoxide, polysulfone, and PEGylated-polythioether NPs) shows the impact of the modification of the NPs core and the surface functionalization. The oxidized derivatives show a different profile of adsorption than their parent polythioether and are promising alternative to PEGylated bio-nanocarriers, often plagued by the side-effects arising from the accumulation of PEG in the organism.

Overall, the results show that controlling the chemical composition of the core of the NPs through oxidation and the surface chemistry by grafting biomolecules or polymer chains influences the NPs in biological media. More characterization of those systems coupled with the cellular uptake of these NPs could be used to predict the fate of those NPs *in vivo*. Furthermore, the combination of core oxidation and surface functionalization to impart specific interactions with receptors and cells would be of interest for applications of those NPs as drug-delivery systems.

5 Summary and Perspectives

5.1 Summary

This thesis highlights the potential of thiol-ene chemistry to generate fully customizable polymer nanoparticles, which could find applications in a wide range of fields, from non-leaching materials, nanocarriers for biomedical use, high barrier packaging film, and chromatography columns. The photopolymerization of thiol-ene systems in miniemulsion offers a tunable platform to tackle this challenge. Thiol-ene polymerization and thiol-ene coupling are the synthetic platforms of choice, given the versatility in terms of building blocks and the ubiquitous presence of sulfhydryl groups in biomolecules. The thesis is divided into three main parts (Figure 5.1.1), where, firstly, the mechanisms and kinetics of the thiol-ene photopolymerization in miniemulsion were studied to produce well-designed nanoparticles. Then, the resulting nanoparticles were chemically modified by oxidation; by controlling the chemical composition of the core of these particles, the physicochemical properties of the nanoparticles can be finely tuned. Finally, the surface modifications promoted by the thiol-ene click chemistry itself provided another level of control over the properties of the final systems, for example leading to important changes in the interactions of the modified particles with proteins.

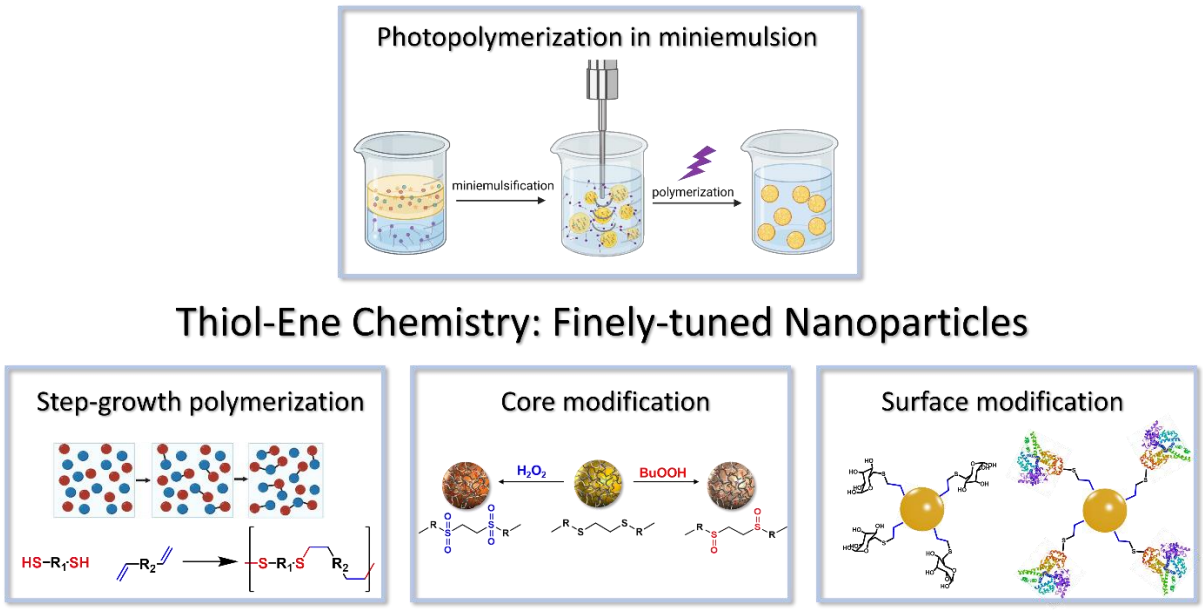

Figure 5.1.1. Schematic representation of the aspects covered by this thesis, from the thiol-ene step-growth photopolymerization in miniemulsion (Section 4.1), to the core (Section 4.2) and surface modification (Section 4.3) of the polythioether nanoparticles, to control the properties of the nanoparticles.

Here, every aspect of the thiol-ene chemistry was investigated in those systems. In section 4.1, the kinetic of this step-growth polymerization in miniemulsion was studied. Thiol-ene photopolymerization in miniemulsion is not only an elegant way to produce nanosystems, but also to promote, through a confinement effect within the miniemulsion droplets, improvement in the reaction rate and the final molecular weight of the polymer synthesized from a given monomer system in comparison to the same reaction in bulk. Also, results indicated that the thiol-ene reaction kept virtually the same kinetics and thus molecular weights even when the complementary monomers were present in the system at an off-stoichiometric ratio due to the confinement effect offered by the miniemulsion.

Following that, post-polymerization modifications of the polythioether nanoparticles were evaluated. Oxidizing the sulfur-centers of the main polymer backbones promoted the formation of the partially oxidized derivative polysulfoxide and the fully oxidized one, polysulfone. By employing mild conditions and different oxidants, tert-butyl hydroperoxide and hydrogen peroxide, each of these derivatives were separately produced directly from the parent miniemulsion of polysulfide (polythioether) nanoparticles. The method has shown to be mild enough to preserve the colloidal stability and the polymer chains integrity, as well as robust to work with polysulfides produced with different monomer pairs. The oxidation carried out in the suspension of the parent polysulfide nanoparticles yielded systems where all the sulfur centers were oxidized either to sulfone or sulfoxide. The selective production of these materials allowed the harnessing of their individual properties, with the oxidized derivatives displaying improved hydrophilicity in comparison to the parent polysulfide, and polysulfones exhibiting an increase in the glass transition temperature.

The core modifications were then followed by the modifications made on the surface of the polythioether particles. Nanoparticles prepared with a non-stoichiometric ratio between the functionalities presented unreacted end-groups that could be used for further coupling on the surface. Molecules of different sizes and structures were attached to nanoparticles bearing accessible C=C double bonds. The grafting of thiolated poly(ethylene glycol), a benchmark compound used to tune the protein adhesion on nanocarriers, was successful and the grafting density could be controlled by the reaction conditions. In addition, thioglucose and bovine serum albumin were used as models for the attachment of carbohydrates and proteins, which are known to affect the fate of nanoparticles in vivo. These results highlight the high level of control and selectivity offered by the thiol-ene coupling. Naked nanoparticles, i.e., nanoparticles with free surfaces, of polythioether, polysulfoxide, and polysulfone were compared to polythioether nanoparticles functionalized with thiolated polyethylene glycol in terms of their protein adhesion profile. The study showed promising results, especially for

the oxidized derivatives, that could potentially be used in the future to tune interactions in biological media without the need to attach another group on the surface of the carrier.

In conclusion, the results presented in this thesis show that thiol-ene chemistry can be used to both produce and control the properties of polymer nanoparticles. Using one polymer system, samples with distinct, well-defined, properties can be readily produced. The platform is versatile in terms of compatible monomers and provides multiple handles to control the thermomechanical properties of the system either through the selection of the monomer or oxidation, and the behavior of the nanoparticles in suspension through surface modification.

5.2 Perspectives

The results reported in this thesis pave the way to a broad range of applications of thiol-ene polymer nanoparticles. Such nanoparticles could also find application as nanocarriers but to this end, more systematic *in vitro* and *in vivo* studies should be conducted to bring new information about the behavior of these thiol-based systems in terms of their behavior in biological medium. More insights into the *in cellulo* fate of the nanocarrier are needed to optimize the design in terms of degradability, targeting ability, and release mechanism. For example, some biomolecules, such as heparin and hyaluronic acid, could be used to modify the surface of the polythioether nanocarriers to enable the selectively targeting of a given tissue. Moreover, polythioethers are redox-sensitive polymers, and the over-oxidation of these nanocarriers could be employed as a mechanism of release of cargo in areas with high concentrations of reactive oxidating species, i.e., inflamed tissues. The chemical composition of the monomer system could also be modified to introduce additional functionalities in the nanoparticles. For example, redox, pH, and temperature sensitive functionalities could be introduced in the monomer feed.

Furthermore, polythioether and its oxidized derivatives have great potential as high-performance materials. Polysulfones are already used commercially as filter membranes and resins toughener. The methodology described here could expand their application to other fields that already use colloidal suspensions, such as coatings and films. For example, thiol-ene based films with improved thermomechanical properties could potentially substitute materials such as vinylidene chloride copolymer coating (PVDC) as oxygen barrier waterborne coatings, offering a halogen-free and more sustainable alternative for the food packaging industry.

Those nanoparticles could also potentially be applied as scaffolds, in photoresist for lithography, and chromatographic columns packing material, all of which require polymer with enhanced thermomechanical resistance. A more detailed study on the mechanical stability of the polysulfoxide produced could also direct new applications since traditionally such materials cannot be produced in a straightforward manner. At this point, the improved hydrophilicity and different protein adhesion profile seem to hold great potential for polysulfoxides as drug-delivery systems. Hopefully, this protocol of selective oxidation will pave the way for more and more diverse applications of main chain polysulfoxide materials.

6 References

(1) Jasinski, F.; Zetterlund, P. B.; Braun, A. M.; Chemtob, A. Photopolymerization in Dispersed Systems. *Prog. Polym. Sci.* **2018**, *84*, 47–88. DOI:10.1016/j.progpolymsci.2018.06.006.

(2) Posner, T. Beiträge Zur Kenntniss Der Ungesättigten Verbindungen. II. Ueber Die Addition von Mercaptanen an Ungesättigte Kohlenwasserstoffe. *Berichte der Dtsch. Chem. Gesellschaft* **1905**, *38* (1), 646–657.

(3) Kolb, H. C.; Finn, M. G.; Sharpless, K. B. Click Chemistry: Diverse Chemical Function from a Few Good Reactions. *Angew. Chemie - Int. Ed.* **2001**, *40* (11), 2004–2021.

(4) Hoyle, C. E.; Bowman, C. N. Thiol-Ene Click Chemistry. *Angew. Chemie Int. Ed.* **2010**, *49* (9), 1540–1573. DOI:10.1002/anie.200903924.

(5) Hoyle, C. E.; Lee, T. A. I. Y.; Roper, T. Thiol – Enes : Chemistry of the Past with Promise for the Future. **2004**, *42*, 5301–5338. DOI:10.1002/pola.20366.

(6) Lowe, A. B. Thiol-Ene '" Click "' Reactions and Recent Applications in Polymer and Materials Synthesis. **2010**, 17–36. DOI:10.1039/b9py00216b.

(7) Lowe, A. B. Thiol-Ene "Click" Reactions and Recent Applications in Polymer and Materials Synthesis: A First Update. *Polym. Chem.* **2014**, *5* (17), 4820–4870. DOI:10.1039/c4py00339j.

(8) Liu, Y.; Hou, W.; Sun, H.; Cui, C.; Zhang, L.; Jiang, Y.; Wu, Y.; Wang, Y.; Li, J.; Sumerlin, B. S.; Liu, Q.; Tan, W. Thiol-Ene Click Chemistry: A Biocompatible Way for Orthogonal Bioconjugation of Colloidal Nanoparticles. *Chem. Sci.* **2017**, *8* (9), 6182–6187. DOI:10.1039/c7sc01447c.

(9) Stenzel, M. H. Bioconjugation Using Thiols: Old Chemistry Rediscovered to Connect Polymers with Nature's Building Blocks. *ACS Macro Lett.* **2013**, *2* (1), 14–18. DOI:10.1021/mz3005814.

(10) Mckenas, C. G.; Fehr, J. M.; Liu, B.; Donley, C. L.; Lockett, M. R.; Carolina, N.; States, U. Mechanistic Insights into UV-Initiated Thiol–Ene Reactions on Amorphous Carbon Films. *J. Phys. Chem. C* **2018**, *122*, 21854–21860. DOI:10.1021/acs.jpcc.8b04359.

(11) Magennis, E. P.; Hook, A. L.; Williams, P.; Alexander, M. R. Making Silicone Rubber Highly Resistant to Bacterial Attachment Using Thiol-Ene Grafting. *ACS Appl. Mater. Interfaces* **2016**, *8* (45), 30780–30787. DOI:10.1021/acsami.6b10986.

(12) Yang, H.; Chen, Y.; Liu, Y.; Nie, L.; Yao, S. One-Pot Synthesis of (3-Sulfopropyl Methacrylate Potassium)-Silica Hybrid Monolith via Thiol-Ene Click Chemistry for CEC. *Electrophoresis* **2013**, *34* (4), 510–517. DOI:10.1002/elps.201200354.

(13) Sticker, D.; Geczy, R.; Häfeli, U. O.; Kutter, J. P. Thiol-Ene Based Polymers as Versatile Materials for Microfluidic Devices for Life Sciences Applications. *ACS Appl. Mater. Interfaces* **2020**, *12* (9), 10080–10095. DOI:10.1021/acsami.9b22050.

(14) Campos, L. M.; Killops, K. L.; Sakai, R.; Paulusse, J. M. J.; Damiron, D.; Drockenmuller, E.; Messmore, B. W.; Hawker, C. J. Development of Thermal and Photochemical Strategies for Thiol-Ene Click Polymer Functionalization. *Macromolecules* **2008**, *41* (19), 7063–7070. DOI:10.1021/ma801630n.

(15) Dondoni, A.; Marra, A. Recent Applications of Thiol–Ene Coupling as a Click Process for Glycoconjugation. *Chem. Soc. Rev.* **2012**, *41* (2), 573–586. DOI:10.1039/C1CS15157F.

(16) Chen, Y.; Triola, G.; Waldmann, H. Bioorthogonal Chemistry for Site-Specific Labeling and Surface Immobilization of Proteins. **2011**, *44* (9), 32. DOI:10.1021/ar200046h.

(17) Mosiewicz, K. A.; Kolb, L.; Van Der Vlies, A. J.; Martino, M. M.; Lienemann, P. S.; Hubbell, J. A.; Ehrbar, M.; Lutolf, M. P. In Situ Cell Manipulation through Enzymatic Hydrogel Photopatterning. *Nat. Mater.* **2013**, *12* (11), 1072–1078. DOI:10.1038/nmat3766.

(18) Jonkheijm, P.; Weinrich, D.; Köhn, M.; Engelkamp, H.; Christianen, P. C. M.; Kuhlmann, J.; Maan, J. C.; Nüsse, D.; Schroeder, H.; Wacker, R.; Breinbauer, R.; Niemeyer, C. M.; Waldmann, H. Photochemical Surface Patterning by the Thiol-Ene Reaction. *Angew. Chemie - Int. Ed.* **2008**, *47* (23), 4421–4424. DOI:10.1002/anie.200800101.

(19) Colak, B.; Soares, T. A.; Gautrot, J. E. Impact of the Molecular Environment on Thiol − Ene Coupling For Biofunctionalization and Conjugation. **2016**. DOI:10.1021/acs.bioconjchem.6b00349.

(20) Thalhauser, S.; Breunig, M. Considerations for Efficient Surface Functionalization of Nanoparticles with a High Molecular Weight Protein as Targeting Ligand. *Eur. J. Pharm. Sci.* **2020**, *155* (105520), 105520. DOI:10.1016/j.ejps.2020.105520.

(21) Renault, K.; Fredy, J. W.; Renard, P. Y.; Sabot, C. Covalent Modification of Biomolecules through Maleimide-Based Labeling Strategies. *Bioconjug. Chem.* **2018**, *29* (8), 2497–2513.

DOI:10.1021/acs.bioconjchem.8b00252.

(22) Smith, M. E. B.; Schumacher, F. F.; Ryan, C. P.; Tedaldi, L. M.; Papaioannou, D.; Waksman, G.; Caddick, S.; Baker, J. R. Protein Modification, Bioconjugation, and Disulfide Bridging Using Bromomaleimides. *J. Am. Chem. Soc.* **2010**, *132* (6), 1960–1965. DOI:10.1021/ja908610s.

(23) Tallec, G.; Loh, C.; Liberelle, B.; Garcia-Ac, A.; Duy, S. V.; Sauvé, S.; Banquy, X.; Murschel, F.; De Crescenzo, G. Adequate Reducing Conditions Enable Conjugation of Oxidized Peptides to Polymers by One-Pot Thiol Click Chemistry. *Bioconjug. Chem.* **2018**, *29* (11), 3866–3876. DOI:10.1021/acs.bioconjchem.8b00684.

(24) Obermeier, B.; Frey, H. Poly(Ethylene Glycol-Co-Allyl Glycidyl Ether)s: A PEG-Based Modular Synthetic Platform for Multiple Bioconjugation. *Bioconjug. Chem.* **2011**, *22* (3), 436–444. DOI:10.1021/bc1004747.

(25) Schöttler, S.; Becker, G.; Winzen, S.; Steinbach, T.; Mohr, K.; Landfester, K.; Mailänder, V.; Wurm, F. R. Protein Adsorption Is Required for Stealth Effect of Poly(Ethylene Glycol)- and Poly(Phosphoester)-Coated Nanocarriers. *Nat. Nanotechnol.* **2016**, *11* (4), 372–377. DOI:10.1038/nnano.2015.330.

(26) Li, M.; Jiang, S.; Simon, J.; Paßlick, D.; Frey, M. L.; Wagner, M.; Mailander, V.; Crespy, D.; Landfester, K. Brush Conformation of Polyethylene Glycol Determines the Stealth Effect of Nanocarriers in the Low Protein Adsorption Regime. *Nano Lett.* **2021**, *21* (4), 1591–1598. DOI:10.1021/acs.nanolett.0c03756.

(27) Gupta, N.; Lin, B. F.; Campos, L. M.; Dimitriou, M. D.; Hikita, S. T.; Treat, N. D.; Tirrell, M. V; Clegg, D. O.; Kramer, E. J.; Hawker, C. J. A Versatile Approach to High-Throughput Microarrays Using Thiol-Ene Chemistry. *Nat. Chem.* **2010**, *2* (2), 138–145. DOI:10.1038/nchem.478.

(28) Danhier, F.; Vroman, B.; Lecouturier, N.; Crokart, N.; Pourcelle, V.; Freichels, H.; Jérôme, C.; Marchand-Brynaert, J.; Feron, O.; Préat, V. Targeting of Tumor Endothelium by RGD-Grafted PLGA-Nanoparticles Loaded with Paclitaxel. *J. Control. Release* **2009**, *140* (2), 166–173. DOI:10.1016/j.jconrel.2009.08.011.

(29) Aravind, A.; Jeyamohan, P.; Nair, R.; Veeranarayanan, S.; Nagaoka, Y.; Yoshida, Y.; Maekawa, T.; Kumar, D. S. AS1411 Aptamer Tagged PLGA-Lecithin-PEG Nanoparticles for Tumor Cell Targeting and Drug Delivery. *Biotechnol. Bioeng.* **2012**, *109* (11), 2920–2931. DOI:https://doi.org/10.1002/bit.24558.

(30) Lou, S.; Gao, S.; Wang, W.; Zhang, M.; Zhang, J.; Wang, C.; Li, C.; Kong, D.; Zhao, Q. Galactose-Functionalized Multi-Responsive Nanogels for Hepatoma-Targeted Drug Delivery. *Nanoscale* **2015**, *7* (7), 3137–3146. DOI:10.1039/C4NR06714B.

(31) Pei, M.; Xu, R.; Zhang, C.; Wang, X.; Li, C.; Hu, Y. Mannose-Functionalized Antigen Nanoparticles for Targeted Dendritic Cells, Accelerated Endosomal Escape and Enhanced MHC-I Antigen Presentation. *Colloids Surfaces B Biointerfaces* **2021**, *197*, 111378. DOI:https://doi.org/10.1016/j.colsurfb.2020.111378.

(32) Cengiz, N.; Gevrek, T. N.; Sanyal, R.; Sanyal, A. Orthogonal Thiol-Ene "click" Reactions: A Powerful Combination for Fabrication and Functionalization of Patterned Hydrogels †. *This J. is Cite this Chem. Commun* **2017**, *53*, 8894. DOI:10.1039/c7cc02298k.

(33) Goldmann, A. S.; Walther, A.; Nebhani, L.; Joso, R.; Ernst, D.; Loos, K.; Barner-Kowollik, C.; Barner, L.; Müller, A. H. E. Surface Modification of Poly(Divinylbenzene) Microspheres via Thiol-Ene Chemistry and Alkyne-Azide Click Reactions. *Macromolecules* **2009**, *42* (11), 3707–3714. DOI:10.1021/ma900332d.

(34) Stein, H. L. Ultra-High Molecular Weight Polyethylene (UHMWPE). Guide to Engineering Plastics Families: Thermoplastic Resins. *Eng. Mater. Handb.* **1999**, *2*.

(35) Sherazi, T. A. Ultrahigh Molecular Weight Polyethylene. In *Encyclopedia of Membranes*; Drioli, E., Giorno, L., Eds.; Springer Berlin Heidelberg: Berlin, Heidelberg, 2015; pp 1–2. DOI:10.1007/978-3-642-40872-4_591-2.

(36) Mishra, V.; Desai, J.; Patel, K. I. High-Performance Waterborne UV-Curable Polyurethane Dispersion Based on Thiol–Acrylate/Thiol–Epoxy Hybrid Networks. *J. Coatings Technol. Res.* **2017**, *14* (5), 1069–1081. DOI:10.1007/s11998-016-9906-1.

(37) Sarapas, J. M.; Tew, G. N. Poly(Ether-Thioethers) by Thiol-Ene Click and Their Oxidized Analogues as Lithium Polymer Electrolytes. *Macromolecules* **2016**, *49* (4), 1154–1162. DOI:10.1021/acs.macromol.5b02513.

(38) Teixeira, L. I.; Landfester, K.; Thérien-Aubin, H. Selective Oxidation of Polysulfide Latexes to Produce Polysulfoxide and Polysulfone in a Waterborne Environment. **2021**, *54*, 3659–3667. DOI:10.1021/acs.macromol.1c00382.

(39) Jasinski, F.; Rannée, A.; Schweitzer, J.; Fischer, D.; Lobry, E.; Croutxé-Barghorn, C.; Schmutz, M.;

Le Nouen, D.; Criqui, A.; Chemtob, A. Thiol-Ene Linear Step-Growth Photopolymerization in Miniemulsion: Fast Rates, Redox-Responsive Particles, and Semicrystalline Films. *Macromolecules* **2016**, *49* (4), 1143–1153. DOI:10.1021/acs.macromol.5b02512.

(40) Marvel, C. S.; Aldrich, P. H. Polyalkylene Sulfides. II. Preparation of Polyhexamethylene Sulfide in Emulsion. *J. Am. Chem. Soc.* **1950**, *72* (5), 1978–1981.

(41) Okay, O.; Reddy, S. K.; Bowman, C. N. Molecular Weight Development during Thiol-Ene Photopolymerizations. *Macromolecules* **2005**, *38* (10), 4501–4511. DOI:10.1021/ma050080x.

(42) Jiang, K.; Liu, Y.; Yan, Y.; Wang, S.; Liu, L.; Yang, W. Combined Chain- and Step-Growth Dispersion Polymerization toward PSt Particles with Soft, Clickable Patches. *Polym. Chem.* **2017**, *8* (8), 1404–1416. DOI:10.1039/C6PY02094A.

(43) Li, Y.; Dong, X.-H.; Guo, K.; Wang, Z.; Chen, Z.; Wesdemiotis, C.; Quirk, R. P.; Zhang, W.-B.; Cheng, S. Z. D. Synthesis of Shape Amphiphiles Based on POSS Tethered with Two Symmetric/Asymmetric Polymer Tails via Sequential “Grafting-from” and Thiol–Ene “Click” Chemistry. *ACS Macro Lett.* **2012**, *1* (7), 834–839. DOI:10.1021/mz300196x.

(44) Carlborg, C. F.; Haraldsson, T.; Öberg, K.; Malkoch, M.; Van Der Wijngaart, W. Beyond PDMS: Off-Stoichiometry Thiol-Ene (OSTE) Based Soft Lithography for Rapid Prototyping of Microfluidic Devices. *Lab Chip* **2011**, *11* (18), 3136–3147. DOI:10.1039/c1lc20388f.

(45) Khire, B. V. S.; Yi, Y.; Clark, N. A.; Bowman, C. N. Formation and Surface Modification of Nanopatterned Thiol-Ene Substrates Using Step and Flash Imprint Lithography **. **2008**, *80309*, 3308–3313. DOI:10.1002/adma.200800672.

(46) Kade, M. J.; Burke, D. J.; Hawker, C. J. The Power of Thiol-Ene Chemistry. *J. Polym. Sci. Part A Polym. Chem.* **2010**, *48* (4), 743–750. DOI:10.1002/pola.23824.

(47) Podgórski, M.; Wang, C.; Yuan, Y.; Konetski, D.; Smalyukh, I.; Bowman, C. N. Pristine Polysulfone Networks as a Class of Polysulfide-Derived High-Performance Functional Materials. *Chem. Mater.* **2016**, *28* (14), 5102–5109. DOI:10.1021/acs.chemmater.6b02026.

(48) Miller, D. J.; Dreyer, D. R.; Bielawski, C. W.; Paul, D. R.; Freeman, B. D. Surface Modification of Water Purification Membranes. *Angew. Chemie - Int. Ed.* **2017**, *56* (17), 4662–4711.

(49) Idris, A.; Mat Zain, N.; Noordin, M. Y. Synthesis, Characterization and Performance of Asymmetric Polyethersulfone (PES) Ultrafiltration Membranes with Polyethylene Glycol of

Different Molecular Weights as Additives. *Desalination* **2007**, *207* (1–3), 324–339.

(50) Alenazi, N. A.; Hussein, M. A.; Alamry, K. A.; Asiri, A. M. Modified Polyether-Sulfone Membrane: A Mini Review. *Des. Monomers Polym.* **2017**, *20* (1), 532–546.

(51) Perez, R. M.; Sandler, J. K. W.; Altstädt, V.; Hoffmann, T.; Pospiech, D.; Ciesielski, M.; Döring, M.; Braun, U.; Balabanovich, A. I.; Schartel, B. Novel Phosphorus-Modified Polysulfone as a Combined Flame Retardant and Toughness Modifier for Epoxy Resins. *Polymer (Guildf).* **2007**, *48* (3), 778–790.

(52) Lawrie, K. J.; Blakey, I.; Blinco, J. P.; Cheng, H. H.; Gronheid, R.; Jack, K. S.; Pollentier, I.; Leeson, M. J.; Younkin, T. R.; Whittaker, A. K. Chain Scission Resists for Extreme Ultraviolet Lithography Based on High Performance Polysulfone-Containing Polymers. *J. Mater. Chem.* **2011**, *21* (15), 5629–5637.

(53) Chen, L.; Goh, Y.; Lawrie, K.; Chuang, Y.; Piscani, E.; Zimmerman, P.; Blakey, I.; Whittaker, A. K. Polysulfone Based Non-CA Resists for 193 Nm Immersion Lithography : Effect of Increasing Polymer Absorbance on Sensitivity. *Radiat. Phys. Chem.* **2011**, *80* (2), 242–247. DOI:10.1016/j.radphyschem.2010.07.040.

(54) Cao, Y.; Zhang, G.; Zhang, Y.; Yue, M.; Chen, Y.; Cai, S.; Xie, T.; Feng, X. Direct Fabrication of Stretchable Electronics on a Polymer Substrate with Process-Integrated Programmable Rigidity. *Adv. Funct. Mater.* **2018**, *28* (50), 1–9.

(55) Zhao, Z.; Chen, X.; Wang, Q.; Yang, T.; Zhang, Y.; Yuan, W. Z. Sulphur-Containing Nonaromatic Polymers: Clustering-Triggered Emission and Luminescence Regulation by Oxidation. *Polym. Chem.* **2019**, *10* (26), 3639–3646.

(56) Voutyritsa, E.; Triandafillidi, I.; Kokotos, C. G. Green Organocatalytic Oxidation of Sulfides to Sulfoxides and Sulfones. *Synth.* **2017**, *49* (4), 917–924.

(57) Yu, B.; Liu, A. H.; He, L. N.; Li, B.; Diao, Z. F.; Li, Y. N. Catalyst-Free Approach for Solvent-Dependent Selective Oxidation of Organic Sulfides with Oxone. *Green Chem.* **2012**, *14* (4), 957–962.

(58) Podgórski, M.; Wang, C.; Yuan, Y.; Konetski, D.; Smalyukh, I.; Bowman, C. N. Pristine Polysulfone Networks as a Class of Polysulfide-Derived High-Performance Functional Materials. *Chem. Mater.* **2016**, *28* (14), 5102–5109. DOI:10.1021/acs.chemmater.6b02026.

(59) Jeanmaire, D.; Laliturai, J.; Almalik, A.; Carampin, P.; D'Arcy, R.; Lallana, E.; Evans, R.; Winpenny, R. E. P.; Tirelli, N. Chemical Specificity in REDOX-Responsive Materials: The Diverse Effects of Different Reactive Oxygen Species (ROS) on Polysulfide Nanoparticles. *Polym. Chem.* **2014**, *5* (4), 1393–1404.

(60) El Mohtadi, F.; D'Arcy, R.; Yang, X.; Turhan, Z. Y.; Alshamsan, A.; Tirelli, N.; Mohtadi, F. El; Arcy, R.; Yang, X.; Turhan, Z. Y.; Alshamsan, A.; Tirelli, N. Main Chain Polysulfoxides as Active 'Stealth' Polymers with Additional Antioxidant and Anti-Inflammatory Behaviour. *Int. J. Mol. Sci.* **2019**, *20* (18), 1–14. DOI:10.3390/ijms20184583.

(61) Cao, Y.; Zhang, G.; Zhang, Y.; Yue, M.; Chen, Y.; Cai, S. Direct Fabrication of Stretchable Electronics on a Polymer Substrate with Process-Integrated Programmable Rigidity. **2018**, *1804604*, 1–9. DOI:10.1002/adfm.201804604.

(62) El Mohtadi, F.; d'Arcy, R.; Yang, X.; Turhan, Z. Y.; Alshamsan, A.; Tirelli, N. Main Chain Polysulfoxides as Active "Stealth" Polymers with Additional Antioxidant and Anti-Inflammatory Behaviour. *Int. J. Mol. Sci.* **2019**, *20* (18), 4583. DOI:10.3390/ijms20184583.

(63) Allen, B. L.; Johnson, J. D.; Walker, J. P. Encapsulation and Enzyme-Mediated Release of Molecular Cargo in Polysulfide Nanoparticles. *ACS Nano* **2011**, *5* (6), 5263–5272.

(64) Herrera-Ordóñez, J.; Saldívar-Guerra, E.; Vivaldo-Lima, E. Dispersed-Phase Polymerization Processes. *Handb. Polym. Synth. Charact. Process.* **2013**, 295–315. DOI:10.1002/9781118480793.ch14.

(65) Aerdts, A. M.; Van Herk, A. M.; Klumperman, B.; Kurja, J.; German, A. L. Emulsion Polymerization. *Mater. Sci. Technol. A Compr. Treat.* **2008**, 269–317. DOI:10.1002/9783527619313.ch9.

(66) Schork, F. J.; Luo, Y.; Smulders, W.; Russum, J. P.; Butté, A.; Fontenot, K. Miniemulsion Polymerization. *Adv. Polym. Sci.* **2005**, *175*, 129–255. DOI:10.1007/b100115.

(67) Asua, J. M. Miniemulsion Polymerization. *Prog. Polym. Sci.* **2002**, *27* (7), 1283–1346. DOI:10.1016/S0079-6700(02)00010-2.

(68) Landfester, K. Miniemulsion Polymerization and the Structure of Polymer and Hybrid Nanoparticles. *Angew. Chemie - Int. Ed.* **2009**, *48* (25), 4488–4507. DOI:10.1002/anie.200900723.

(69) Landfester, K. The Generation of Nanoparticles in Miniemulsions. *Adv. Mater.* **2001**, *13* (10), 765–768. DOI:10.1002/1521-4095(200105)13:10<765::AID-ADMA765>3.0.CO;2-F.

(70) Antonietti, M.; Landfester, K. Polyreactions in Miniemulsions. *Prog. Polym. Sci.* **2002**, *27* (4), 689–757. DOI:10.1016/S0079-6700(01)00051-X.

(71) Kabalnov, A. S.; Pertzov, A. V.; Shchukin, E. D. Ostwald Ripening in Emulsions. I. Direct Observations of Ostwald Ripening in Emulsions. *J. Colloid Interface Sci.* **1987**, *118* (2), 590–597. DOI:10.1016/0021-9797(87)90492-9.

(72) Gommes, C. J. Ostwald Ripening of Confined Nanoparticles: Chemomechanical Coupling in Nanopores. *Nanoscale* **2019**, *11* (15), 7386–7393. DOI:10.1039/c9nr01349k.

(73) Dagtepe, P.; Chikan, V. Quantized Ostwald Ripening of Colloidal Nanoparticles. *J. Phys. Chem. C* **2010**, *114* (39), 16263–16269. DOI:10.1021/jp105071a.

(74) Tobita, H. Modeling Controlled/Living Radical Polymerization Kinetics: Bulk and Miniemulsion. *Macromol. React. Eng.* **2010**, *4* (11–12), 643–662. DOI:10.1002/mren.201000029.

(75) Tobita, H. Effect of Small Reaction Locus in Free-Radical Polymerization: Conventional and Reversible-Deactivation Radical Polymerization. *Polymers (Basel).* **2016**, *8* (4). DOI:10.3390/polym8040155.

(76) Amaral, M. Do; Asua, J. M. Synthesis of Large, High-Solid-Content Latexes by Miniemulsion Polymerization. *J. Polym. Sci. Part A Polym. Chem.* **2004**, *42* (17), 4222–4227. DOI:10.1002/pola.20287.

(77) Rodríguez, R.; Barandiaran, M. J.; Asua, J. M. Particle Nucleation in High Solids Miniemulsion Polymerization. **2007**. DOI:10.1021/ma070525c.

(78) Weiss, C. K.; Landfester, K. Encapsulation by Miniemulsion Polymerization. In *Modern Techniques for Nano and Microreactors/-reactions*; Caruso, F., Ed.; Springer US: New York, 2010; Vol. 229, pp 28–37. DOI:10.1007/978-3-642-12873-8.

(79) Landfester, K.; Musyanovych, A.; Mailaender, V. From Polymeric Particles to Multifunctional Nanocapsules for Biomedical Applications Using the Miniemulsion Process. *J. Polym. Sci. Part A Polym. Chem.* **2010**, *48* (3), 493–515. DOI:10.1002/pola.23786.

(80) Guyot, A.; Landfester, K.; Joseph Schork, F.; Wang, C. Hybrid Polymer Latexes. *Prog. Polym. Sci.*

2007, *32* (12), 1439–1461. DOI:10.1016/j.progpolymsci.2007.07.003.

(81) Herrmann, C.; Crespy, D.; Landfester, K. Synthesis of Hydrophilic Polyurethane Particles in Non-Aqueous Inverse Miniemulsions. *Colloid Polym. Sci.* **2011**, *289* (10), 1111–1117. DOI:10.1007/s00396-011-2430-z.

(82) Jasinski, F.; Lobry, E.; Tarablsi, B.; Chemtob, A.; Croutxé-Barghorn, C.; Nouen, D. Le; Criqui, A. Light-Mediated Thiol-Ene Polymerization in Miniemulsion: A Fast Route to Semicrystalline Polysul Fide Nanoparticles. *ACS Macro Lett.* **2014**, *3* (9), 958–962. DOI:10.1021/mz500458s.

(83) Asua, J. M. Challenges in Polymerization in Dispersed Media. *Adv. Polym. Sci.* **2018**, *281*, 1–22. DOI:10.1007/12_2017_21.

(84) Chemtob, A.; Kunstler, B.; Croutxé-Barghorn, C.; Fouchard, S. Photoinduced Miniemulsion Polymerization. *Colloid Polym. Sci.* **2010**, *288* (5), 579–587. DOI:10.1007/s00396-010-2190-1.

(85) Fuchs, A. V.; Will, G. D. Photo-Initiated Miniemulsion Polymerization as a Route to the Synthesis of Gold Nanoparticle Encapsulated Latexes. *Polymer (Guildf).* **2010**, *51* (10), 2119–2124. DOI:10.1016/j.polymer.2010.03.019.

(86) Lobry, E.; Jasinski, F.; Penconi, M.; Chemtob, A.; Ley, C.; Croutxé-Barghorn, C.; Oliveros, E.; Braun, A. M.; Criqui, A. Absorption and Scattering in Concentrated Monomer Miniemulsions: Static and Dynamic Investigations. *Macromol. Chem. Phys.* **2014**, *215* (12), 1201–1211. DOI:10.1002/macp.201400072.

(87) Daniloska, V.; Tomovska, R.; Asua, J. M. Hybrid Miniemulsion Photopolymerization in a Continuous Tubular Reactor-A Way to Expand the Characteristics of Polyurethane/Acrylics. *Chem. Eng. J.* **2012**, *184*, 308–314. DOI:10.1016/j.cej.2012.01.040.

(88) Penconi, M.; Lobry, E.; Jasinski, F.; Chemtob, A.; Croutxé-Barghorn, C.; Criqui, A.; Braun, A. M.; Oliveros, E. The Use of Chemical Actinometry for the Evaluation of the Light Absorption Efficiency in Scattering Photopolymerizable Miniemulsions. *Photochem. Photobiol. Sci.* **2015**, *14* (2), 308–319. DOI:10.1039/c4pp00323c.

(89) Hoijemberg, P. A.; Chemtob, A.; Croutxé-Barghorn, C.; Poly, J.; Braun, A. M. Radical Photopolymerization in Miniemulsions. Fundamental Investigations and Technical Development. *Macromolecules* **2011**, *44* (22), 8727–8738. DOI:10.1021/ma201753d.

(90) Lobry, E.; Jasinski, F.; Penconi, M.; Chemtob, A.; Croutxé-Barghorn, C.; Oliveros, E.; Braun, A.

M.; Criqui, A. Continuous-Flow Synthesis of Polymer Nanoparticles in a Microreactor via Miniemulsion Photopolymerization. *RSC Adv.* **2014**, *4* (82), 43756–43759. DOI:10.1039/c4ra06814a.

(91) Piradashvili, K.; Alexandrino, E. M.; Wurm, F. R.; Landfester, K. Reactions and Polymerizations at the Liquid–Liquid Interface. *Chem. Rev.* **2016**, *116* (4), 2141–2169. DOI:10.1021/acs.chemrev.5b00567.

(92) Crespy, D.; Landfester, K. Making Dry Fertile: A Practical Tour of Non-Aqueous Emulsions and Miniemulsions, Their Preparation and Some Applications. *Soft Matter* **2011**, *7* (23), 11054–11064. DOI:10.1039/c1sm06156a.

(93) Crespy, D.; Stark, M.; Hoffmann-Richter, C.; Ziener, U.; Landfester, K. Polymeric Nanoreactors for Hydrophilic Reagents Synthesized by Interfacial Polycondensation on Miniemulsion Droplets. *Macromolecules* **2007**, *40* (9), 3122–3135. DOI:10.1021/ma0621932.

(94) Alkanawati, M. S.; Da Costa Marques, R.; Mailänder, V.; Landfester, K.; Thérien-Aubin, H. Polysaccharide-Based PH-Responsive Nanocapsules Prepared with Bio-Orthogonal Chemistry and Their Use as Responsive Delivery Systems. *Biomacromolecules* **2020**, *21* (7), 2764–2771. DOI:10.1021/acs.biomac.0c00492.

(95) Alkanawati, M. S.; Machtakova, M.; Landfester, K.; Thérien-Aubin, H. Bio-Orthogonal Nanogels for Multiresponsive Release. *Biomacromolecules* **2021**, acs.biomac.1c00378. DOI:10.1021/acs.biomac.1c00378.

(96) Machtakova, M.; Han, S.; Yangazoglu, Y.; Lieberwirth, I.; Thérien-Aubin, H.; Landfester, K. Self-Sustaining Enzyme Nanocapsules Perform on-Site Chemical Reactions †. **2021**, *13*, 4051. DOI:10.1039/d0nr08116g.

(97) Zetterlund, P. B. Controlled/Living Radical Polymerization in Nanoreactors: Compartmentalization Effects. *Polym. Chem.* **2011**, *2* (3), 534–549. DOI:10.1039/c0py00247j.

(98) Lancaster, L.; Abdallah, W.; Banta, S.; Wheeldon, I. Engineering Enzyme Microenvironments for Enhanced Biocatalysis. *Chem. Soc. Rev.* **2018**, *47* (14), 5177–5186. DOI:10.1039/c8cs00085a.

(99) Baumann, P.; Spulber, M.; Fischer, O.; Car, A.; Meier, W. Investigation of Horseradish Peroxidase Kinetics in an "Organelle-Like" Environment. *Small* **2017**, *13* (17), 10–12. DOI:10.1002/smll.201603943.

(100) Yu, J.; Zhang, Y.; Liu, S. Enzymatic Reactivity of Glucose Oxidase Confined in Nanochannels. *Biosens. Bioelectron.* **2014**, *55*, 307–312. DOI:10.1016/j.bios.2013.12.042.

(101) Rivas, G.; Minton, A. P. Macromolecular Crowding In Vitro, In Vivo, and In Between. *Trends Biochem. Sci.* **2016**, *41* (11), 970–981. DOI:10.1016/j.tibs.2016.08.013.

(102) Laurino, P.; Hernandez, H. F.; Bräuer, J.; Krüger, K.; Grützmacher, H.; Tauer, K.; Seeberger, P. H. Snowballing Radical Generation Leads to Ultrahigh Molecular Weight Polymers. *Macromol. Rapid Commun.* **2012**, *33* (20), 1770–1774. DOI:10.1002/marc.201200384.

(103) Alexandrino, E. M.; Buchold, P.; Wagner, M.; Fuchs, A.; Kreyes, A.; Weiss, C. K.; Landfester, K.; Wurm, F. R. A Molecular "Screw-Clamp": Accelerating Click Reactions in Miniemulsions. *Chem. Commun.* **2014**, *50* (72), 10495–10498. DOI:10.1039/c4cc04119d.

(104) Lopez, E.; Simon, S. L. Trimerization Reaction Kinetics and T g Depression of Polycyanurate under Nanoconfinement. *Macromolecules* **2015**, *48* (13), 4692–4701. DOI:10.1021/acs.macromol.5b00167.

(105) Petrosko, S. H.; Johnson, R.; White, H.; Mirkin, C. A. Nanoreactors: Small Spaces, Big Implications in Chemistry. *J. Am. Chem. Soc.* **2016**, *138* (24), 7443–7445. DOI:10.1021/jacs.6b05393.

(106) Baumann, E. Ueber Eine Einfache Methode Der Darstellung von Benzoësäureäthern. *Berichte der Dtsch. Chem. Gesellschaft* **1886**, *19* (2), 3218–3222. DOI:10.1002/CBER.188601902348.

(107) Schotten, C. Ueber Die Oxydation Des Piperidins. *Berichte der Dtsch. Chem. Gesellschaft* **1883**, *16* (1), 643–649. DOI:10.1002/cber.188301601144.

(108) Qu, P.; Kuepfert, M.; Jockusch, S.; Weck, M. Compartmentalized Nanoreactors for One-Pot Redox-Driven Transformations. *ACS Catal.* **2019**, *9* (4), 2701–2706. DOI:10.1021/acscatal.8b04667.

(109) Lu, J.; Dimroth, J.; Weck, M. Compartmentalization of Incompatible Catalytic Transformations for Tandem Catalysis. *J. Am. Chem. Soc.* **2015**, *137* (40), 12984–12989. DOI:10.1021/jacs.5b07257.

(110) Balasubramanian, V.; Correia, A.; Zhang, H.; Fontana, F.; Mäkilä, E.; Salonen, J.; Hirvonen, J.; Santos, H. A. Biomimetic Engineering Using Cancer Cell Membranes for Designing Compartmentalized Nanoreactors with Organelle-Like Functions. *Adv. Mater.* **2017**, *29* (11), 1–

7. DOI:10.1002/adma.201605375.

(111) Peters, R. J. R. W.; Louzao, I.; Van Hest, J. C. M. From Polymeric Nanoreactors to Artificial Organelles. *Chem. Sci.* **2012**, *3* (2), 335–342. DOI:10.1039/c2sc00803c.

(112) Zhou, H.-X.; Rivas, G.; Minton, A. P. Macromolecular Crowding and Confinement: Biochemical, Biophysical, and Potential Physiological Consequences. *Annu. Rev. Biophys.* **2008**, *37* (1), 375–397. DOI:10.1146/annurev.biophys.37.032807.125817.

(113) Dong, B.; Pei, Y.; Zhao, F.; Goh, T. W.; Qi, Z.; Xiao, C.; Chen, K.; Huang, W.; Fang, N. In Situ Quantitative Single-Molecule Study of Dynamic Catalytic Processes in Nanoconfinement. *Nat. Catal.* **2018**, *1* (2), 135–140. DOI:10.1038/s41929-017-0021-1.

(114) Cotanda, P.; Lu, A.; Patterson, J. P.; Petzetakis, N.; O'Reilly, R. K. Functionalized Organocatalytic Nanoreactors: Hydrophobic Pockets for Acylation Reactions in Water. *Macromolecules* **2012**, *45* (5), 2377–2384. DOI:10.1021/ma2027462.

(115) Jo, S. M.; Wurm, F. R.; Landfester, K. Biomimetic Cascade Network between Interactive Multicompartments Organized by Enzyme-Loaded Silica Nanoreactors. *ACS Appl. Mater. Interfaces* **2018**, *10* (40), 34230–34237. DOI:10.1021/acsami.8b11198.

(116) Bakshi, S. F.; Guz, N.; Zakharchenko, A.; Deng, H.; Tumanov, A. V.; Woodworth, C. D.; Minko, S.; Kolpashchikov, D. M.; Katz, E. Nanoreactors Based on DNAzyme-Functionalized Magnetic Nanoparticles Activated by Magnetic Field. *Nanoscale* **2018**, *10* (3), 1356–1365. DOI:10.1039/c7nr08581h.

(117) Dai, L.; Jones, J. J.; Klotz, A. R.; Levy, S.; Doyle, P. S. Nanoconfinement Greatly Speeds up the Nucleation and the Annealing in Single-DNA Collapse. *Soft Matter* **2017**, *13* (37), 6363–6371. DOI:10.1039/c7sm01249g.

(118) Bentein, L.; D'Hooge, D. R.; Reyniers, M. F.; Marin, G. B. Kinetic Modeling of Miniemulsion Nitroxide Mediated Polymerization of Styrene: Effect of Particle Diameter and Nitroxide Partitioning up to High Conversion. *Polymer (Guildf).* **2012**, *53* (3), 681–693. DOI:10.1016/j.polymer.2011.12.044.

(119) Tobita, H. RAFT Miniemulsion Polymerization Kinetics, 1 - Polymerization Rate. *Macromol. Theory Simulations* **2009**, *18* (2), 108–119. DOI:10.1002/mats.200800069.

(120) Crespy, D.; Landfester, K. Miniemulsion Polymerization as a Versatile Tool for the Synthesis of

Functionalized Polymers. *Beilstein J. Org. Chem.* **2010**, *6*, 1132–1148. DOI:10.3762/bjoc.6.130.

(121) Willert, M.; Landfester, K. Amphiphilic Copolymers from Miniemulsified Systems. *Macromol. Chem. Phys.* **2002**, *203* (5–6), 825–836. DOI:10.1002/1521-3935(20020401)203:5/6<825::AID-MACP825>3.0.CO;2-R.

(122) Renggli, K.; Baumann, P.; Langowska, K.; Onaca, O.; Bruns, N.; Meier, W. Selective and Responsive Nanoreactors. *Adv. Funct. Mater.* **2011**, *21* (7), 1241–1259. DOI:10.1002/adfm.201001563.

(123) Roa, R.; Kim, W. K.; Kanduč, M.; Dzubiella, J.; Angioletti-Uberti, S. Catalyzed Bimolecular Reactions in Responsive Nanoreactors. *ACS Catal.* **2017**, *7* (9), 5604–5611. DOI:10.1021/acscatal.7b01701.

(124) Patterson, J. P.; Cotanda, P.; Kelley, E. G.; Moughton, A. O.; Lu, A.; Epps, T. H.; O'Reilly, R. K. Catalytic Y-Tailed Amphiphilic Homopolymers-Aqueous Nanoreactors for High Activity, Low Loading SCS Pincer Catalysts. *Polym. Chem.* **2013**, *4* (6), 2033–2039. DOI:10.1039/c3py21137a.

(125) Küchler, A.; Yoshimoto, M.; Luginbühl, S.; Mavelli, F.; Walde, P. Enzymatic Reactions in Confined Environments. *Nat. Nanotechnol.* **2016**, *11* (5), 409–420. DOI:10.1038/nnano.2016.54.

(126) Yang, H. Q.; Zhang, L.; Zhong, L.; Yang, Q. H.; Li, C. Enhanced Cooperative Activation Effect in the Hydrolytic Kinetic Resolution of Epoxides on [Co(Salen)] Catalysts Confined in Nanocages. *Angew. Chemie - Int. Ed.* **2007**, *46* (36), 6861–6865. DOI:10.1002/anie.200701747.

(127) Brown, J. M.; Baker, S. K.; Colens, A.; Darwent, J. . *Enzymic and Non-Enzymic Catalysis*; Dunnill, P., Wiseman, A., Blakebrough, N., Eds.; E. Horwood: Chichester : New York, 1980.

(128) Dwars, T.; Paetzold, E.; Oehme, G. Reactions in Micellar Systems. *Angew. Chemie - Int. Ed.* **2005**, *44* (44), 7174–7199. DOI:10.1002/anie.200501365.

(129) Khan, M.; Guimarães, T. R.; Zhou, D.; Moad, G.; Perrier, S.; Zetterlund, P. B. Exploitation of Compartmentalization in RAFT Miniemulsion Polymerization to Increase the Degree of Livingness. *J. Polym. Sci. Part A Polym. Chem.* **2019**, *57* (18), 1938–1946. DOI:10.1002/pola.29329.

(130) Zetterlund, P. B.; D'Hooge, D. R. The Nanoreactor Concept: Kinetic Features of Compartmentalization in Dispersed Phase Polymerization. *Macromolecules* **2019**, *52* (21),

7963–7976. DOI:10.1021/acs.macromol.9b01037.

(131) Suzuki, K.; Kanematsu, Y.; Miura, T.; Minami, M.; Satoh, S.; Tobita, H. Experimental Method to Discriminate RAFT Models between Intermediate Termination and Slow Fragmentation via Comparison of Rates of Miniemulsion and Bulk Polymerization. *Macromol. Theory Simulations* **2014**, *23* (3), 136–146. DOI:10.1002/mats.201300150.

(132) Rausch, K.; Reuter, A.; Fischer, K.; Schmidt, M. Evaluation of Nanoparticle Aggregation in Human Blood Serum. *Biomacromolecules* **2010**, *11* (11), 2836–2839. DOI:10.1021/bm100971q.

(133) Rodriguez, E. D.; Luo, X.; Mather, P. T. Linear/Network Poly(ε-Caprolactone) Blends Exhibiting Shape Memory Assisted Self-Healing (SMASH). *ACS Appl. Mater. Interfaces* **2011**, *3* (2), 152–161. DOI:10.1021/am101012c.

(134) Zhang, L.; Ren, X.; Zhang, Y.; Zhang, K. Step-Growth Polymerization Method for Ultrahigh Molecular Weight Polymers. *ACS Macro Lett.* **2019**, *8* (8), 948–954. DOI:10.1021/acsmacrolett.9b00475.

(135) Hoyle, C. E.; Bowman, C. N. Thiol–Ene Click Chemistry. *Angew. Chemie Int. Ed.* **2010**, *49* (9), 1540–1573. DOI:https://doi.org/10.1002/anie.200903924.

(136) Love, D.; Fairbanks, B.; Bowman, C. Reaction Environment Effect on the Kinetics of Radical Thiol-Ene Polymerizations in the Presence of Amines and Thiolate Anions. *ACS Macro Lett.* **2020**, 174–179. DOI:10.1021/acsmacrolett.9b00960.

(137) Le, C. M. Q.; Vidal, L.; Schmutz, M.; Chemtob, A. Droplet Nucleation in Miniemulsion Thiol–Ene Step Photopolymerization. *Polym. Chem.* **2021**, *12* (14), 2084–2094. DOI:10.1039/d1py00139f.

(138) Zhao, H. Y.; Simon, S. L. Equilibrium Free-Radical Polymerization of Methyl Methacrylate under Nanoconfinement. *Polymer (Guildf).* **2015**, *66*, 173–178. DOI:10.1016/j.polymer.2015.04.017.

(139) Monteiro, M. J. Nanoreactors for Polymerizations and Organic Reactions. *Macromolecules* **2010**, *43* (3), 1159–1168. DOI:10.1021/ma902348r.

(140) Müller, K.; Klapper, M.; Müllen, K. Preparation of High Molecular Weight Polyurethane Particles by Nonaqueous Emulsion Polyaddition. *Colloid Polym. Sci.* **2007**, *285* (10), 1157–1161. DOI:10.1007/s00396-007-1670-4.

(141) Sutherland, B. P.; Kabra, M.; Kloxin, C. J. Expanding the Thiol-X Toolbox: Photoinitiation and

Materials Application of the Acid-Catalyzed Thiol-Ene (ACT) Reaction. *Polym. Chem.* **2021**, *12* (10), 1562–1570. DOI:10.1039/d0py01593h.

(142) Claudino, M.; Jonsson, M.; Johansson, M. Thiol-Ene Coupling Kinetics of d-Limonene: A Versatile "non-Click" Free-Radical Reaction Involving a Natural Terpene. *RSC Adv.* **2013**, *3* (27), 11021–11034. DOI:10.1039/c3ra40696b.

(143) Jasinski, F.; Rannée, A.; Schweitzer, J.; Fischer, D.; Lobry, E.; Croutxé-Barghorn, C.; Schmutz, M.; Le Nouen, D.; Criqui, A.; Chemtob, A. Thiol-Ene Linear Step-Growth Photopolymerization in Miniemulsion: Fast Rates, Redox-Responsive Particles, and Semicrystalline Films. *Macromolecules* **2016**, *49* (4), 1143–1153. DOI:10.1021/acs.macromol.5b02512.

(144) Hoyle, C. E.; Bowman, C. N. Thiol – Ene Click Chemistry. *Angew. Chemie Int. Ed.* **2010**, 1540–1573. DOI:10.1002/anie.200903924.

(145) Lee, T. Y.; Smith, Z.; Reddy, S. K.; Cramer, N. B.; Bowman, C. N. Thiol-Allyl Ether-Methacrylate Ternary Systems. Polymerization Mechanism. *Macromolecules* **2007**, *40* (5), 1466–1472. DOI:10.1021/ma062494b.

(146) Senyurt, A. F.; Wei, H.; Hoyle, C. E.; Piland, S. G.; Gould, T. E. Ternary Thiol-Ene/Acrylate Photopolymers: Effect of Acrylate Structure on Mechanical Properties? *Macromolecules* **2007**, *40* (14), 4901–4909. DOI:10.1021/ma062534b.

(147) Lungu, A.; Ghitman, J.; Cernencu, A. I.; Serafim, A.; Florea, N. M.; Vasile, E.; Iovu, H. POSS-Containing Hybrid Nanomaterials Based on Thiol-Epoxy Click Reaction. *Polymer (Guildf).* **2018**, *145*, 324–333. DOI:10.1016/j.polymer.2018.05.015.

(148) Stößer, T.; Li, C.; Unruangsri, J.; Saini, P. K.; Sablong, R. J.; Meier, M. A. R.; Williams, C. K.; Koning, C. Bio-Derived Polymers for Coating Applications: Comparing Poly(Limonene Carbonate) and Poly(Cyclohexadiene Carbonate). *Polym. Chem.* **2017**, *8* (39), 6099–6105. DOI:10.1039/c7py01223c.

(149) Colak, B.; Da Silva, J. C. S.; Soares, T. A.; Gautrot, J. E. Impact of the Molecular Environment on Thiol-Ene Coupling for Biofunctionalization and Conjugation. *Bioconjug. Chem.* **2016**, *27* (9), 2111–2123. DOI:10.1021/acs.bioconjchem.6b00349.

(150) Cramer, N. B.; Couch, C. L.; Schreck, K. M.; Boulden, J. E.; Wydra, R.; Stansbury, J. W.; Bowman, C. N. Properties of Methacrylate-Thiol-Ene Formulations as Dental Restorative Materials. *Dent.*

Mater. **2010**, *26* (8), 799–806. DOI:10.1016/j.dental.2010.04.005.

(151) Shanmuganathan, K.; Sankhagowit, R. K.; Iyer, P.; Ellison, C. J. Thiol-Ene Chemistry: A Greener Approach to Making Chemically and Thermally Stable Fibers. *Chem. Mater.* **2011**, *23* (21), 4726–4732. DOI:10.1021/cm2015093.

(152) Jenjob, R.; Seidi, F.; Crespy, D. Recent Advances in Polymerizations in Dispersed Media. *Adv. Colloid Interface Sci.* **2018**, *260*, 24–31. DOI:10.1016/j.cis.2018.08.002.

(153) Sandström, N.; Shafagh, R. Z.; Vastesson, A.; Carlborg, C. F.; van der Wijngaart, W.; Haraldsson, T. Reaction Injection Molding and Direct Covalent Bonding of OSTE+ Polymer Microfluidic Devices. *J. Micromechanics Microengineering* **2015**, *25* (7), 075002. DOI:10.1088/0960-1317/25/7/075002.

(154) Cramer, N. B.; Davies, T.; O'Brien, A. K.; Bowman, C. N. Mechanism and Modeling of a Thiol-Ene Photopolymerization. *Macromolecules* **2003**, *36* (12), 4631–4636. DOI:10.1021/ma034072x.

(155) Brandup, J.; Immergut, E. H.; Grulke, E. A. *Polymer Handbook*, 4th ed.; Abe, A., Bloch, D. R., Eds.; John Wiley & Sons, Inc.: New York, 1999; Vol. 1.

(156) Odian, G. Chain Copolymerization. In *Principles of Polymerization*; John Wiley & Sons, Ltd: New York, 2004; pp 464–543. DOI:https://doi.org/10.1002/047147875X.ch6.

(157) Asua, J. M. Challenges for Industrialization of Miniemulsion Polymerization. *Prog. Polym. Sci.* **2014**, *39* (10), 1797–1826. DOI:10.1016/j.progpolymsci.2014.02.009.

(158) Aguilar-Vega, M., Elizalde, L. E., Santiago-García J. L., S.-V. G. Step- Growth Polymerization. In *Handbook of Polymer Synthesis, Characterization and Processing*; John Wiley & Sons, Inc., 2013; pp 43–63.

(159) El-Hibri, M. J.; Weinberg, S. A. Polysulfones. In *Encyclopedia of Polymer Science and Technology*; American Cancer Society, 2001. DOI:https://doi.org/10.1002/0471440264.pst291.

(160) Podgórski, M.; Chatani, S.; Bowman, C. N. Development of Glassy Step-Growth Thiol-Vinyl Sulfone Polymer Networks. *Macromol. Rapid Commun.* **2014**, *35* (17), 1497–1502. DOI:10.1002/marc.201400260.

(161) Kortan, A. M.; Cannizzaro, R. J.; Robb, M. J.; Knauss, D. M. Poly(Ether Sulfone)s Using a Rigid Dibenzothiophene Dioxide Heterocycle. *J. Polym. Sci. Part A Polym. Chem.* **2016**, *54* (19), 3127–3131. DOI:10.1002/pola.28197.

(162) Chemtob, A.; Feillée, N.; Ley, C.; Ponche, A.; Rigolet, S.; Soraru, C.; Ploux, L.; Le Nouen, D. Oxidative Photopolymerization of Thiol-Terminated Polysulfide Resins. Application in Antibacterial Coatings. *Prog. Org. Coatings* **2018**, *121*, 80–88. DOI:https://doi.org/10.1016/j.porgcoat.2018.04.017.

(163) Ebnesajjad, S.; Landrock, A. H. Characteristics of Adhesive Materials. In *Adhesives Technology Handbook*; Elsevier, 2015; pp 84–159. DOI:10.1016/b978-0-323-35595-7.00005-x.

(164) Montembault, V.; Fontaine, L. Polyphosphoesters. In *Phosphorus-Based Polymers: From Synthesis to Applications*; The Royal Society of Chemistry, 2014; pp 97–124. DOI:10.1039/9781782624523-00097.

(165) Sun, Y.; Dong, T.; Lu, C.; Xin, W.; Yang, L.; Liu, P.; Qian, Y.; Zhao, Y.; Kong, X.-Y.; Wen, L.; Jiang, L. Tailoring A Poly(Ether Sulfone) Bipolar Membrane: Osmotic-Energy Generator with High Power Density. *Angew. Chemie Int. Ed.* **2020**, *59* (40), 17423–17428. DOI:https://doi.org/10.1002/anie.202006320.

(166) Jeon, Y.-M.; Lim, T.-H.; Kim, S.-H.; Kim, J.-G.; Gong, M.-S. Preparation of Amine-Containing Poly(Amide-Sulfone)s Using Vinylsulfone Reactive Monomers and Their Properties. *Macromol. Res.* **2007**, *15* (1), 17–21. DOI:10.1007/BF03218747.

(167) Rao, V. L. Polyether Sulfones. *J. Macromol. Sci. - Rev. Macromol. Chem. Phys.* **1999**, *39 C* (4), 655–711. DOI:10.1081/mc-100101430.

(168) Bulman Page, P. C.; Buckley, B. R.; Elliott, C.; Chan, Y.; Dreyfus, N.; Marken, F. Chemoselective Oxidation of Sulfides to Sulfoxides with Urea–Hydrogen Peroxide Complex Catalysed by Diselenide. *Synlett* **2016**, *27* (01), 80–82.

(169) El-Mohtadi, F.; D'Arcy, R.; Tirelli, N. Oxidation-Responsive Materials: Biological Rationale, State of the Art, Multiple Responsiveness, and Open Issues. *Macromol. Rapid Commun.* **2019**, *40* (1), 1–24.

(170) Durham, O. Z.; Shipp, D. A. Polymer Colloids from Step-Growth Thiol-X Polymerizations. *Polym. Rev.* **2021**, *61* (1), 54–79. DOI:10.1080/15583724.2020.1743307.

(171) Machado, T. O.; Cardoso, P. B.; Feuser, P. E.; Sayer, C.; Araújo, P. H. H. Thiol-Ene Miniemulsion Polymerization of a Biobased Monomer for Biomedical Applications. *Colloids Surfaces B Biointerfaces* **2017**, *159*, 509–517. DOI:10.1016/j.colsurfb.2017.07.043.

(172) Cao, Y.; Zhang, G.; Zhang, Y.; Yue, M.; Chen, Y.; Cai, S.; Xie, T.; Feng, X. Direct Fabrication of Stretchable Electronics on a Polymer Substrate with Process-Integrated Programmable Rigidity. *Adv. Funct. Mater.* **2018**, *28* (50), 1804604. DOI:https://doi.org/10.1002/adfm.201804604.

(173) Cheng, F.; Su, T.; Luo, K.; Pu, Y.; He, B. The Polymerization Kinetics, Oxidation-Responsiveness, and in Vitro Anticancer Efficacy of Poly(Ester-Thioether)S. *J. Mater. Chem. B* **2019**, *7* (6), 1005–1016. DOI:10.1039/c8tb02980f.

(174) Zhao, Z.; Chen, X.; Wang, Q.; Yang, T.; Zhang, Y.; Yuan, W. Z. Sulphur-Containing Nonaromatic Polymers: Clustering-Triggered Emission and Luminescence Regulation by Oxidation. *Polym. Chem.* **2019**, *10* (26), 3639–3646. DOI:10.1039/c9py00519f.

(175) Jeanmaire, D.; Lalituraі, J.; Almalik, A.; Carampin, P.; D'Arcy, R.; Lallana, E.; Evans, R.; Winpenny, R. E. P.; Tirelli, N. Chemical Specificity in REDOX-Responsive Materials: The Diverse Effects of Different Reactive Oxygen Species (ROS) on Polysulfide Nanoparticles. *Polym. Chem.* **2014**, *5* (4), 1393–1404. DOI:10.1039/c3py01475d.

(176) Allen, B. L.; Johnson, J. D.; Walker, J. P. Encapsulation and Enzyme-Mediated Release of Molecular Cargo in Polysulfide Nanoparticles. *ACS Nano* **2011**, *5* (6), 5263–5272. DOI:10.1021/nn201477y.

(177) Claudino, M.; Jonsson, M.; Johansson, M. Utilizing Thiol–Ene Coupling Kinetics in the Design of Renewable Thermoset Resins Based on d-Limonene and Polyfunctional Thiols. *RSC Adv.* **2014**, *4* (20), 10317–10329. DOI:10.1039/C3RA47922F.

(178) Hu, P.; Tirelli, N. Scavenging ROS: Superoxide Dismutase/Catalase Mimetics by the Use of an Oxidation-Sensitive Nanocarrier/Enzyme Conjugate. *Bioconjug. Chem.* **2012**, *23* (3), 438–449. DOI:10.1021/bc200449k.

(179) Yan, B.; Zhang, Y.; Wei, C.; Xu, Y. Facile Synthesis of ROS-Responsive Biodegradable Main Chain Poly(Carbonate-Thioether) Copolymers. *Polym. Chem.* **2018**, *9* (7), 904–911. DOI:10.1039/C7PY01908D.

(180) Mahmoud, E. A.; Sankaranarayanan, J.; Morachis, J. M.; Kim, G.; Almutairi, A. Inflammation Responsive Logic Gate Nanoparticles for the Delivery of Proteins. *Bioconjug. Chem.* **2011**, *22* (7), 1416–1421. DOI:10.1021/bc200141h.

(181) Fan, Z.; Xu, H. Recent Progress in the Biological Applications of Reactive Oxygen Species-Responsive Polymers. *Polym. Rev.* **2020**, *60* (1), 114–143. DOI:10.1080/15583724.2019.1641515.

(182) Lee, S.; Stubelius, A.; Olejniczak, J.; Jang, H.; Huu, V. A. N.; Almutairi, A. Chemical Amplification Accelerates Reactive Oxygen Species Triggered Polymeric Degradation. *Biomater. Sci.* **2018**, *6* (1), 107–114. DOI:10.1039/C7BM00758B.

(183) Fernandez-rodriguez, P.; Haber, J.; Kleinbeck, F.; Kamptmann, S.; Susanne, F.; Hoehn, P.; Lanz, M.; Pellegatti, L.; Venturoni, F.; Robertson, J.; Willis, C. Toolbox Study for Application of Hydrogen Peroxide as a Versatile, Safe and Industrially-Relevant Green Oxidant in Continuous Flow Mode. *Green Chem.* **2017**, *19*, 1439–1448. DOI:10.1039/c6gc02899c.

(184) Arcy, R.; Gennari, A.; Donno, R.; Tirelli, N. Linear, Star, and Comb Oxidation-Responsive Polymers: Effect of Branching Degree and Topology on Aggregation and Responsiveness. *Macromol. Rapid Commun.* **2016**, *37*, 1918–1925. DOI:10.1002/marc.201600481.

(185) Herzberger, J.; Fischer, K.; Leibig, D.; Bros, M.; Thiermann, R.; Frey, H. Oxidation-Responsive and "Clickable" Poly(Ethylene Glycol) via Copolymerization of 2-(Methylthio)Ethyl Glycidyl Ether. *J. Am. Chem. Soc.* **2016**, *138* (29), 9212–9223. DOI:10.1021/jacs.6b04548.

(186) Gibian, M. J.; Ungermann, T. Reaction of Tert-Butyl Hydroperoxide Anion with Dimethyl Sulfoxide. On the Pathway of the Superoxide-Alkyl Halide Reaction. *J. Org. Chem.* **1976**, *41* (14), 2500–2502. DOI:10.1021/jo00876a037.

(187) Das, T. N.; Dhanasekaran, T.; Alfassi, Z. B.; Neta, P. Reduction Potential of the Tert-Butylperoxyl Radical in Aqueous Solutions. *J. Phys. Chem. A* **1998**, *5639* (97), 280–284. DOI:10.1021/jp972903t.

(188) Krumova, K.; Cosa, G. Overview of Reactive Oxygen Species. In *Singlet Oxygen: Applications in Biosciences and Nanosciences, Volume 1*; The Royal Society of Chemistry, 2016; Vol. 1, pp 1–21. DOI:10.1039/9781782622208-00001.

(189) Lallana, E.; Tirelli, N. Oxidation-Responsive Polymers: Which Groups to Use, How to Make

Them, What to Expect From Them (Biomedical Applications). *Macromol. Chem. Phys.* **2013**, *214*, 143–158. DOI:10.1002/macp.201200502.

(190) Wood, P. M. The Redox Potential for Dimethyl Sulphoxide Reduction to Dimethyl Sulphide. Evaluation and Biochemical Implications. *FEBS Lett.* **1981**, *124* (1), 11–14. DOI:10.1016/0014-5793(81)80042-7.

(191) Ratnikov, M. O.; Doyle, M. P. Mechanistic Investigation of Oxidative Mannich Reaction with Tert-Butyl Hydroperoxide. The Role of Transition Metal Salt. *J. Am. Chem. Soc.* **2013**, *135*, 1549–1557. DOI:10.1021/ja3113559.

(192) Goldstein, S.; Samuni, A. Kinetics and Mechanism of Peroxyl Radical Reactions with Nitroxides. *J. Phys. Chem. A* **2007**, *111*, 1066–1072. DOI:10.1021/jp0655975.

(193) Kim, G.; Weiss, S. J.; Levine, R. L. Methionine Oxidation and Reduction in Proteins. *Biochim. Biophys. Acta* **2014**, *1840* (2), 901–905. DOI:https://doi.org/10.1016/j.bbagen.2013.04.038.

(194) Thalhauser, S.; Breunig, M. Considerations for Efficient Surface Functionalization of Nanoparticles with a High Molecular Weight Protein as Targeting Ligand. *Eur. J. Pharm. Sci.* **2020**, *155* (105520), 1–11. DOI:10.1016/j.ejps.2020.105520.

(195) Arcy, R.; Iturrospe, A.; Arbe, A.; Tirelli, N.; Pe, R. A.; Mu, A. J. Influence of Chain Primary Structure and Topology (Branching) on Crystallization and Thermal Properties: The Case of Polysulfides. *Macromolecules* **2019**, *52*, 2093–2104. DOI:10.1021/acs.macromol.8b02659.

(196) Drago, R. S.; Wayland, B.; Carlson, R. L. Donor Properties of Sulfoxides, Alkyl Sulfites, and Sulfones. *J. Am. Chem. Soc.* **1963**, *85* (20), 3125–3128. DOI:10.1021/ja00903a016.

(197) Prezhdo, V. V.; Prezhdo, O. V.; Vaschenko, E. V. Studies on Proton Acceptor Ability of SOx-Containing Compounds. *J. Mol. Struct.* **1995**, *356* (1), 7–13. DOI:10.1016/0022-2860(95)08920-Q.

(198) Rodriguez, A. R.; Kramer, J. R.; Deming, T. J. Enzyme-Triggered Cargo Release from Methionine Sulfoxide Containing Copolypeptide Vesicles. *Biomacromolecules* **2013**, *14* (10), 3610–3614. DOI:10.1021/bm400971p.

(199) Yu, Y.; Xu, W.; Huang, X.; Xu, X.; Qiao, R.; Li, Y.; Han, F.; Peng, H.; Davis, T. P.; Fu, C.; Whittaker, A. K. Proteins Conjugated with Sulfoxide-Containing Polymers Show Reduced Macrophage Cellular Uptake and Improved Pharmacokinetics. *ACS Macro Lett.* **2020**, *9*, 799–805.

DOI:10.1021/acsmacrolett.0c00291.

(200) Li, S.; Chung, H. S.; Simakova, A.; Wang, Z.; Park, S.; Fu, L.; Cohen-karni, D.; Averick, S.; Matyjaszewski, K. Biocompatible Polymeric Analogues of DMSO Prepared by Atom Transfer Radical Polymerization. *Biomacromolecules* **2017**, *18*, 475–482. DOI:10.1021/acs.biomac.6b01553.

(201) Qiao, R.; Fu, C.; Li, Y.; Qi, X.; Ni, D.; Nandakumar, A.; Siddiqui, G.; Wang, H.; Zhang, Z.; Wu, T.; Zhong, J.; Tang, S. Y.; Pan, S.; Zhang, C.; Whittaker, M. R.; Engle, J. W.; Creek, D. J.; Caruso, F.; Ke, P. C.; Cai, W.; Whittaker, A. K.; Davis, T. P. Sulfoxide-Containing Polymer-Coated Nanoparticles Demonstrate Minimal Protein Fouling and Improved Blood Circulation. *Adv. Sci.* **2020**, *7* (13), 1–13. DOI:10.1002/advs.202000406.

(202) Kaiser, D.; Klose, I.; Oost, R.; Neuhaus, J.; Maulide, N. Bond-Forming and -Breaking Reactions at Sulfur (IV): Sulfoxides, Sulfonium Salts, Sulfur Ylides, and Sulfinate Salts. *Chem. Rev.* **2019**, *119*, 8701–8780. DOI:10.1021/acs.chemrev.9b00111.

(203) Cook, R. E.; Dainton, F. S.; Ivin, K. J. Effect of Olefin Structure on the Ceiling Temperature for Olefin Polysulfone Formation. *J. Polym. Sci.* **1957**, *26* (114), 351–364. DOI:https://doi.org/10.1002/pol.1957.1202611410.

(204) Naylor, M. A.; Anderson, A. W. Thermal Stability of Various Olefin-SO2 Polymers. *J. Am. Chem. Soc.* **1954**, *76* (15), 3962–3965. DOI:10.1021/ja01644a028.

(205) Onaca-Fischer, O.; Liu, J.; Inglin, M.; G. Palivan, C. Polymeric Nanocarriers and Nanoreactors: A Survey of Possible Therapeutic Applications. *Curr. Pharm. Des.* **2012**, *18* (18), 2622–2643. DOI:10.2174/138161212800492822.

(206) Navya, P. N.; Kaphle, A.; Srinivas, S. P.; Bhargava, S. K.; Rotello, V. M.; Daima, H. K. Current Trends and Challenges in Cancer Management and Therapy Using Designer Nanomaterials. *Nano Converg.* **2019**, *6* (1). DOI:10.1186/s40580-019-0193-2.

(207) Blanco, E.; Shen, H.; Ferrari, M. Principles of Nanoparticle Design for Overcoming Biological Barriers to Drug Delivery. *Nat. Biotechnol.* **2015**, *33* (9), 941–951. DOI:10.1038/nbt.3330.

(208) Zęibacz, N.; Wieczorek, S. A.; Kalwarczyk, T.; Fiałkowski, M.; Hołyst, R. Crossover Regime for the Diffusion of Nanoparticles in Polyethylene Glycol Solutions: Influence of the Depletion Layer. *Soft Matter* **2011**, *7* (16), 7181–7186. DOI:10.1039/c0sm01357a.

(209) Smilgies, D.-M.; Folta-Stogniew, E. Molecular Weight–Gyration Radius Relation of Globular Proteins: A Comparison of Light Scattering, Small-Angle X-Ray Scattering and Structure-Based Data. *J. Appl. Crystallogr.* **2015**, *48* (5), 1604–1606. DOI:10.1107/S1600576715015551.

(210) Johnsen, K. B.; Burkhart, A.; Melander, F.; Kempen, P. J.; Vejlebo, J. B.; Siupka, P.; Nielsen, M. S.; Andresen, T. L.; Moos, T. Targeting Transferrin Receptors at the Blood-Brain Barrier Improves the Uptake of Immunoliposomes and Subsequent Cargo Transport into the Brain Parenchyma. *Scientific Reports*. 2017. DOI:10.1038/s41598-017-11220-1.

(211) Pelegri-O'Day, E. M.; Lin, E.-W.; Maynard, H. D. Therapeutic Protein–Polymer Conjugates: Advancing Beyond PEGylation. *J. Am. Chem. Soc.* **2014**, *136* (41), 14323–14332. DOI:10.1021/ja504390x.